FACULTY OF ENGINEERING AND ARCHITECTURE

Printability and early age shrinkage of cementitious materials with superabsorbent polymers

Rens De Coensel
Student number: 01305337

Supervisors: Prof. dr. Kim Van Tittelboom, Dr. ir. Didier Snoeck
Counsellor: Jolien Van Der Putten

Master's dissertation submitted in order to obtain the academic degree of
Master of Science in Civil Engineering

Academic year 2018-2019

GHENT UNIVERSITY

This page is intentionally left blank.

PRINTABILITY AND EARLY AGE SHRINKAGE OF CEMENTITIOUS MATERIALS WITH SUPERABSORBENT POLYMERS

MASTER'S THESIS

AD Bartlett Show (event). (2015, October 1). Team Amalgamma 3D printed concrete table [photograph]. London, Bartlett School of Architecture (UCL)

GHENT UNIVERSITY

FACULTY OF ENGINEERING AND ARCHITECTURE

DEPARTMENT OF STRUCTURAL ENGINEERING
FACULTY OF ENGINEERING AND ARCHITECTURE

SUPERVISORS: prof. dr. ing. Kim Van Tittelboom
dr. ir. Didier Snoeck

COUNSELLOR: ir. Jolien Van Der Putten

Rens De Coensel
01305337

Master's dissertation submitted in order to obtain the academic degree of Master of Science in Civil Engineering

Academic year 2018-2019

This page is intentionally left blank.

Acknowledgements

"To all those who lead monotonous lives, in the hope that they may experience at second hand the delights and dangers of ~~adventure~~ experimental research on properties of fresh and hardened concrete with superabsorbent polymers."

Original quote by Agatha Christie from her novel The Secret Adversary.

This thesis would not have been what it is as it is being read by you, dear reader, without the help and support of the many people and institutions mentioned below. I am proud to present it to you together with my gratitude to my Maecenases.

Thank you, professor Van Tittelboom, for your confidence in my academic abilities.

Thank you, Didier, for all the invaluable help in all stages of my experimental research: pre-, intra- and post-.

Thank you, Jolien, for the many formal and informal conversations that made the daily trip to the laboratory worthwhile, even when all tests failed.

Thank you, laboratory Magnel and all its members of staff.

Thank you, Mom, for all the unconditional love and support in all that I do, have done and ever will do.

Thank you, dear family, for all the wisdom of life you provide me with.

Thank you, brothers from other mothers and sisters I never had, for all the pleasure in life you bring.

Thank you, Ghent University and its professors for setting out a challenging course in applied sciences and shaping the one to come.

And thank you, Vulcain for already believing in me and trusting me with a great responsibility, though I have not proven myself to you yet.

"Now this is not the end. It is not even the beginning of the end. But it is, perhaps, the end of the beginning."

Original quote by Winston Churchill from his 1942 Alamein speech at London's Mansion House.

Overview

PRINTABILITY AND EARLY AGE SHRINKAGE OF CEMENTITIOUS MATERIALS WITH SUPERABSORBENT POLYMERS
By Rens De Coensel

Supervisors: prof. dr. ing. Kim Van Tittelboom & dr. ir. Didier Snoeck
Counsellor: ir. Jolien Van Der Putten

Master's dissertation submitted in order to obtain the academic degree of
Master of Science in Civil Engineering

Department of Structural Engineering
Faculty of Engineering and Architecture
Academic year 2018-2019

Abstract

In 3D printing of concrete (3DPC) the cementitious material needs to fulfil conflicting requirements for pumpability, extrudability and buildability that define its overall printability. Superabsorbent polymers (SAPs) are added to mortar mixtures to stimulate internal curing that mitigates early age shrinkage and associated cracking. In this research printed specimens of mixtures with and without SAPs (having different characteristics) are studied with respect to their printability, early age shrinkage and mechanical properties. The effective water-cement ratio (w/c) in each was 0.365 and the 2D printing procedure was not altered. The specimens were printed on manipulated substrates that allowed them to shrink as unrestrained as possible. The mix designs were optimised, based on flow table workability in comparison to the reference mixture without SAPs (REF). Slight variations on the preceding mixing process, in combination with the swelling kinetics and geometrical characteristics of the SAPs, proved to influence the flow table diameter. Printability was evaluated by means of 5 criteria, covering early workability, viscosity, surface quality and dimensional stability under normal and increased hydrostatic pressure. These affect the mechanical properties as air can get trapped at the interface. Some SAPs have a lubricating tendency in the delivery system. It is believed the printing process increases the overall air content. The setting characteristics were established via the Vicat needle test and compared to those obtained from early age shrinkage measurements. SAPs tend to retard the onset and duration of setting. The macro- and microporosity were established by microscopy and automated RapidAir air void analysis. An increased air content generally led to a greater reduction in mechanical strength. Nanoporosity was studied at the lower, inter- and upper layer of double-layered printed specimens by means of mercury intrusion porosimetry (MIP). The bottom layer showed a lower nanoporosity ascribed to a denser matrix under increased loading of the superposed layer. The autogenous shrinkage was measured on corrugated tubes by automated dilatometry and unprotected shrinkage, subject to evaporation, was evaluated by means of photographic image analysis. The difference in order of magnitude between the measurements amounted to a factor 10^3. All mixtures with SAPs show a reduced shrinkage. The unprotected shrinkage transverse to the printing direction depends on the perimeter and longitudinal shrinkage of the filament. The mechanical properties mostly depend on the time gap, size and shape of voids by SAPs, and possibly entrapped air at the interlayer. It was concluded that a good surface moisture is not a necessary requirement for good interlayer bonding strength, but the water management capacity of the SAP is. The larger the (estimated) total horizontally projected area of SAPs, the greater the reduction in continuous mortar matrix and as such the greater its reduction in resistance to tensile loads.

Printability and early age shrinkage of cementitious materials with superabsorbent polymers

Rens De Coensel
Supervisors: prof. dr. ing. Kim Van Tittelboom & dr. ir. Didier Snoeck
Counsellor: ir. Jolien Van Der Putten

Abstract – In 3D printing of concrete (3DPC) the cementitious material needs to fulfil conflicting requirements for pumpability, extrudability and buildability that define its overall printability. Superabsorbent polymers (SAPs) are added to mortar mixtures to stimulate internal curing that mitigates early age shrinkage and associated cracking. In this research printed specimens of mixtures with and without SAPs (having different characteristics) are studied with respect to their printability, early age shrinkage and mechanical properties. The effective water-cement ratio (w/c) in each was 0.365 and the 2D printing procedure was not altered. The specimens were printed on manipulated substrates that allowed them to shrink as unrestrained as possible. The mix designs were optimised, based on flow table workability in comparison to the reference mixture without SAPs (REF). Slight variations on the preceding mixing process, in combination with the swelling kinetics and geometrical characteristics of the SAPs, proved to influence the flow table diameter. Printability was evaluated by means of 5 criteria, covering early workability, viscosity, surface quality and dimensional stability under normal and increased hydrostatic pressure. These affect the mechanical properties as air can get trapped at the interface. Some SAPs have a lubricating tendency in the delivery system. It is believed the printing process increases the overall air content. The setting characteristics were established via the Vicat needle test and compared to those obtained from early age shrinkage measurements. SAPs tend to retard the onset and duration of setting. The macro- and microporosity were established by microscopy and automated RapidAir air void analysis. An increased air content generally led to a greater reduction in mechanical strength. Nanoporosity was studied at the lower, inter- and upper layer of double-layered printed specimens by means of mercury intrusion porosimetry (MIP). The bottom layer showed a lower nanoporosity ascribed to a denser matrix under increased loading of the superposed layer. The autogenous shrinkage was measured on corrugated tubes by automated dilatometry and unprotected shrinkage, subject to evaporation, was evaluated by means of photographic image analysis. The difference in order of magnitude between the measurements amounted to a factor 10^3. All mixtures with SAPs show a reduced shrinkage. The unprotected shrinkage transverse to the printing direction depends on the perimeter and longitudinal shrinkage of the filament. The mechanical properties mostly depend on the time gap, size and shape of voids by SAPs, and possibly entrapped air at the interlayer. It was concluded that a good surface moisture is not a necessary requirement for good interlayer bonding strength, but the water management capacity of the SAP is. The larger the (estimated) total horizontally projected area of SAPs, the greater the reduction in continuous mortar matrix and as such the greater its reduction in resistance to tensile loads.

Keywords – 3D printing of concrete (3DPC), superabsorbent polymer (SAP), internal curing, printability, autogenous shrinkage, self-desiccation, drying plastic shrinkage, setting behaviour, interlayer bonding strength

1. Introduction

1.1. Printability

3DPC is one type of additive manufacturing (AM), which comprises all modern techniques of fabricating building elements layer by layer. It shows great prospects with respect to freedom of design [1], time and cost management of a project [2][3]. An optimal construction process not only depends on the paste mixture or the envisioned 3D model, but on construction time and design of the delivery system as well [4]. Specific jargon in the field of 3DPC includes: pumpability, extrudability and buildability.

Pumpability describes the mobility and stability of the paste, when it is put under pressure [5]. Fresh cementitious materials are widely accepted to behave as visco-plastic Bingham materials [6]. Stability under pressure translates into averting the possibility of segregation and potential additional bleeding. Not only is the mix design no longer homogenous, weakening overall mechanical properties, but segregation may also lead to blockage in the tubes of the delivery system. Pressure might also reduce the amount of air voids in the mixture, while suction pressure will make air bubbles grow. Both eventually alter the final (printed) volumetric mixture composition and need to not be overlooked [5].

Extrudability has comparable requirements to those of pumpability. However, extrusion happens at the nozzle at the very end of the delivery system, localising the notion of extrudability to that narrow but crucial section. The (smallest) curvature that the extruded material is exposed to might induce tearing of the outer edge of the material [7]. Tensile stresses above the capacity of the fresh mortar introduce unwanted surface defects [8].

Buildability comes into play from the moment the extruded filament leaves the nozzle and becomes part of the printed element. It is a very broad material property with contradicting requirements to those of pump- and extrudability. The fresh layer has to withstand its own gravitational load and keep its form, contrary to cast concrete elements, in which case this function is served by the formwork [5]. The new layer has an initial yield stress τ_{c0}, shear strain γ_{c0} and elastic (shear) modului G_0 and E_0. Because of setting of the cementitious material, the layer becomes stronger ($\tau_c \uparrow$) and more rigid ($G\uparrow \sim E\uparrow$) over time [9]. A new layer will deform (i.e. compress) the underlying one by increase of

hydrostatic pressure. The time between the deposition of filament at a certain location and the filament that comes on top is called the time gap [10]. During this time gap the lower layers of paste must grow sufficient strength to support additional ones on top. However, they may not have set completely for a good adhesion between two layers is imperative for the overall stability [11].

Printability encompasses all three of the above definitions: pump-, extrude- and buildability. A printable material is then one with reasonable properties in all three aspects [12].

Papachristoforou et al. [13] found that the flow table test was the most consistent workability assessment of all in deriving a printability quotation according to a predefined set of criteria.

The mechanical properties of hardened multi-layered printed elements vary depending on the time gap [10], the surface moisture [14] and the load direction with respect to the printing direction [14][15][16][17]. The results of these researches tend to disagree and as such, no conclusive statements can be drawn from them [18]. The interlayer bonding strength is commonly referred to as the most important property in 3DPC. The interlayer bonding strength is a type of adhesion, combining both mechanical and chemical linkage. At microscale the chemical forces (attractive or repulsive) rule, while at macroscale surface roughness and interlocking gain importance. It is influenced by the presence of a cold joint (when the sublayer is dry and rigid) [14] and surface moisture (too moist is not good either) [15] in combination with time [11]. Chemically, it is influenced by a higher concentration of weak hydroxide at the interface between two printed layers [19]. Other dependencies were found in the difference of early shrinkage between two stacked layers [11] and the surface quality as a result of the printing process [20].

1.2. Shrinkage

Especially when the deformations are restrained, shrinkage may lead to (tensile) stresses and cracking that degrade the quality of the printed element. Shrinkage can be categorised according to two characteristics: (1) time (and duration) and (2) chemical and/or physical cause [21].

Plastic shrinkage happens in the concrete's plastic state, i.e. when the paste is still fresh and can be considered as solid particles suspended in cement-water. The printing environment might cause rapid loss of water to the surroundings by evaporation. First, shrinkage is simply due to the volumetric loss of water. After a while, the loss can no longer be replenished fast enough and menisci start to form between the inter-solid pores, giving rise to capillary tension. Under continued evaporation, the menisci will break up and hydration is limited [22]. A possible solution to plastic shrinkage is curing. Both external and internal curing are adequate [23].

Chemical shrinkage is the loss of volume due to denser hydration products than their reactants. The volume reduction will induce autogenous shrinkage on its part. The absolute volume is the sum of volumes of solids and liquids, while the apparent also includes the internal voids and gases. The whole external volume of the specimen corresponds to its apparent volume. By definition, chemical shrinkage acts on the absolute volume, while autogenous shrinkage will change the whole apparent volume [21].

Autogenous shrinkage acts by two different methods, depending on the stage in time: before or after structuration has commenced. During hydration but before gaining much rigidity, chemical shrinkage will use up. Since percolation is not yet fully developed, the voids created will collapse under self-weight. As such, the absolute volume change is equal to the apparent deformation. This means that before structuration, autogenous and chemical shrinkage cannot be distinguished from each other. After some time however, percolation will lead to structuration and the chemical loss of water manifests as voids supported by a skeleton of hydration products. From then on, the absolute and apparent volume changes will no longer be alike. Microscopically a lot of fine pores and voids are created due to chemical removal of water. This is to be called chemical shrinkage, since it affects the absolute volume. Macroscopically, however, not much volume change is noticed since the voids can be upheld by the gain in structure. From the start of structuration on, autogenous shrinkage is also known as self-desiccation. The apparent volume change is then caused by capillary pore water tension [21][24]. Baroghel-Bouny et al. [25] concluded a dependency of chemical and autogenous shrinkage upon: changes in temperature, w/c, chemical-structural crystallisation pressure under formation and growth of more voluminous products and internal relative humidity.

Drying shrinkage is volume loss, continued over the whole lifetime, caused by evaporation of internal water in hardened concrete [26].

Carbonation shrinkage is caused by dehydration and decalcification as a result of the carbonation process. Dehydration, or loss of bound H_2O, triggers

the same mechanism as in drying shrinkage. Decalcification results in a structural reorganisation that leads to shrinkage of the overall [27].

Thermal shrinkage occurs due to the exothermic cement hydration. This will heat up the setting concrete as well as unbound water, which might evaporate to the environment [28].

1.3. Superabsorbent polymers

1.3.1. In general

Superabsorbent polymers (SAPs) are 3D cross-linked poly-electrolytes that can absorb up to 1,500 times their own weight in water (or aqueous solutions), forming hydrogels. Developed in the 80s, their first application was found in hygiene industry and more specifically in diapers. Since then the demand has been steadily growing, opening up new markets in, amongst others, the construction industry [29][30][31].

SAPs are natural or synthetic, three-dimensional networks of polymer chains that are chemically (covalently) or physically (electrostatically) cross-linked and have hydrophilic functional groups in them. The production process is defining for the geometrical characteristics of the polymers. Bulk produced polymers tend to be of an irregular, edged shape. Suspension polymerisation will lead to spherical polymers. By extruding the batch, fibres can be formed and cut to length. The important issue is that the chemical process will influence the shape; meaning not only the chemistry needs to be engineered properly, but the process as well [31][39].

The main driving force for the (water) absorption capacity of SAPs is their internal osmotic pressure. The polymer links keep the electrically charged or polar functional groups close together, resulting in a high osmotic pressure on the inside. Absorbing water reduces this pressure by dilution of the electrically opposing charges [40]. The swelling capacity is limited by three opposing forces until a state of equilibrium is met and the SAP is fully saturated. The first opposing force comes from the elastic restraint in the polymer links. Secondly, a difference in osmotic pressure from the surroundings might cause water to flow back and out of the SAP. Thirdly, the hydrogels might be subjected to external mechanical loading. The polymers are then literally squeezed due to which they may lose water [30].

The main function of SAPs in concrete technology is controlling the water and as such controlling the rheological properties in fresh concrete and curing abilities in hardened concrete [32]. In [33] a list is given by Cusson, Mechtcherine and Lura, with all possible improvements of concrete properties by means of SAP addition: shrinkage reduction due to internal curing [34][35]; frost resistance due to greater microporosity [31]; rheology modification of mortar [33]; controlled water release under environmental changes [36]; waterproofing [37]; crack healing [31][37][38]; etc.

Their effectiveness in cementitious materials depends on: their size, influencing swelling capacity and time [41][42]; the outer surface which is less active than the inner bulk [41]; the chemical composition of the mixing water, reducing the swelling capacity [43].

1.3.2. Effect on printability

The addition of SAPs to a cementitious mix design, without additional water to compensate their absorption, is comparable to simply removing water from the mixture. In that case, the workability will diminish, and with it pump- and extrudability as well. On the other hand, the increase in yield stress and higher plastic viscosity that result from a reduction of (effective) w/c, improve buildability [44].

1.3.3. Effect on shrinkage

SAP addition reduces the amount of plastic deformation in the first hours after mixing, i.e. in the time span of plastic shrinkage. It is assumed that, though an overall increase of hydration will result, it is delayed a bit at first: spreading out the heat production of the exothermic reaction over a longer period. The thermal shrinkage influence, happening parallel to plastic shrinkage is thus diminished too. Another influencer was the reduced capillary pressure that showed when using SAPs [21].

Since SAPs improve the rate of hydration, they will increase the rate of chemical shrinkage as well. Indeed, the highest loss (−25 %) of volume by hydration was observed in mixtures with SAPs instead of in reference mixtures [21].

Extensive research by many institutions have come to the same conclusion: SAPs lead to a reduction of autogenous shrinkage and sometimes even a volume expansion [21]. (1) Small-sized polymers released curing water more gradually leading to longer controlled internal curing and a better mitigation of autogenous shrinkage [21][31]. (2) A uniform distribution of SAPs is paramount for a good mitigation of self-desiccation [21].

SAPs have a positive (lowering) effect on drying shrinkage but would not seem able to completely

avert shrinking over longer time (except possibly for a SAP-to-cement ratio of over 0.4 mass percentage points [21].

1.3.4. Effect on mechanical properties

The size and amount of SAPs, the additional and effective w/c and the way of addition of SAPs (i.e. saturated or dry) are the three most important influencers of the hardened structure. SAPs filled with water will act as soft aggregate; when they are empty, they act as voids. Their dispersion rate will influence mechanical properties [45]. Due to the internal curing effect, hydration is stimulated locally and globally [34][35]. When no additional water was added to compensate the swelling, little to no difference in overall porosity [45][46]. However, when extra water was used, the total porosity did increase a couple of percentage points [47]. According to Kovler [48]: "No pronounced negative effects on compressive strength are found upon adding SAP, if a right amount of extra water is added for the purpose of internal curing." Generally, there is a (small) reduction of compressive strength with respect to reference samples (10 % to 20 % depending on the age) [41].

1.4. This research

Four commercial bulk-produced superabsorbent polymers are studied. With each an optimal mix design is obtained based on the flow table workability. The optimal mixtures are then tested for their printability, early age shrinkage behaviour and mechanical properties, focussing on the interlayer bonding strength. The results as well as the influence of some of the preceding practices are discussed in the next chapters.

2. Materials and methods

2.1. Materials

Ordinary Portland cement CEM I 52.5 N Strong (Holcim Belgium) was used in all mixtures. It has a normal structuration development and a mass density of 3,160 kg/m^3.

Standardised sand (Normensand Germany) with grain sizes ranging from 0.08 mm to 2.00 mm was used in all mixtures. The moisture content is guaranteed to be below 0.2 % and the mass density equals 1,241 kg/m^3.

Tap water at a temperature of 20 °C was used for executing all tests. The mass density used in calculations is 1,000 kg/m^3.

As superplasticiser (SP) MasterGlenium 51 con. 35 % (BASF The Netherlands) was used in all mixtures. Its mass density equals 1,075 kg/m^3.

Table 1 and Figure 1 hold the details of the bulk-produced SAPs used in this research. The following abbreviations are used: swelling capacity (SC), swelling time (ST), demineralised water (DW), cement filtrate (CF).

SAPs A, G, M and P all have bulk densities of around 700 kg/m^3 and true densities of ca. 1,400 kg/m^3.

All dry materials including SAPs, and the SP were stored in sealed containers at a temperature of 20 °C and deprived of light. Tap water at a temperature of 20 °C was used during testing.

2.2. Mixtures

A mix design based on the work of Khalil et al. [49] was used as reference for developing new mixes with superabsorbent polymers. The reference mixture (denoted REF) has a total water cement ratio of 0.365, equal to the effective water-cement ratio, as no additional water is used in absence of SAPs. The composition is given in Table 2.

Table 2: Mix design of reference mixture REF

Component	Mass [g]	m% of cement
CEM I 52.5 N Strong	675.00	N.A.
CEN standard sand	1350.00	N.A.
Water	246.38	36.50
MasterGlenium 51 con. 35 %	1.01	0.15

In the mixtures with superabsorbent polymers, an additional mass of 37.125 g water is added to obtain a total w/c of 0.42, following from Powers' model. The amount of SAPs is then determined by trial and error to compensate the additional mixing water and reduce the effective w/c to 0.365, in accordance

Table 1: Bulk-polymerised SAPs used in this research [31]

SAP	Type	Production	Company	Size [µm]	SC [g/g]		ST [s]
					DW	CF	
A	copolymer of acrylamide and sodium acrylate	Bulk	BASF	100±22	305±4	61±1	10
G	cross-linked acrylate polymer	Bulk	SNF Floerger	157±82	332±6	47±2	22
M	cross-linked potassium salt polyacrylate	Bulk	Evonik Industries	486±141	285±2	59±1	65
P	cross-linked potassium salt polyacrylate	Bulk	Evonik Industries	190±61	286±1	58±2	14

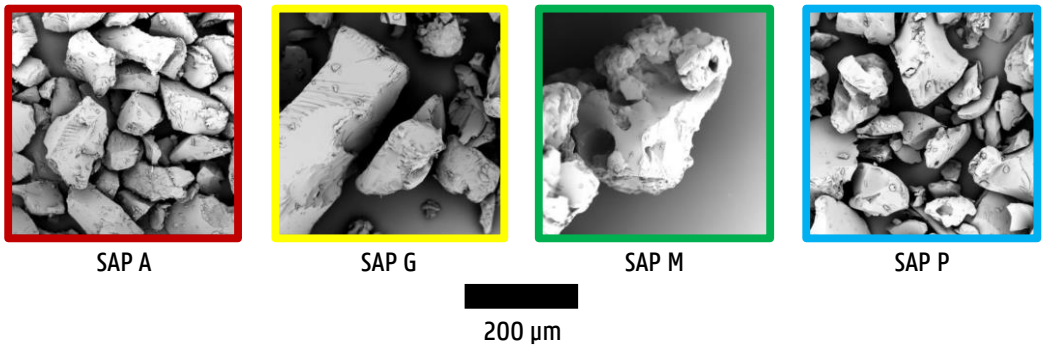

Figure 1: Bulk-polymerised SAPs used in this research [31]

with REF. The exact optimisation process is explained in the chapter 3.

2.3. Methods

2.3.1. Preparation

2.3.1.1. Mixing procedure

The mixing procedure followed prior to printing is given in Table 3.

Table 3: Mixing procedure prior to printing

Step	Duration [s]	Speed [rpm]	Description
1	30	140	Mixing of sand + cement + SAP
2	30	140	Immediately adding water + SP and mixing the whole
3	30	285	Increased rotational speed
4	30	0	Scraping off material from the sides of the bowl
5	60	0	Rest
6	60	285	Increased rotational speed
+	240	N.A.	Total mixing time

2.3.1.2. Printing procedure

2D printing of mortar was done by means of a Quikpoint mortar gun with a Black & Decker 5.2 Amp drill built in (Figure 2) [50].

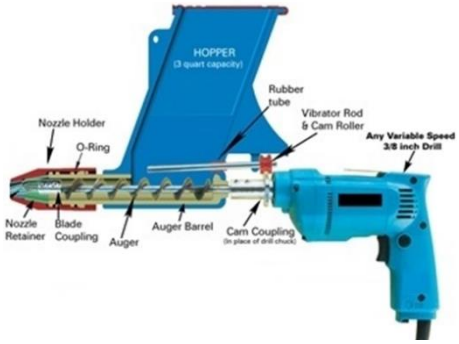

Figure 2: Quikpoint mortar gun [50]

The mortar gun was mounted vertically on a fixed steel frame, in turn fixed to a rigid printing table. The printing table was provided with a sliding steel carrier in which the printing substrate could be placed. The mortar gun could be altered in height for the nozzle to have the required clearance above the printing substrate.

The flow rate of the reference mixture provided by the mortar gun in the conditions described above, amounted to 8.4 cm^3/s: that is 1.7 cm/s translational speed times 1.5 cm of layer height times 3.3 cm of layer width. It was intended to keep the width of the extruded layer within 10 % deviation on the nozzle width for all mix designs.

2.3.1.3. Printing substrate

A proper printing substrate treatment was needed that allowed the printed elements to deform as freely as possible on the supportive surface. Clear glass plates were manipulated consistently for all experiments in the following way (Figure 3): (1) a layer of talcum powder (ca. 0.05 g/cm^2) was applied on the entire plate surface; (2) cling film was cut to the dimensions of a glass plate and put on top of it; (3) after printing, the cling film was cut just in front and after the layer(s) with a sharp knife, freeing the movement of the specimen. This was done carefully as to not move the filament or introduce shear stress in it.

Figure 3: Printing substrates

2.3.1.4. Laboratory conditions

All mixing and printing procedures as well as most experiments were carried out in a climatized room, where a temperature of 20 °C ± 3 °C and relative humidity of 65 % ± 5 % were upheld throughout. All samples were stored in this room until the day of testing.

2.3.2. Characterisation

2.3.2.1. Surface moisture

The evolution of the surface moisture of printed filaments in one hour was observed by gently pressing (uniform pressure of 77.5 Pa ± 0.1 Pa) blotting paper strips on top of it every 15 min and measuring their change in mass. The Aurora ref. 10 blotting paper with an areal density of 125 g/m^2 was cut to strips of approximately 7.5 cm x 2.5 cm, to allow three of them to fit on the surface of one filament

2.3.2.2. Setting times

A MATEST Vicatronic served in the automatic Vicat testing of all studied mortars according to NBN EN 196 3. The device automatically measures the penetration depth of its probing needle (∅ 1 mm) every 15 min over a period of 21.5 hours. The results of the Vicat tests were analysed according to NBN EN 196-3 to obtain the initial and final setting times of each mixture.

2.3.2.3. Microscopy

The sizes of dry and swollen SAPs as well as the pores in longitudinal sections of hardened double-layered specimens were visually inspected and photographed by means of a Leica DFC295 digital microscope colour camera. The acquired images were then analysed making use of the software ImageJ.

2.3.2.4. Air content

The air content was analysed according to the linear traverse method as described in ASTM C457 by means of a fully automated Concrete Experts International RapidAir 457 device. The double-layered printed filaments are longitudinally sawn in half at an age of 28 days and both sides are polished with variable grading and dried afterwards at 35 °C for one hour. After polishing, the surface of the samples was treated with black ink and barium sulphate ($BaSO_4$) to increase the contrast between the air void and cementitious matrix.

2.3.2.5. Mercury intrusion porosimetry

Capillary pores, having a diameter between 10 nm and 10 µm, were studied with mercury intrusion porosimetry (MIP) measurements (PASCAL series 140 and 440, Thermo Fisher Scientific Inc).

2.3.3. Printability

2.3.3.1. Workability

The workability of all mix designs was evaluated according to the flow table test (NBN EN 12350 5) performed at 3, 10, 15, 20, 25 and 30 min after finalising the mixing process. The mix design optimisation in this research was based on these workability results, keeping the flow diameter in the range of ± 0.5 cm of that of REF by means of trial and error.

2.3.3.2. Printability qualification

The following properties are observed to evaluate the printability of the mortar mixtures:

A) the flow table workability, three minutes after mixing as a measure for immediate pumpability;

B) the mortar gun drill voltage needed for a flow rate of 8.4 cm^3/s as a measure for the viscosity of the mixture and its associated pumpability too;

C) the surface roughness R as a measure for extrudability;

D) the dimensional stability of a single layer as a measure for its buildability;

E) the dimensional stability of the lower layer when a new one is printed on top, as a measure for its buildability.

The evaluation happened with respect to REF.

2.3.4. Early age shrinkage

2.3.4.1. Autogenous shrinkage by means of corrugated tube measurements

The autogenous shrinkage of all studied mortars was monitored on corrugated tubes with digital dilatometers according to ASTM C1698.

2.3.4.2. Unprotected shrinkage in the horizontal plane by means of photographic image digital analysis

Single-layer printed filaments were photographed with 5-minute intervals, taking the first picture 10 min after the first contact of water and cement. Figure 4 shows the setup of the Logitech C920 Full HD 1080p webcam and underlying object. The object is a mortar filament of about 15 cm long that has 5 fluorescent yellow focussing points randomly placed on its surface. They serve to aid the digital image analysis software GOM Correlate to register the changes in time of the same surface of interest. That measures about 33 mm x 72 mm or respectively 285 x 622 pixels at a focal length of around 6 cm. Comparison of the results to those

obtained with the experimental setup by Slowik [51] proved the procedure to be accurate, however a higher precision camera would be more reliable as the possible strain error using the current setup amounted to about 1.6 ‰ longitudinally and 3.5 ‰ transversally.

Figure 4: Camera setup for the unprotected shrinkage measurement

2.3.5. Mechanical properties

In all of the following tests, drilled cylindrical samples with a diameter of 25 mm are used (Figure 5) and test results show the properties of these samples at an age of 28 days.

Figure 5: Cylindrical samples used in mechanical property tests

2.3.5.1. Compressive strength

The compressive strength perpendicular to the printing plane, f_c [N/mm^2] was determined by means of a Walter+Bai Series DBC testing machine.

2.3.5.2. Interlayer bonding strength

The drilled cylindrical specimens were sawn to a height of approximately 10 mm, making sure the interlayer was positioned right at the centre of the piece. The top and bottom bases were then coated in Sikadur 30 two-component epoxy and glued to steel dollies (Figure 6, left).

Figure 6: Interlayer tensile strength test setup

One of the steel mounts was then anchored to a rigid table, while the other one was connected to the testing knob of a Proceq DY-2 pull-off device (Figure 6, right). The tensile test was executed according to NBN EN 1542.

The same procedure was followed to assess the ultimate shear strength f_s [N/mm^2] of the interlayer. This time however, the setup was slightly altered to the one shown in Figure 7.

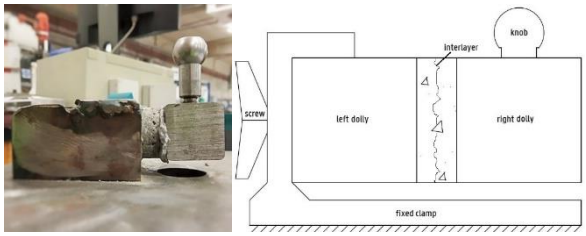

Figure 7: Interlayer shear strength test setup

3. Results and discussions

The notation X123 is used in which X denotes the SAP type: A, G, M or P and 1, 2, 3 denote the amount of X added in units of 1 m%, 0.1 m% and 0.01 m% of cement.

3.1. Printability

3.1.1. Flow optimised mix designs

The reference mixture, as defined in § 2.2, serves as standard for and basis of the new mix designs. As it has a water-cement ratio of 0.365, there is room for improvement with respect to full hydration optimisation. The additional amount of water w_{add} required to this end is then 37.125 g. The reference mixture with additional water is denoted REF* and has a total w/c of 0.42, enabling complete cement hydration according to Powers' model. REF* is the basic mix design to which a varying amount of SAPs is added, evaluated regarding their workability and optimised by trial and error. Table 4 holds the optimal mass percentages of additional SAPs.

Table 4: Optimised mass percentages of additional SAPs

SAP	Initial estimate	Optimal amount
A	0.18 m%	0.17 m%
G	0.23 m%	0.25 m%
M	0.19 m%	0.22 m%
P	0.19 m%	0.15 m%

The initial estimate (Table 4) was based on the swelling capacities in cement filtrate as recorded in Table 1 [31] and halving those as recommended by Kovler [48]. This seems a valid estimation formula.

Prior tests with other SAPs: one fibre (extrusion) and one grapes-like (suspension) showed the influence of the mixing procedure as the SAPs were broken during increases rotational speed.

Small alterations in the mixing procedure, such as order of addition of ingredients, had a reasonable influence on the flow table test results, especially for mixtures that did not have the optimal amount of SAPs added to them (Table 4).

In the remainder of this research only the following mix designs will be considered: REF, (REF*,) A017, G025, M022 and P015. A015 is added to this list as well as it was originally thought optimised and it was already subject in prior testing. It serves as a valuable comparison to A017.

3.1.2. Printability qualification

The printability of each mix design was evaluated by the five criteria, defined in § 2.3.3.2. Scores of −2 to +2 were given to them in case they showed a worse, respectively better result than REF. Figure 8 shows the qualification in a spider chart.

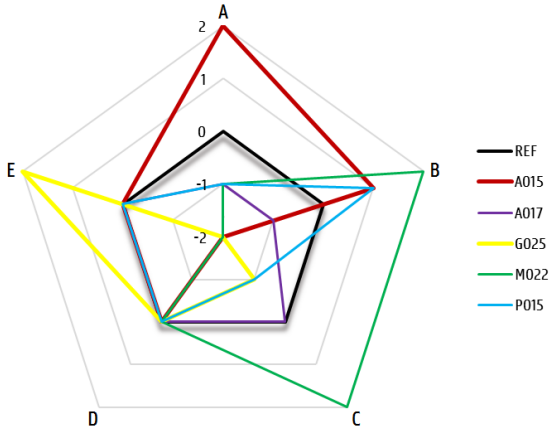

Figure 8: Spider chart of printability qualification

A) The first qualification is based on the flow diameters 3 minutes after mixing, as a measure for immediate pumpability. Initially, the flow diameters differed the most from REF, but over time the evolutions clearly align.

B) The higher the drill voltage had to be placed in order to get the reference mortar flow rate of 8.4 cm^3/s, the more energy was lost to overcome the internal viscous shear stress. A positive score denotes a less viscous mixture than REF. The lowest viscosity of M022 is ascribed to the largest swollen particle sizes which create sand-size water compartments that tend to reduce the internal shear stress and friction with the auger and barrel surfaces (Figure 2). The mix design with SAP G shows the worst results for both workability and viscosity. Its high viscosity is ascribed to a relatively dry mixture. Future research could perhaps include a mix with a lower mass percentage of G, as at this point it is assumed that the polymers take a little too much of the additional water in, reducing the early effective w/c.

C) To substantiate the surface qualification, the surface roughness R [mm] was calculated from automated laser measurement along the length of the a single-layered filament (Table 5, n = 3).

Table 5: Surface roughness of single-layered specimens (n = 3)

Mix	Mean roughness [mm]	Standard deviation [mm]
REF	0.30	0.02
A015	0.43	0.10
G025	0.41	0.10
M022	0.27	0.13
P015	0.35	0.12

D) All printed singular filaments are dimensionally stable: they do not deform under their own weight.

E) When a second layer is printed on top of a first one, all mixtures show good buildability and do not deform noticeably more than REF, except for mortars containing SAPs G and M. G025 (Figure 9, above) shows 'no' deformation when a new layer is printed on top, while the first layer of M022 (Figure 9, below) is compressed considerably under a second layer. Both are ascribed to their respective viscosities. The evaluation was done by visual inspection as only these two mix designs showed a noticeable difference.

Figure 9: Visual inspection of the stability of the first layer when a second one is superposed (above: G025; below: M022)

3.2. Characterisation

3.2.1. Surface moisture evolution

Figure 10 shows the mean surface moisture evolution [g/m^2] in time after printing (n = 3; $\sigma \leq 0.57\mu$).

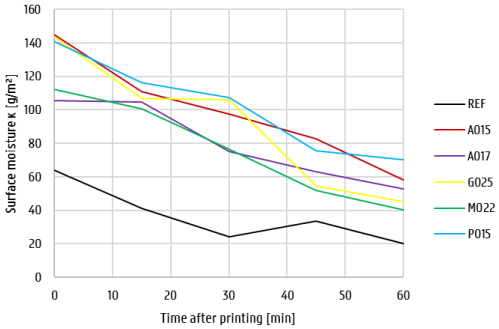

Figure 10: Surface moisture evolution (n = 3)

Unlike the findings of Marchement et al. [10], the mixtures do not show a pronounced inverted bell curve pattern with a minimum around 20 min after printing. Instead, the mixtures with SAPs show a more or less linear reduction of surface moisture. REF on the other hand has a minimum around 30 min after printing.

3.2.2. Macro- and microporosity

The diameter of a swollen particle (in DW) is about 5 to 6 times that of a dry particle.

The diameter of the void one polymer leaves behind in hardened specimens is about 3 to 4 times that of a dry particle. A considerably lower value (i.e. 2.4) is found for SAP M, which is ascribed to the visual measuring technique (2D section versus 3D volume of an irregular-shaped particle). Also, the set void volume an M particle leaves behind lies in the same size range as sand particles. During mixing, they are more resistant to desorption under sand attack, but they seem to be hindered to reach their maximum capacity as well. This reasoning needs to be substantiated with the kinetic properties of the SAP.

The total air content and void frequency in hardened specimens increase with SAP addition and the exact increase is more or less proportional to the amount of SAPs added, or equivalently the amount of dry volume added (as the true densities are equal and around 1,400 kg/m^3). A linear relation exists between the air content and the estimated total set volume, based on the measured diameter factor of set and dry particle (from microscopy). The exception to this rule is M022 which shows the largest air content while its estimated set volume is smallest. This is ascribed to an increased count of voids around its interlayer, compared to other studied samples (Figure 11). The reason why M022 is likely to suffer more from entrapped air at the interface between two superposed printed layers is accounted to its relatively dry surface (Figure 10) even at zero time gap in combination with its relatively worst dimensional stability (Figure 8).

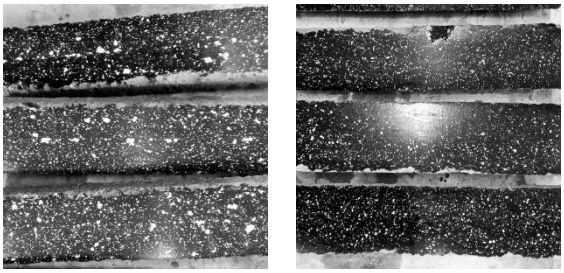

Figure 11: Studied specimens for air content

In this research, the printing process was carried out consistently, reducing the effect of the nozzle standoff distance or printing speed for that matter. The possibility of swollen SAP particles segregating and migrating to the outer edges of the cementitious mixture was not actively studied in this research. Though the photograph of M022 specimens in Figure 11 might prove it interesting for future research.

Comparison to research by Snoeck [31] suggest that the process of sample preparation plays a large role in the overall air content: printing could induce additional air in the mixture, or at least not remove the air already present after mixing. Jolting on the other hand, densifies the matrix by driving the air upwards through vibrational motion.

3.2.3. Nanoporosity

Mixtures with SAPs tend to increase the total nanoporosity in all layers of hardened specimens by 5 % to 25 % with respect to the reference. This conforms with the conclusion stated by Baroghel-Bouny in [25]: when the (total) w/c decreases, the nanoporosity decreases as well. This is associated to the denser matrix that results from a reduction in total amount of mixing water.

No conclusive statement can be made about which layer (top, interface or bottom) has the largest total nanoporosity, however there is a clear difference in continuous pore network. In general, the bottom layer has the network with the smallest continuous pore diameter. This is ascribed to the densification under additional hydrostatic pressure in fresh state, exerted by the top layer. G025 does not follow this trend as it is believed that due to its relatively best dimensional stability (Figure 8) the added weight of a second layer will have a smaller effect. The pore network with the largest continuous diameter is found in either the top layer or interlayer. It is generally true that the top layer is less dense than the underlying layer as it is subject to only its own hydrostatic pressure. At the interface on the other hand, air can get trapped as new layer is printed on

top of an older one. The pore network in the interlayer (micro-scale) is believed to be influenced by the surface roughness (with sufficient rigidity) of one or both meeting layers, and their outer surface moisture, as larger water voids will after hydration have a wider connection of pores (nano-scale).

In general, SAPs tend to reduce the amount of nanopores in the range of 100 nm to 500 nm and increase the amount of voids with a diameter above 700 nm. This is ascribed to a better hydration rate around the SAPs, closing up the smaller pores, as well as to their autogenous shrinkage mitigation that reduces the amount of micro-cracking. Their influence on sizes below 100 nm is inconclusive. and/or capillary tension from a larger water mass in its proximity. This would explain the relatively large fraction of small pores (< 100 nm) that get closed off, and small fraction of intermediate nanopores (400 nm to 1,100 nm) in G025, that keep reducing in pore diameter as type G SAPs provides them with water to maintain hydration. Accordingly, the other mixtures would seem less efficient in supplying water to their surroundings as they show a greater presence of larger nanopores (500 nm to 1,000 nm) associated with accumulated water that was not able to migrate away and take place in hydration. M022 shows a tendency similar to G025.

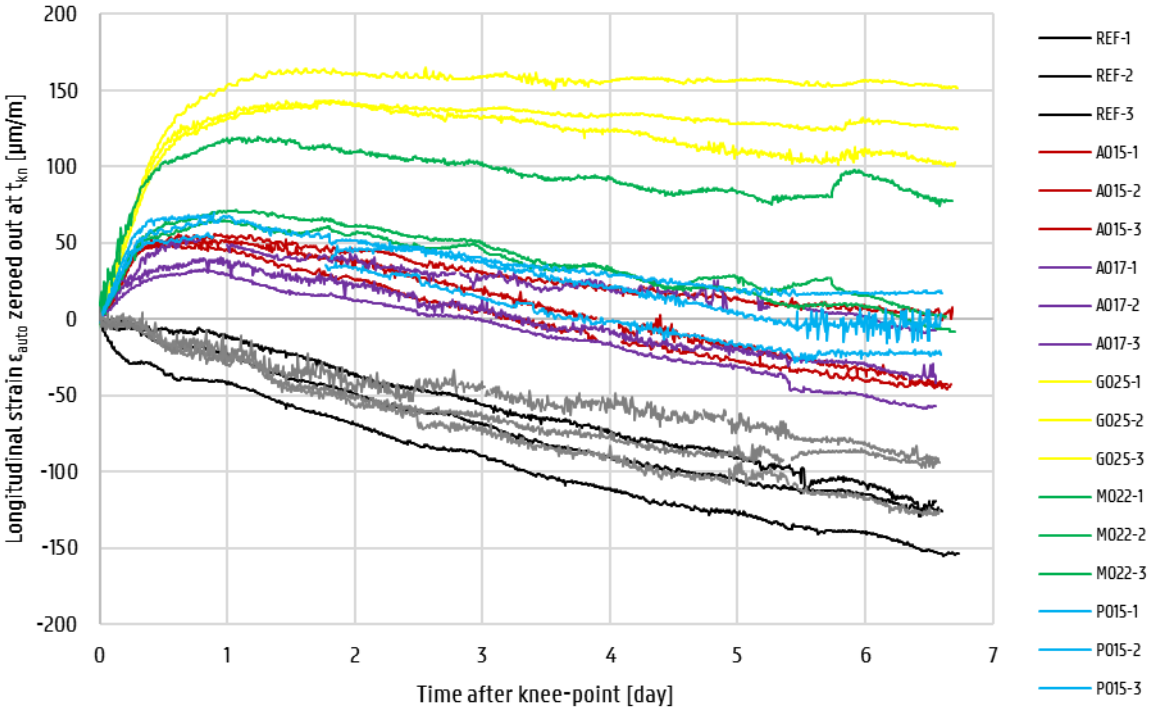

Figure 12: Autogenous shrinkage after knee-point (self-desiccation)

G025 shows a distinct increase in pore diameters ranging from 10 nm to 100 nm, while it shows a reduction in the amount of pores with a diameter above 400 nm, unlike all other studied mixtures. G025 is even denser than REF in every layer, which would suggest a lower effective w/c. This is validated by previous printability tests, such as the flow table test and viscosity evaluation (Figure 8). The water that is released by the swollen particles over time, will migrate away from the polymer and take part in hydration, reducing the diameter of the porous path it followed. As such, it is believed the water will close off the porous network by chemically connecting the sides. The water might not be able to penetrate the smallest pore connections as an air pocket is entrapped for example, under cohesion to the matrix, adhesion

3.3. Early age shrinkage

3.3.1. Autogenous shrinkage

Figure 12 plots the curves of autogenous strain zeroed out at knee-point (i.e. from self-desiccation on). Two distinct bending points are observed for all measurements. The first bending point marks the first real change in chemical structure: i.e. the initial setting time or the moment the specimen goes from a pure suspension state to a percolated structure. The second bending point indicates the final setting time and as such a completely percolated structure of irreversible chemical bonds. From this point on the overall shrinkage is mostly due to the apparent volume change rather than the absolute, as the latter stagnates when the hydration rate diminishes. Consequently, from that moment on, the

autogenous shrinkage is self-desiccative. By definition the knee-point coincides with the second bending point.

Both reference mixtures, with and without additional water (REF*, respectively REF) continue to shrink at the same rate after the knee-point. They show no swelling behaviour as do the mixtures with SAPs.

The swelling behaviour immediately after knee-point up to about a day after is present in all mixtures with SAPs. This is ascribed to their capacity to recapture possible bleeding water as well as to them mitigating the additional water. An overall chemical-structural swelling is present in all specimens. However, it can only manifest in combination with a water management capacity, as otherwise capillary tension will annihilate it.

G025's best autogenous shrinkage mitigation is explained by former conclusions for the mixture. SAP G, which is abundantly present in G025 is able to take up more of the mixing water than it was designed for (w_{add}) due to its good SC. It seems to retain the water the longest as well (infra) and it has the largest ratio of set to dry size. Therefore, less bleeding water will be lost to the interface of tube and specimen compared to other mixtures and the effective w/c will be relatively lower too. When the period of free strain commences, SAP G is more efficient in providing the surrounding cement particles with water for the following reasons: (1) internal curing water is only provided within a 2 mm range around the reservoir [52]; (2) the particles are relatively small, abundant and well spread out over the specimen; (3) the type G particles still hold most of their initially absorbed water while other SAPs might have lost part to bleeding that localises water at the top and therefore on average further away from unhydrated cement particles. All of these lead to an efficient supply of water to cement by the SAP G particles and as such a reduction in setting duration (i.e. the period of free strain).

This notion of efficiency can be used to describe the behaviour of SAPs as well.

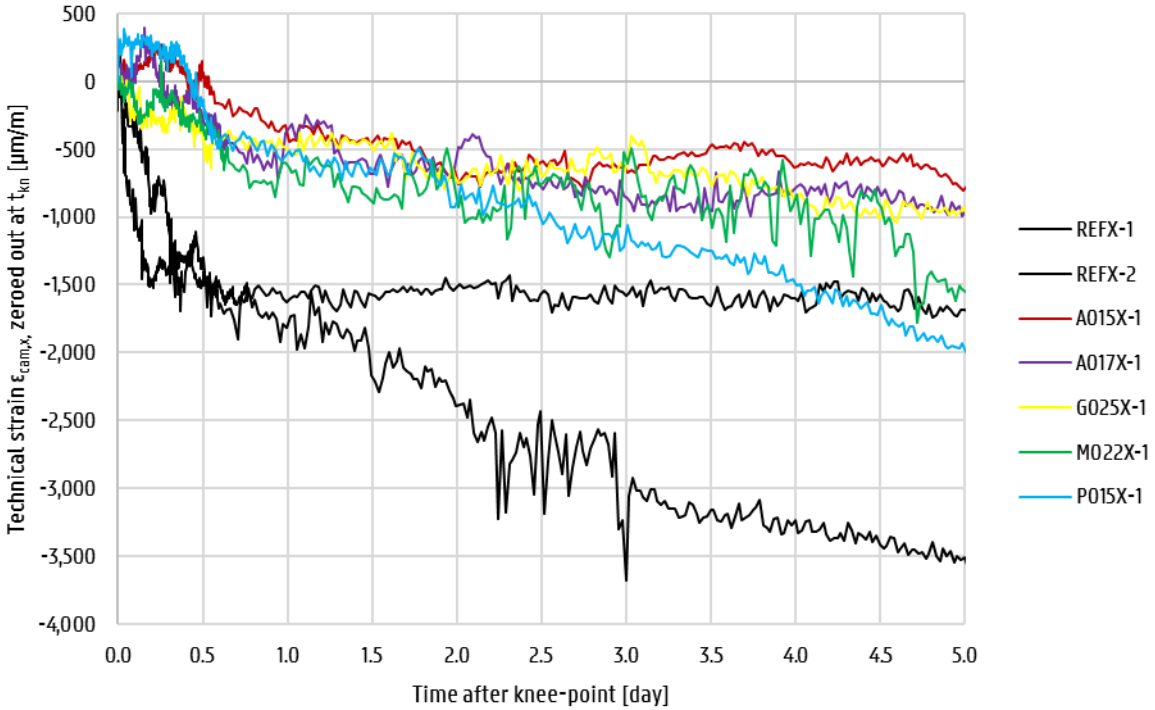

Figure 13: Unprotected shrinkage along the printing direction, zeroed out at knee-point

3.3.2. Unprotected early age shrinkage

Figure 13 shows the unprotected shrinkage measured along the direction of printing, by means of photographic image analysis, zeroed out at the respective knee-point (the two distinct bending points also showed for unprotected shrinkage).

All mix designs will shrink, however mixtures with SAPs know a minor expansion of about + 300 µm/m during the first 12 to 24 hours after knee-point. During this period the reference specimens show a relatively big shrinkage of about - 1,500 µm/m.

The expansive effect of SAP addition is ascribed to a combination of their water mitigation capacity and a chemical swelling present in all mixtures, but in the case of REF not strong enough to overcome the

omnipresent capillary tension. After final setting a crystallisation pressure exists due to delayed formation and growth of calcium hydroxide a.o., that counteracts the capillary pore water tension that induces self-desiccation.

Once hydration slows down as it reaches its optimum, i.e. about a day after the knee-point, all mixtures can only shrink under endured evaporation. The shrinkage rates then align for all mixtures to about - 200 µm/m/day. On average, this rate is about - 40 µm/m/day lower for the reference mixture. More measurements are required to make a significant conclusion around the difference in rate at later age.

As to why G025 does not show a noticeably better shrinkage mitigation, is attributed to the difference in testing conditions: protected from loss of water to the surroundings, in which case the polymer particles can hold on to their absorbed water; or not, in which case they will lose some to the environment under capillary tension.

With respect to the unprotected shrinkage transverse to the printing direction, the same general trend as observed in longitudinal direction holds: SAPs tend to mitigate the shrinkage. The reference mixtures have both in longitudinal and transversal directions the same outcome. The results in transverse direction of mixtures with SAPs are greatly dependent on their behaviour in longitudinal direction, in combination with the length of the sample (along the printing direction). For samples of sufficient length, i.e. around 15 cm, the shrinkage in transversal direction seems a magnification of the one in longitudinal direction. Shorter samples (11 cm), show the opposite behaviour, ascribed to Poisson deformation.

Of course, in the field of 3DPC, the longitudinal shrinkage will be of greater importance than the transversal shrinkage, as their linear dimensions are considerably different. From the last observations, it follows that the unprotected shrinkage will depend on the continues length (or dimensions, in general) of the printed specimen. As the perimeter increases, the volume will do too and as such the specimen will restrain itself more from shrinking.

3.3.3. Setting behaviour

Figure 14 compares the differences in setting behaviour obtained from the different measurement techniques (Vicat, autogenous shrinkage and unprotected shrinkage).

The onset of setting according to Vicat (n = 1) is postponed with the addition of SAPs (and w_{add}). It takes about 30 min longer to reach final setting, compared to REF. This is due to the SAPs mitigating the additional water to compensate the loss due to evaporation at the top surface, which is bare to the environment. Since the Vicat test will conclude final setting as the moment the needle can no longer penetrate the top surface, its state of freshness (i.e. moisture) is crucial for the results. The REF mixture surface will be drier sooner and as such the needle will not be able to penetrate it sooner than for mix designs with SAPs.

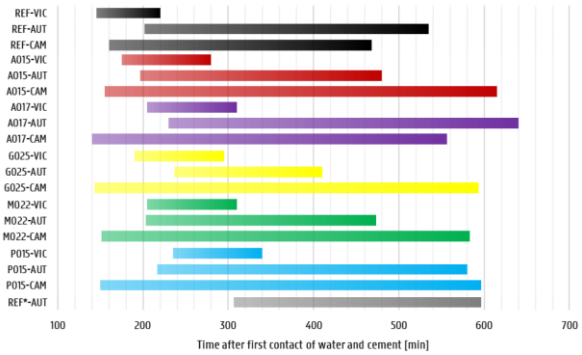

Figure 14: Setting behaviour according to different measurements (VIC = Vicat, n = 1; AUT = autogenous shrinkage, n = 3; CAM = camera testing, n = 3)

The same analogy explains the difference in initial setting time for different techniques. All unprotected shrinkage tests (less distinct for REF) conclude an initial setting time before the one from the Vicat testing. This is explained by the fact that relatively more outer surface is subject to evaporation in the camera tests, creating a drier outer surface with a lower elasticity than the underlying part. On photographs especially, they will appear set, though it might not be completely so. It seems that specimens shielded from the environment in the corrugated tubes harden later, as no mixing water is lost and keeps the mortar fresh. Depending on the retention capacity of the polymers the effective w/c is different, leading to the small differences observed in Figure 14. The larger the effective w/c, or equivalently the less retaining the SAPs are, the later the initial setting time is marked, cf. REF* with the highest effective w/c equal to the total w/c.

The duration of free strain in unprotected specimens is longer than in protected specimens as the latter have a higher effective water-cement ratio, expediting the hydration reaction and as such the hardening process.

The conclusion drawn by Justs et al. [53] and Dudziak et al. [54] that internal curing retards the setting behaviour of cement mixtures, is also valid for the results of this research (Figure 14).

As final remark to this section, the sensibility of the camera setup for unprotected shrinkage measurements is reported. Several data sets of longer periods of monitoring were discarded as the photographing software (operating ceaselessly for months on end) malfunctioned and freezed the image due to movement nearby.

3.4. Mechanical properties

Figure 15 shows the compressive strength of double-layered specimens printed with a zero time gap.

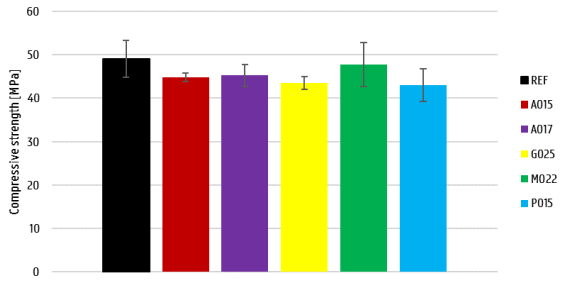

Figure 15: Compressive strength of double-layered specimens at zero time gap

Statistically the difference in compression strengths of all mixtures is insignificant, however two observations stand out: the values of REF and M022. The observation that REF has the largest compressive strength is explained by its low total air content and low void frequency (cf. § 3.2) that result in a denser matrix. Contradictory to this result is the high compressive strength in case of M022 which has the largest air content. In this case the result is explained by the fact that SAP M particles are the largest in dry and swollen state. This means that the larger total air content compared to other mixtures is actually divided over a smaller amount of voids in the specimen. Consequently, the matrix connections between the voids are thicker and stronger (internal curing) to compression and enable dome action around the SAP particles. Also, by having a larger volume the irregularly shaped voids create less stress concentrations than they would do if they were smaller. M022 has the least total horizontally projected area of SAPs of all mixtures with SAPs: 8,090 mm^2 of SAPs M compared to 14,390 mm^2 of SAPs G in G025. This explains the relatively low compression strength of G025 as well.

In general, the compressive strength is reduced with 2.4 % to 14.0 %.

Figure 16 shows the compressive strength of double-layered specimens of REF, A015 and A017 printed at different time gaps (of 0, 15 and 30 min; with notations: T0, T15 and T30).

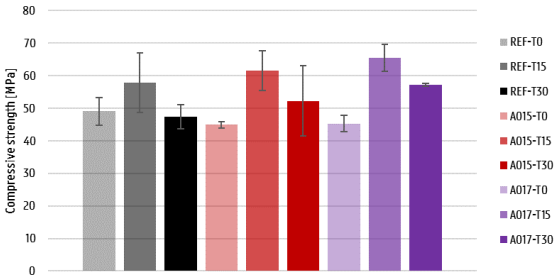

Figure 16: Compressive strength of double-layered specimens at different time gaps

The compressive strength is the largest at T15. This is ascribed to the denser first layer, which can shrink more freely compared to double-layered specimens (T0) since the second layer will increase the outward hydrostatic pressure that counteracts the longitudinal contraction. The unprotected shrinkage strain can amount to −4 ‰ even after 15 min, proving the importance of duration of time gap. The second layer is also restricted more in its early shrinkage and results in a denser matrix as well. The difference between T15 and T30 is ascribed to air that gets entrapped more for older sublayers as it is drier at the surface (Figure 10), more rigid and therefore disables air to be squeezed out of the interface when another filament is superposed. The difference in strength between different mixtures is explained by the difference in retention capacity of the polymers or the lack of water retention at all. A017 can retain more water due to its larger SAP mass percentage added compared to A015, loses less permanently to the environment and is therefore more able to connect the fresh and older layers by gradual release over time. This is reflected in the surface moisture of Figure 10 as well: A017 seems drier at the surface as it retains the water longer internally.

Figure 17 and Figure 18 respectively show the interlayer tensile and shear strength at zero time gap.

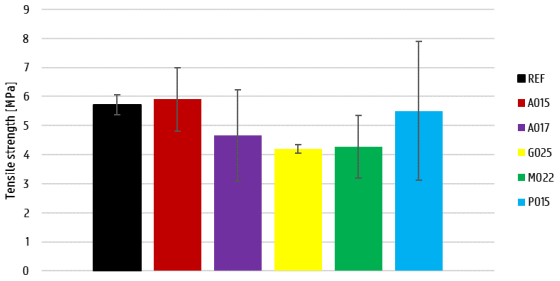

Figure 17: Interlayer tensile strength of double-layered specimens at zero time gap

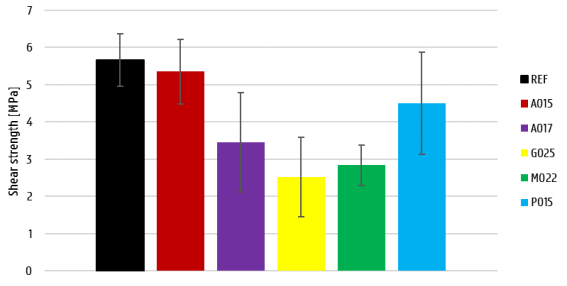

Figure 18: Interlayer shear strength of double-layered specimens at zero time gap

The interlayer tensile and shear strengths are inversely proportional to the air content of the specimens, being in turn proportional to the mass of SAPs added. A linear relationship exists between the total horizontally projected area of SAP particles over the volume of specimen and its bonding strength. The larger the total projected area of SAPs, the greater the reduction in continuous mortar matrix and as such the greater its reduction in resistance to tensile loads. Most of the time, a crack will initiate near the interface as this is the preferred location for larger entrapped air voids, but it propagates through a regularly dense matrix, which determines the final strength. The influence of nanoporosity was noted but no conclusive relation could be remarked. In the same respect, the influence of a good hydration stimulation by SAPs is noted (e.g. G025) but deemed of minor importance compared to the micro- and macroporosity of the matrix.

Figure 19 and Figure 20 respectively compare the interlayer tensile and shear strength for different time gaps.

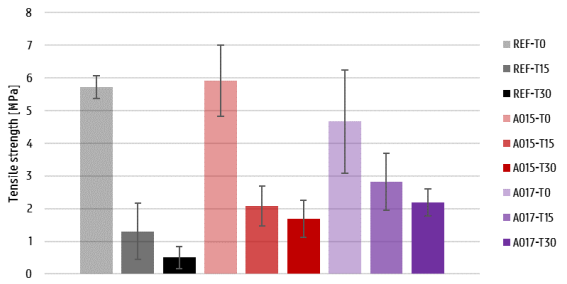

Figure 19: Interlayer tensile strength of double-layered specimens at different time gaps

The interlayer bonding strength reduction at longer time gaps is ascribed to the entrapment of air between a drier and more rigid first layer and a new layer, as well as to their differential shrinkage strain. In the case of compressive strength this might be beneficial as the two layers end up with a denser matrix. The restriction of the sublayer to the free shrinkage of the upper layer might however lead to (micro-)cracking in the connections between the layers. These reduce the resistance to tensile (and shear) loading.

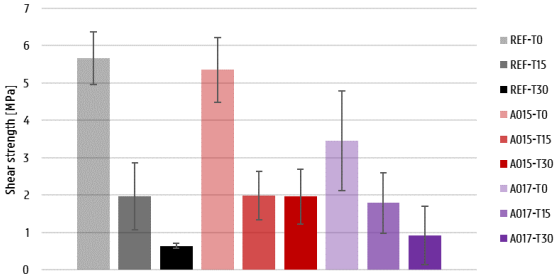

Figure 20: Interlayer shear strength of double-layered specimens at different time gaps

4. Conclusions

4.1. On printability

The flow table test results depend on the preceding mixing procedure, i.e. its effect on the behaviour of the superabsorbent polymers. Small (dry ∅ ca. 100 µm), irregular and fast-swelling (< 10 s) polymers, such as SAP A, are less affected by the hindrance of sand granulates that tend to slow down the swelling rate and sometimes destroy the (swollen) polymers altogether. Big (dry ∅ ca. 500 µm), irregular and slow-swelling (> 60 s) polymers, alike SAP M, seem not influenced by the mixing procedure. Their size, elasticity and shape help them against possible sand attack and their swelling behaviour is quite inert to a variation in mixing duration. SAPs with intermediate properties (cf. G and P) show a greater susceptibility to flow dissimilarities as they are more vulnerable to sand, especially in (quasi)-swollen state and more influenced by a change in mixing order or duration.

Larger polymer particles (200 µm ≲ dry particle size < 500 µm) tend to make the mortar less viscous as they have a lubricating capacity that reduces the internal shear and friction to the sides of the pumping system, when put in motion. The lower viscosity will in turn lead to a smoother surface of the printed filament but a lower dimensional stability when a second layer is put on top as well.

The chemical structure of the SAPs and their associated properties are of paramount importance. This in combination with the physical, especially geometrical characteristics, defines their behaviour in fresh mortar. More specialised research is required to perfect and validate the previous theories.

4.2. On the printing process

Both the printing process and the mixture to be printed influence each other's characteristics.

Mixtures with SAPs tend to retard the onset and duration of setting compared to the reference mixture without SAPs. This influences the duration of open time of printing and the choice of time gap.

The workability reduces quite quickly over time: flow table diameter from 21 cm to 18 cm in 30 min. This will influence the printing procedure in the mortar production (e.g. volume of a batch, continuity of production, …) and in time gap as well.

Mixtures with larger SAP particles (200 µm $\lesssim$ dry particle size $<$ 500 µm) tend to show a lubricating behaviour that reduces the energy loss due to friction on the sides of the pumping hose. The possibility of swollen SAP particles segregating and migrating to the outside of the printed filament was noted, but nothing conclusive follows from this research.

Air can get trapped at the interface of two superposed layers. The likeliness to find a higher air content in the interlayer is dependent on the printing procedure as well as on characteristics of the printed mixture. The dimensional stability of a printed layer under its own weight or that of a superposed one, in combination with their respective states of viscosity influence the interlayer quality. Layers with a low buildability and high viscosity (M022) show more entrapped air at the interlayer than layers with a high stability and low viscosity (G025). Air entrapment may also result from slight variations in the process or mixture, which are variable in nature and cannot be eliminated.

The bottom layer has, in comparison to the inter- and top layer, a lower nanoporosity, ascribed to its denser matrix under increased hydrostatic pressure of superposed layers. The density of the matrix at the interlayer is influenced by entrapped air and water pockets that might have influence on both micro- and nanoporosity.

Comparison with other research showed that it is likely the air content in printed specimens is higher than in mould casts of the same mixture, especially if the latter are compacted.

The duration of time gap is an important influencer of the degree of free (i.e. less restrained) shrinkage. The latter also depends on the perimeter of the printed specimens. A newly printed layer is restricted in its shrinkage by its own size (the larger, the more restriction) and by the layer underneath that, depending on the time gap, has reached a higher shrinkage strain. This differential shrinkage may lead to (micro-)cracking of the connections between the two layers and as such to a reduction in interlayer bonding strength.

4.3. On early age shrinkage

For both environmental conditions (protected from evaporation or not) the shrinkage plots in time show two distinct bending points, between 2 and 10 hours after first contact of water and cement, marking changes in the chemical structure of the specimen. The first bending point is observed at the transition of suspension state to percolation and will as such slow down the vast plastic shrinkage. The second bending point, i.e. by definition the knee-point, indicates the final setting time after which the autogenous shrinkage is mostly self-desiccative. In between lies a period of free (autogenous) strain, so-called as the apparent volume is not different from the absolute.

The water management characteristics of SAPs will influence the onset of setting and its duration. SAPs who absorb more than the additional mass of water, reduce the effective water-cement ratio and stall as such the hydration. Their spatial distribution and chemical ability to supply water to the unhydrated cement particles determine the duration of free strain: a better efficiency leads to faster setting. Setting times and durations also depend on the condition of testing: a greater surface subject to evaporation will commonly lead to faster initial setting and later final setting.

The shrinkage mitigation capacity of any mixture can be explained by the notion of efficiency in water supply, based on the spatial distribution, retention and recapture tendencies of its internal water reservoirs.

The unprotected shrinkage development, transverse to the printing direction is dependent on the longitudinal shrinkage evolution. It will show some magnification of the longitudinal effect, except for when the length over width ratio of the printed specimen drops below 3.5: in that case it will expand as the specimen contracts in length, and vice versa, due to increased effect of Poisson deformation.

There is a difference in order of magnitude of shrinkages (and rates) monitored in both environmental conditions, of about 10^3 (unprotected conditions amount to substantially more shrinkage).

4.4. On mechanical properties

The compressive strength is not substantially reduced by the addition of SAPs: a reduction of

2.5 % to 14.0 % depending on the mixture. But it is remarked that a lower number of larger polymers is less compromising than an equal total swollen volume divided over smaller and therefore more particles. This is due to the effect on a continuous matrix and the shape of the particles creating stress concentrations. Relatively big but less abundant irregular particles enable dome action.

For layers printed with an intermediate time gap of 15 minutes, the compressive strength is larger than for a zero time gap. This is ascribed to the difference in restriction of shrinkage between one- and two-layered specimens. In the latter the initial unprotected shrinkage is counteracted more by a larger hydrostatic pressure, as it has double the height of a single filament. The more freely deforming single sublayer has a denser matrix after 15 minutes and will in turn restrict the shrinkage of the second layer more. A denser matrix leads to a higher compressive strength. From a time gap of 30 minutes on, the gain in strength has become marginal as the outer surface of the sublayer is believed too dry and rigid, enabling air being stuck at the interface.

A linear relationship exists between the total horizontally projected area of SAP particles over the volume of specimen and its bonding strength. The larger the total projected area of SAPs, the greater the reduction in continuous mortar matrix and as such the greater its reduction in resistance to tensile loads. Most of the time, a crack will initiate near the interface as this is the preferred location for larger entrapped air voids, but it propagates through a regularly dense matrix, which determines the final strength.

The interlayer bonding strength reduction at longer time gaps is ascribed to the entrapment of air between a drier and more rigid first layer and a new layer, as well as to their differential shrinkage strain. The restriction of the sublayer to the free shrinkage of the upper layer might however lead to (micro-)cracking in the connections between the layers. These reduce the resistance to tensile (and shear) loading.

The surface moisture is believed to be a necessity rather than a sufficiency in the bonding strength of the interlayer. It is a sign of active water management by SAPs but, as a possible cold joint is temporary in nature (in SAP mixtures), not an exclusive one.

References

[1] Nematollahi B., Xia M., Sanjayan J. (2017). Current progress of 3D concrete printing technologies. Proceedings of 34th International Symposium on Automation and Robotics in Construction, Taiwan, pp. 260–267.

[2] Lloret E., Shahab A. R., Linus M., Flatt R. J., Gramazio F., Kohler M., Langenberg S. (2015). Complex concrete structures: merging existing casting techniques with digital fabrication. Comput-Aided Des 60, 40–49.

[3] Rouhana C. M., Aoun M. S., Faek F. S., Eljazzar M. S., Hamzeh F. R. (2014). The reduction of construction duration by implementing contour crafting (3D printing), in: Proceedings of the 22nd Annual Conference of the International Group for Lean Construction: Understanding and Improving Project Based Production (IGLC). The International Group for Lean Construction Oslo, Norway, pp. 1031–1042.

[4] Le, T. T., Austin, S. A., Lim, S., Buswell, R. A., Gibb, A. G. F., & Thorpe, T. (2012). Mix design and fresh properties for high-performance printing concrete. Materials and Structures/Materiaux et Constructions.

[5] Jolin, M., Burns, D., Bissonnette, B., Gagnon, F., Bolduc, L. S. (2009. Understanding the pumpability of concrete. Proceedings: Shotcrete for Underground Support XI, Engineering Conferences International.

[6] Roussel, N. (2018). Rheological requirements for printable concretes. Cement and Concrete Research.

[7] Bos, F., Wolfs, R., Ahmed, Z., & Salet, T. (2016). Additive manufacturing of concrete in construction: potentials and challenges of 3D concrete printing. Virtual and Physical Prototyping.

[8] Miller, E., & Rothstein, J. P. (2004). Control of the sharkskin instability in the extrusion of polymer melts using induced temperature gradients. Rheologica Acta.

[9] Mewis, J., & Wagner, N. J. (2009). Thixotropy. Advances in Colloid and Interface Science, 147–148, 214–227.

[10] Marchment, T., Xia, M., Dodd, E., Sanjayan, J., & Nematollahi, B. (2017). Effect of delay time on the mechanical properties of extrusion-based 3D printed concrete. In International Symposium on Automation and Robotics in Construction.

[11] Buswell, R. A., Leal de Silva, W. R., Jones, S. Z., & Dirrenberger, J. (2018). 3D printing using concrete extrusion: A roadmap for research. Cement and Concrete Research.

[12] Ma, G., Li, Z., & Wang, L. (2018). Printable properties of cementitious material containing copper tailings for extrusion based 3D printing. Construction and Building Materials.

[13] Papachristoforou, M., Mitsopoulos, V., & Stefanidou, M. (2018). Evaluation of workability parameters in 3D printing concrete. Procedia Structural Integrity.

[14] Le, T. T., Austin, S. A., Lim, S., Buswell, R. A., Law, R., Gibb, A. G. F., & Thorpe, T. (2012). Hardened properties of high-performance printing concrete. Cement and Concrete Research.

[15] Sanjayan, J. G., Nematollahi, B., Xia, M., & Marchment, T. (2018). Effect of surface moisture on inter-layer strength of 3D printed concrete. Construction and Building Materials.

[16] Nerella, V. N., Krause, M., Näther, M., & Mechtcherine, V. (2016). Studying printability of fresh concrete for formwork free Concrete on-site 3D Printing technology technology (CONPrint3D). Rheologische Messungen an Baustoffen, (March), 236–246.

[17] Feng, P., Meng, X., Chen, J. F., & Ye, L. (2015). Mechanical properties of structures 3D printed with cementitious powders. Construction and Building Materials, 93, 486–497.

[18] Paul, S. C., Tay, Y. W. D., Panda, B., & Tan, M. J. (2018). Fresh and hardened properties of 3D printable cementitious materials for building and construction. Archives of Civil and Mechanical Engineering.

[19] Zareiyan, B., & Khoshnevis, B. (2017). Interlayer adhesion and strength of structures in Contour Crafting - Effects of aggregate size, extrusion rate, and layer thickness. Automation in Construction.

[20] Panda, B., Paul, S. C., Mohamed, N. A. N., Tay, Y. W. D., & Tan, M. J. (2018). Measurement of tensile bond strength of 3D printed geopolymer mortar. Measurement: Journal of the International Measurement Confederation.

[21] Mechtcherine, V., & Dudziak, L. (2012). Effects of superabsorbent polymers on shrinkage of concrete: Plastic, autogenous, drying. In Application of Super Absorbent

Polymers (SAP) in Concrete Construction: State-of-the-Art Report Prepared by Technical Committee 225-SAP.
[22] Slowik, V., Schmidt, M., & Fritzsch, R. (2008). Capillary pressure in fresh cement-based materials and identification of the air entry value. Cement and Concrete Composites.
[23] ACI Committee 308. (2001). Guide to Curing Concrete. American Concrete Institute, ACI Special Publication.
[24] Jensen, O. M., & Hansen, P. F. (2001). Autogenous deformation and RH-change in perspective. Cement and Concrete Research.
[25] Baroghel-Bouny, V., Mounanga, P., Khelidj, A., Loukili, A., & Rafaï, N. (2006). Autogenous deformations of cement pastes: Part II. W/C effects, micro-macro correlations, and threshold values. Cement and Concrete Research, 36(1), 123–136.
[26] Li, J., & Yao, Y. (2001). A study on creep and drying shrinkage of high performance concrete. Cement and Concrete Research.
[27] Šavija, B., & Luković, M. (2016). Carbonation of cement paste: Understanding, challenges, and opportunities. Construction and Building Materials.
[28] Snoeck, D., Jensen, O. M., & De Belie, N. (2015). The influence of superabsorbent polymers on the autogenous shrinkage properties of cement pastes with supplementary cementitious materials. Cement and Concrete Research.
[29] Reinhardt, H. W., Cusson, D., Mechtcherine, V. (2012). Terminology. In Application of Super Absorbent Polymers (SAP) in Concrete Construction: State-of-the-Art Report Prepared by Technical Committee 225-SAP.
[30] Friedrich, S. (2012). Superabsorbent polymers (SAP). In Application of Super Absorbent Polymers (SAP) in Concrete Construction: State-of-the-Art Report Prepared by Technical Committee 225-SAP.
[31] Snoeck, D. (2016). Self-Healing and Microstructure of Cementitious Materials with Microfibres and Superabsorbent Polymers. Civil Engineering Department, Ghent University, Belgium. Ph.D. Thesis.
[32] Mechtcherine, V. (2012). Introduction. In Application of Super Absorbent Polymers (SAP) in Concrete Construction: State-of-the-Art Report Prepared by Technical Committee 225-SAP.
[33] Cusson, D., Mechtcherine, V. & Lura, P. (2012). Practical Applications of Superabsorbent Polymers in Concrete and Other Building Materials. In Application of Super Absorbent Polymers (SAP) in Concrete Construction: State-of-the-Art Report Prepared by Technical Committee 225-SAP.
[34] Snoeck, D., Pel, L., & De Belie, N. (2018). Superabsorbent polymers to mitigate plastic drying shrinkage in a cement paste as studied by NMR. Cement and Concrete Composites, 93, 54–62.
[35] Snoeck, D., Pel, L., & De Belie, N. (2017). The water kinetics of superabsorbent polymers during cement hydration and internal curing visualized and studied by NMR. Scientific Reports, 7(1), 9514.
[36] Buchholz, F., & L.; Peppas, N. A., E. (1994). Superabsorbent Polymer. Science and Technology. American Chemical Society: Washington, DC, 16, 193–202.
[37] Snoeck, D., Van Tittelboom, K., De Belie, N., Steuperaert, S., & Dubruel, P. (2012). The use of superabsorbent polymers as a crack sealing and crack healing mechanism in cementitious materials. 3rd International Conference on Concrete Repair, Rehabilitation and Retrofitting, ICCRRR 2012, September 3, 2012 - September 5, (December 2013), 152–157.
[38] Mignon, A., Snoeck, D., Dubruel, P., Vlierberghe, S. Van, & De Belie, N. (2017). Crack mitigation in concrete: Superabsorbent polymers as key to success? Materials. MDPI AG.
[39] Vandenhaute, M., Snoeck, D., Vanderleyden, E., De Belie, N., Van Vlierberghe, S., & Dubruel, P. (2017). Stability of Pluronic® F127 bismethacrylate hydrogels: Reality or utopia? Polymer Degradation and Stability, 146, 201–211.
[40] Imran, A. B. & Takeoka, Y. (2014). The development of novel “stimuli-sensitive” hydrogels for various applications. In Nature Communications (electronic version).
[41] Jensen, O. M., & Hansen, P. F. (2001). Water-entrained cement-based materials - I. Principles and theoretical background. Cement and Concrete Research.
[42] Esteves, L. P. (2011). Superabsorbent polymers: On their interaction with water and pore fluid. Cement and Concrete Composites, 33(7), 717–724.
[43] Lura, P., Friedemann, K., Stallmach, F., Mönnig, S., Wyrzykowski, M., Esteves, L. P. (2012). Kinetics of Water Migration in Cement-Based Systems Containing Superabsorbent Polymers. In Application of Super Absorbent Polymers (SAP) in Concrete Construction: State-of-the-Art Report Prepared by Technical Committee 225-SAP.
[44] Toledo Filho, R. D., Silva, E. F., Lopes, A. N. M., Mechtcherine, V., & Dudziak, L. (2012). Effect of Superabsorbent Polymers on the Workability of Concrete and Mortar. In Application of Super Absorbent Polymers (SAP) in Concrete Construction: State-of-the-Art Report Prepared by Technical Committee 225-SAP.
[45] Mönnig, S. (2009). Superabsorbing additions in concrete – applications, modelling and comparison of different internal water sources. Fakultät Bau- und Umweltingenieurwissenschaften, Universität Stuttgart, Germany. Ph.D. Thesis.
[46] Snoeck, D., Velasco, L. F., Mignon, A., Van Vlierberghe, S., Dubruel, P., Lodewyckx, P., & De Belie, N. (2015). The effects of superabsorbent polymers on the microstructure of cementitious materials studied by means of sorption experiments. Cement and Concrete Research.
[47] Ye, G., van Breugel, K., Lura, P. & Mechtcherine, V. (2012). Effect of Superabsorbent Polymers on Hardening Process of Binder Paste and Microstructure Development. In Application of Super Absorbent Polymers (SAP) in Concrete Construction: State-of-the-Art Report Prepared by Technical Committee 225-SAP.
[48] Kovler, K. (2012). Effect of Superabsorbent Polymers on the Mechanical Properties of Concrete. In Application of Super Absorbent Polymers (SAP) in Concrete Construction: State-of-the-Art Report Prepared by Technical Committee 225-SAP.
[49] Khalil, N., et al. (2017). Use of calcium sulfoaluminate cements for setting control of 3D-printing mortars. Construction and Building Materials, 157: p. 382-391.
[50] Quikpoint (2019). Quikpoint™ Mortar Gun (w/ Black & Decker, 5.2 Amps). [online] www.quikpoint.com. Available at: https://www.quikpoint.com/Quikpoint-Mortar-Gun-p/3600.htm [Accessed 13 May. 2019].
[51] Slowik, V., Schmidt, M., Fritzsch, R. (2008). Capillary pressure in fresh cement-based materials and identification of the air entry value. Cement and Concrete Composites. Volume 30, Issue 7, 2008, Pages 557-565.
[52] Trtik, P., Münch, B., Weiss, W.J., Kaestner, A., Jerjen, I., Josic, L., Lehmann, E., & Lura, P. (2011). Release of internal curing water from lightweight aggregates in cement paste investigated by neutron and X-ray tomography. Nuclear Instruments and Methods in Physics Research Section A, 651(1), 244-249.
[53] Justs, J., Wyrzykowski, M., Bajare, D., Lura, P. (2015). Internal curing by superabsorbent polymers in ultra-high performance concrete. Cement and Concrete Research. Volume 76, 2015, Pages 82-90.
[54] Dudziak, L., Mechtcherine, V. (2010). Enhancing early-age resistance to cracking in high strength cement-based materials by means of internal curing using Super Absorbent Polymers. International Rilem Conference On Material Science. 3. 129-139.

This page is intentionally left blank.

PRINTABILITY AND EARLY AGE SHRINKAGE OF CEMENTITIOUS MATERIALS WITH SUPERABSORBENT POLYMERS

AD Bartlett Show (event). (2015, October 1). Team Amalgamma 3D printed concrete table [photograph]. London, Bartlett School of Architecture (UCL)

This page is intentionally left blank.

Table of contents

List of abbreviations and symbols

3D	Three-dimensional	§ 1
3DPC	3D printing of concrete	§ 2.1
A	Area [m²]	§ 2.1.4.1
A015	Optimised mix design with 0.15 m% of SAP A	§ 5.1.1
A017	Optimised mix design with 0.17 m% of SAP A	§ 5.1.1
AM	Additive manufacturing	§ 2.1
ANOVA	Analysis of variance	§ 4.6
ASTM	American Society for Testing and Materials	§ 2.1
A_{thix}	Structuration or thixotropy rate [Pa/s]	§ 2.1.4.1
c	Mass of cement in a normal batch of mortar, i.e. 675 g	§ 5.1.1
CF	Cement filtrate	§ 2.3.4
CSH	Calcium silicate hydrate	§ 2.1.4.1
d	Capillary pore diameter [m]	§ 4.2.7
d_i	Diameter with i: dry, sat, set or air in accordance to the particle state or void [mm]	§ 5.2.4
d_m	Median capillary pore diameter [m]	§ 4.2.7
dQ/dt	Heat flow during hydration reaction [J/s]	§ 4.2.3
DW	Demineralised water	§ 3.5
E	Modulus of elasticity or Young's modulus [Gpa]	§ 2.1.2.3
E(d)	Expected diameter [mm]	§ 5.2.4
f_c	Compressive strength perpendicular to the printing plane [N/mm²]	§ 4.5.1
F_c	Maximum compressive force perpendicular to the printing plane [N]	§ 4.5.1
FRP	Free radical polymerisation	§ 2.3.1.2
F_s	Shear force at failure [kN]	§ 4.5.3
f_s	Shear strength of the interlayer [N/mm²]	§ 4.5.3
F_t	Tensile force at failure [kN]	§ 4.5.2
f_t	Tensile strength of the interlayer [N/mm²]	§ 4.5.2
G	Shear modulus [Gpa]	§ 2.1.4.1
g	Gravitational acceleration [m/s²]	§ 2.1.4.1
G025	Optimised mix design with 0.25 m% of SAP G	§ 5.1.1
H	Final 3DPC element height [m]	§ 2.1.4.1
$\dot{H}$	Rising rate of the 3DPC element [m/s]	§ 2.1.4.1
h_0	Height of 1 extruded filament [m]	§ 2.1.4.1
H_c	Critical buckling height of the 3DPC element [m]	§ 2.1.4.1
I	Quadratic moment of inertia [m⁴]	§ 2.1.4.1
IUPAC	International Union of Pure and Applied Chemistry	§ 2.1.2.3
L	Length [m]	§ 4.4.2
l_0	Initial length [m]	§ 4.4.3

M022	Optimised mix design with 0.22 m% of SAP M	§ 5.1.1
m%	Mass percentage, relative to the mass of a reference component, usually cement [%]	§ 2.3.4
MU	Moisture uptake [g/g]	§ 3.5
n	Sample size [-]	§ 4.6
N.A.	Not applicable	§ 3.6
N_{voids}	Total number of voids encoutered in a RapidAir 457 test	§ 4.2.6
OPC	Ordinary Portland cement	§ 2.2.2
P	Printing contour perimeter [m]	§ 2.1.4.1
p	Pressure applied in MIP [Pa]	§ 4.2.7
P015	Optimised mix design with 0.15 m% of SAP P	§ 5.1.1
PAA	Polyacrylic acid	§ 2.3.1.1
PEG	Polyethylene glycol	§ 2.3.1.1
PEO	Polyethylene oxide	§ 2.3.1.1
PLA	Polylactic acid	§ 2.3.1.1
PMA	Polymethacrylate	§ 2.3.1.1
r	Capillary pore radius [m]	§ 4.2.7
R	Surface roughness [mm]	§ 5.1.2
REF	Reference mixture with w/c = 0.365	§ 3.6
REF*	Reference mixture with w/c = 0.42	§ 5.1.1
RH	Relative humidity [%]	§ 2.3.1.3
rpm	Rotations per minute	§ 4.1.1
SC	Swelling capacity [g/g]	§ 2.3.1.3
SEM	Scanning electron microscopy	§ 5.3.4
SNK	Student-Newman-Keuls multiple comparison test	§ 4.6
SP	Superplasticiser	§ 2.1.3
ST	Swelling time [s]	§ 3.5
t	Time [s]	§ 2.1.4.1
t_0	First contact of cement and water, by defenition: t_0 = 0 min	§ 4.4.2
t_{fs}	Final setting time, according to Vicat testing [min]	§ 4.4.2
t_{kn}	Time of suspension-to-solid knee-point [min]	§ 4.4.2
t_{max}	Maximum cycle time [s]	§ 2.1.4.3
t_{ref}	Reference time [min], e.g. t_{fs}, t_0, t_{kn}, etc.	§ 4.4.2
UHPC	Ultra-high performance cement	§ 5.3.3
UV	Ultraviolet	§ 4.2.1
V	Nozzle displacement velocity [m/s]	§ 2.1.4.1
V_i	Volume with i: dry, sat, set or air in accordance to the particle state or void [mm]	§ 5.2.4
VMA	Viscosity modifying agent	§ 2.1.3
w/c	Water-cement ratio [g/g]	§ 2.1.4.2
w_{add}	Mass of water added to compensate the absorption by SAPs [g]	§ 5.1.1

w_{dry}	Mass of dry particles [kg]	§ 2.3.1.3
w_{sat}	Mass of saturated particles [kg]	§ 2.3.1.3
$(w/c)_{add}$	Additional water-cement ratio [g/g]	§ 2.3.1.1
$(w/c)_{eff}$	Effective water-cement ratio [g/g]	§ 2.3.1.1
$(w/c)_{entr}$	Entrained water-cement ratio, i.e. the water needed for internal curing [g/g]	§ 2.3.4
$(w/c)_{tot}$	Total water-cement ratio [g/g]	§ 2.3.1.1

Greek

α	Significance level [%]	§ 4.6
α_{eff}	Effective level of significance [%]	§ 4.6
γ	Shear strain [-]	§ 2.1.2.1
γ_c	Critical flow-onset shear strain [-]	§ 2.1.2.1
Δl	Difference in length [m]	§ 4.4.3
ε_{auto}	Linear autogenous strain [µm/m]	§ 4.4.2
ε_{cam}	Mean overall technical strain according to photographic digital analysis [%]	§ 4.4.3
ζ	Surface tension of mercury [N/m]	§ 4.2.7
θ	Contact angle of mercury on concrete, i.e. 140°	§ 4.2.7
κ	Mass of absorbed surface moisture per unit area [g/cm²]	§ 4.2.2
λ	Total length of chord segments intersecting voids, measured with the RapidAir 457 [mm]	§ 4.2.6
Λ	Total chord length measured with the RapidAir 457 [mm]	§ 4.2.6
μ_p	Plastic viscosity [cP]	§ 2.1.4.3
ρ	Mass density [kg/m³]	§ 2.1.4.1
τ	Shear stress [Mpa]	§ 2.1.2.1
τ_c	Critical shear stress [Mpa]	§ 2.1.2.1
Y	Specific pore volume per mass of test cylinder in MIP [mm³/g]	§ 4.2.7

Symbols

$\varnothing$	Diameter [mm]	§ 2.3.1.3

INTRODUCTION

Cum fuerit operis species
grata et elegans
membrorumque commensus
iustas habeat symmetriarum
ratiocinationes.

MARCUS VITRUVIUS POLLIO

DE ARCHITECTURA | LIBER PRIMUS | CAPUT TERTIUM

Beauty is produced by the pleasing appearance and good taste of the whole, and by the dimensions of all the parts being duly proportioned to each other.

1. Introduction

3D printing of concrete is an innovative way of building with traditional concrete; it is the old dog with the new tricks in the world of construction. However, since it features both new technology as well as established theories, old and new obstacles arise.

1.1. Problem statement

During the last decade a lot of research has been performed on 3D printing of cementitious materials. The topic is looked at from many different angles, since a lot of parameters influence its behaviour. The utmost advantage of 3D printing of concrete – the main reason it exists, in fact – is the absence of costly formwork. This formwork usually requires a lot of manual labour, translated these days into a huge cost. The second main advantage is the freedom of form of the printed element. Especially in modern times where waste is justly prohibited to loosen the collar on the environment's neck. The last advantage has a similar effect on the project's economy, as does the first: a cost reduction. This is without doubt what makes 3D printing of concrete such a hot topic.

However, prior to revolution in the construction practice, there is a period of study and optimisation. Concrete for printing needs to fulfil conflicting requirements. First, there is the work- or printability that demands a good flow in the printer tubes and nozzle. The printing material may not settle too fast in the reservoir and blocking in the tubing must be prevented. Second, buildability requires stability of the printed layer: being viscous enough, setting not too fast in order to benefit the bonding surface for, and not too slow to obtain enough strength for support of the next layer. These demands do not solely depend on the cementitious characteristics but on the printing procedure as well. Time plays a leading role in this performance.

Apart from the additional requirements set by the new technology, the concrete faces problems inherent to its mix design, indifferent to the procedure. Shrinkage is one of the major issues in all concrete structures. Only in the last two decades has there gradually been more insight in its many mechanisms. Shrinkage can be subdivided according to moment of occurring and chemical or physical cause. It obviously has an undesirable effect on durability, strength and aesthetics of the element. Shrinkage can lead to cracks, which in their turn facilitate intrusion of (harmful) gases and fluids, corrosion of reinforcement, freeze-thaw attack, etc. and clearly reduce the strength. In (in formwork) cast concrete, drying shrinkage can be mitigated through the use of a curing procedure (actively or passively). However, autogenous shrinkage, which is prone to the core of the element cannot be treated (i.e. cured) externally. External curing might, in the case of 3D printed elements, also complicate the bonding between superposed layers, since the surface of the earliest one is affected.

In search of a possible solution for autogenous shrinkage, scientists have turned to superabsorbent polymers. These can act as internal water pockets in the concrete, due to their (enormous) swelling capacity in aqueous solutions. They are able to provide the concrete core

with the water that is lost by the self-desiccation effect due to autogenous shrinkage. And the surface of the layers is not impaired, quite the contrary even: since water is provided from within the element, drying shrinkage is slightly mitigated as well. This will keep the surface moist, and thusly enhance the bonding possibilities. But superabsorbent polymers alter the workability of the printed material, as they absorb part of the mixing water, reducing the flow properties as such. Additional water, superplasticiser or a combination of both are needed to enhance the printability again. However, these will in turn change the mechanical properties of the element.

1.2. The goal

Solving one of the above problems, simply creates a new. An optimal balance in mix design as well as overall properties are subject in this thesis. Seven commercial superabsorbent polymers are available, covering a broad range in characteristics: size (70 à 500 µm), shape (spherical, fibre, irregular), swelling capacity (15 à 350 g/g), … With each a proper mix design (and printing procedure) is obtained, evaluated and compared. The focus of evaluation lies upon:
(I) printability, (II) early age shrinkage (≤ 7days) and (III) interlayer bonding strength. Other properties (e.g. mechanical) will be treated as well, but not designed for.

1.3. The strategy

First, the available literature is consulted to obtain sufficient knowledge about the three main players in this research: printability, (autogenous) shrinkage and interlayer bonding strength. Since no study covering these three aspects together already exists, the investigation is kept broad in order to include as much influencers as possible. A critical mindset is upheld throughout, looking for (dis)agreeing results and missing links.

The main part of the work will happen in the Magnel Laboratory for Concrete Research. The superabsorbent polymers are studied and compared to tabulated information in literature. Mix designs for each are obtained via trial and error, optimised based on flow properties (which is a good way, as shown in literature). The optimised mixture recipes will be put to test in actual printing of elements. The latter can then be studied in detail with respect to shrinkage, bonding and mechanical properties. During the laboratory phase, specialised literature will still be turned to for the sake of validation of the tests and their results.

Last, general conclusions are drawn and a recommendation for future work will be given.

LITERATURE REVIEW

In ipsis vero moenibus
ea erunt principia.
Primum electio loci saluberrimi.
Is autem erit excelsus
et non nebulosus,
non pruinosus regionesque
caeli spectans necque
aestuosas neque
frigidas sed temperatas.

MARCUS VITRUVIUS POLLIO

DE ARCHITECTURA | LIBER PRIMUS | CAPUT QUARTUM

In setting out the walls of a city
the choice of a healthy situation is
of the first importance:
it should be on high ground,
neither subject to fogs
nor rains;
its aspects should be
neither violently hot nor intensely cold,
but temperate in both respects.

2. Literature review

Firstly, (3D) printing of concrete will be discussed in general, emphasizing conveniences and pitfalls, terminology and most important parameters such as interlayer bond strength. Secondly, the many aspects of shrinkage are considered, with a focus on early age types. And lastly, superabsorbent polymers are studied as well as their influence on printing and printed characteristics.

2.1. 3D printing of concrete

3D printing of concrete (3DPC) is one type of additive manufacturing (AM), which comprises all modern techniques of fabricating building elements layer by layer. Usually the elements are constructed conform a digital model, and fully automated at that. The American Society for Testing and Materials (ASTM) defines AM as "the process of joining materials to make objects from 3D model data, usually layer upon layer [1]."

2.1.1. In general

3DPC has gained a lot of interest over the last years from all sides of the construction industry: researches, prefab constructors, on site constructors, architects, … It does indeed show great prospects with respect to freedom of design, time and cost management of a project. Some of the greatest advantages include but are not restricted to:

- a reduction of overall cost of the concrete element ranging from 35 % to 60 % since this share would be spent on expensive formwork and manual labour [2];
- a reduction of construction time of the printed element of up to 70 % since formwork takes up a lot of preparation and disassembling time [3];
- more freedom of form and more complex geometry of the constructed element (cf. in organic architecture) [4];
- a safer construction site due to a reduction in manual labour and more demanding jobs required for formwork installation [4];
- introducing a new field in the construction profession: high-end-technology-based jobs [4];
- a reduction of waste and spillage as a consequence of already mentioned reductions and as such an increase in construction sustainability [4];
- an (expected) increase in quality control [4].

At this point in time, however, these advantages are yet to be fully developed and first some teething issues must be tackled [5][6].

Figure 1 shows a schematic of a concrete delivery system [7]. Since 3DPC is still being researched, not many standard printing machines exist; most of the time each laboratory has its own rather unique testing equipment. However, each component of the layout in Figure 1 will be present in every printing paste delivery system. And each component will induce some restrictions on and requirements for the mix design.

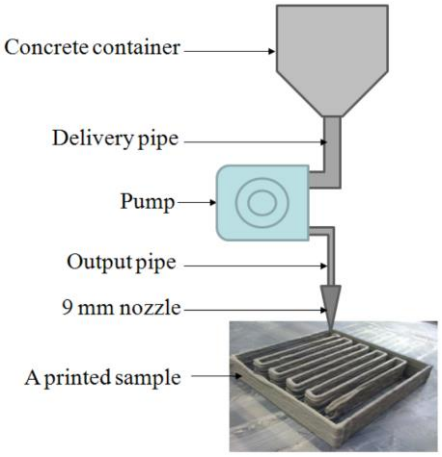

Figure 1: Schematic of a concrete delivery system [7]

It will become clear in next paragraphs and chapters that an optimal construction process not only depends on the paste mixture or the envisioned 3D model, but on construction time and design of the delivery system as well. This makes it sometimes quite challenging to come to concise and generally valid conclusions. Indeed, a larger element to be printed, will not have the same construction time or time gap between consecutive layers; nor is a perfect fit mixture guaranteed to success when the printing machine is changed. It is not the purpose of this thesis to go into too much detail about the equipment and optimise the mix design solely for it. Rather, a mix design with 'good' printing tendency is anticipated, based upon findings from both literature and laboratory testing.

2.1.2. Jargon

Some specific jargon in the field of 3DPC is defined here. It is generally accepted terminology for typical concrete printing features.

2.1.2.1. Pumpability

Pumpability describes the mobility and stability of the paste, when it is put under pressure [8]. Beaupré [9] defined pumpability as the capacity of concrete under pressure to be mobilised while maintaining its initial properties.

The mobility combines two physical properties of fresh paste: rheology and tribology. Rheology is the science that studies the flow of matter and tribology is the science that studies the interaction of surfaces in relative motion [8].
Fresh cementitious materials are widely accepted to behave as visco-plastic Bingham materials. This means that with regards to the shear stress (τ) and strain (γ) relation, there is a threshold value τ_c that needs to be overcome before the material will flow (i.e. $\gamma \neq 0$). This critical stress is called the yield stress (with a subscript c for 'critical'). When τ_c is overcome, the shear strain increases linearly with increasing stress. Fresh pastes are not very fluid and do not return to their original state when deformed (i.e. visco-plastic) [8][10].

Tribology manifests through friction between the paste and the sides of container, tubes and extruder. In the case of printed concrete, also friction between printed layers needs to be investigated [8].

Stability under pressure translates into averting the possibility of segregation and potential additional bleeding. Segregation occurs when the pressure in the mixture pushes the paste through the granulate skeleton, thus separating both. Not only is the mix design no longer homogenous, weakening overall mechanical properties, but segregation may also lead to blockage in the tubes of the delivery system. Pressure might also reduce the amount of air voids in the mixture, while suction pressure will make air bubbles grow. Both eventually alter the final (printed) volumetric mixture composition and need to not be overlooked [8].

Ambiguous results from a study of pumpability and its influencers have led to the definition of the real paste concept. The real paste is the actual amount of paste needed to fill the voids in the granular skeleton itself and between the skeleton and the pipe wall. It can then act as lubricating layer. While the word 'paste' is commonly used, it is now only used to refer to the mixture of binder (cement) and voids (air and water). Since the volume of voids might change depending on the pressure in the delivery system, the amount of paste will change as well. This difference in volume of voids is exactly at the base of the real paste concept. If, for simplistic example, the original mixture volume (binder, water, air (400 l) and granulates (600 l)) equals 1,000 l and under pressure 70 l of air voids is lost, the relative amount of paste reduces from 40 % to 35 %. In order to be pumpable, the 35 % paste will have to be lubricating enough, which will not always be the case. For any given set of boundary conditions (size of granulates, nozzle diameter, hose diameter, etc.) a minimal percentage of 'real paste' exists. Below this percentage, the mixture cannot be continuously pumped. According to Chapdelaine [11] the thickness of the lubricating layer of a pipe filled with flowing concrete is more or less constant and equals about 1 mm, independent of the pipe diameter. Figure 2 shows the relative amount of paste (a) required for the 1 mm thick lubricating layer in the hose. When the porosity of the granulate skeleton (b) is measured, the minimum real paste percentage is then known as the sum of a and b. Of course, this is more like a necessary condition rather than a sufficient one, since pumpability will also depend on granulate size and distribution, rheology, etc [8].

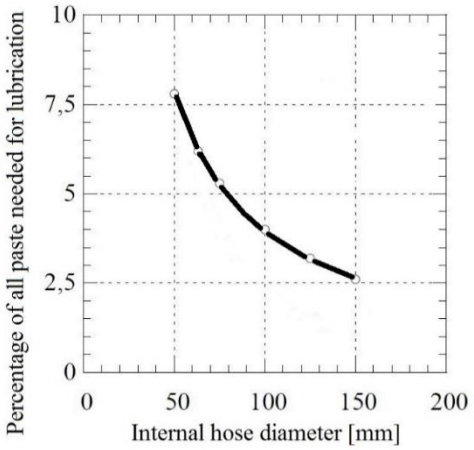

Figure 2: Relative amount of paste required for the 1 mm thick lubricating layer in the hose [%] [11]

2.1.2.2. Extrudability

Extrudability has comparable requirements to those of pumpability. However, some nuances should be made. The cementitious material may be pumped over longer stretches of the delivery system (e.g. hoses), however, the extrusion happens at the nozzle and should form one continuous filament. This literally localises the notion of extrudability to the very end of the delivery system, a narrow but crucial section.

In addition to good pumpability (as a necessary but not sufficient condition), the printed material should also [12]:

- be soft enough to flow through the die;
- be shape stable, i.e. maintain its shape upon extrusion;
- not segregate (cf. § 2.1.2.1);
- require a low possible extrusion pressure;
- have limited surface defects, or preferably none at all.

The focus in this research will be on the last requirement, since it is most influential with respect to interlayer bonding strength (cf. infra).

The surface defects intended here, are the ones induced by the extrusion itself: more specifically the nozzle dimensioning, finishing and orientation with respect to print-on surface. The (smallest) curvature that the extruded material is exposed to might induce tearing of the outer edge of the material [13]. There may also be tensile stresses present in the paste. In plastic polymer extrusion this is known as sharkskin instability (Figure 3): stretching (and tearing) due to local acceleration at the end of the nozzle, hence giving rise to tensile stresses above the capacity of the fresh mortar (or polymer) [14].

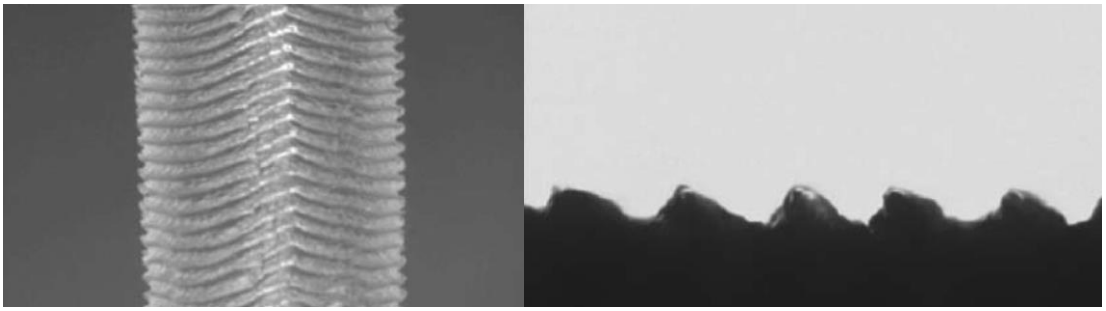

Figure 3: Fully developed sharkskin instability in extrusion of linear low-density polyethylene [14]
Left: top view; right: cross-section

2.1.2.3. Buildability

From the moment the extruded filament leaves the nozzle and becomes part of the printed element, its buildability comes into play. That is a very broad material property with contradicting requirements to those of pump- and extrudability.

The first task of the fresh layer is to withstand its own gravitational load and keep its form. For cast concrete elements, this function is served by the formwork, that can easily balance gravity's effect. In 3DPC the concrete is on its own [10]. The new layer has an initial yield stress τ_{c0}, shear

strain γ_{c0} and elastic shear modulus G_0. Because of setting of the cementitious material, these rheological characteristics change in time: $\tau_c(t)$ and $G(t)$ increase in time, while $\gamma_c(t)$ reduces in time. With increasing shear modulus G, also the Young's modulus E rises. Thus, the layer becomes stronger ($\tau_c\uparrow$) and more rigid ($G\uparrow \sim E\uparrow$) over time (Figure 4) [16]. This tendency of the material to have time-dependent rheological parameters is described by its thixotropy. There exist many different definitions of thixotropy, some juxtaposing, but at the core lie time-dependent rheological parameters. Conform the International Union of Pure and Applied Chemistry (IUPAC), the following definition is generally accepted: "the continuous decrease of viscosity with time when flow is applied to a sample that has been previously at rest and the subsequent recovery of viscosity in time when the flow is discontinued [16]." However, this is not the kind of 'thixotropic behaviour' as encountered in cement pastes: they build up strength and rigidity at rest and the process is not (completely) reversible. Anyhow, the name will be used to describe the time-dependent rheology of concrete as well. In § 2.1.4 more detail is given to the matter.

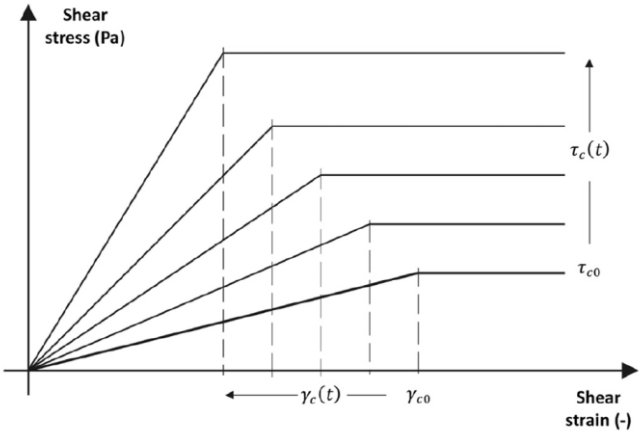

Figure 4: Shear stress-strain relation of cementitious material in time [10]

Self-weight is not only important for the stability of one sole layer but turns more critical with every additional layer that is added to the element. A new layer will deform (i.e. compress) the underlying one by increase of hydrostatic pressure. The time between the deposition of filament at a certain location and the filament that comes on top is called the cycle time (sometimes delay time or time gap) [6]. During this cycle time the lower layers of paste must grow sufficient strength to support additional ones on top. However, they may not have set completely for a good adhesion between two layers is imperative for the overall stability (cf. § 2.1.4.3). Assuming enough strength can be obtained in one cycle time, then still the new filament needs to be positioned with great accuracy. 'Snaking' is the phenomenon where filament shows a curve in the horizontal plane, which was not designed for. As such, a misalignment to the original layers exist and the risk of buckling arises. Snaking can be caused by all stakeholders in the undertaking: either by anomalies in the fresh paste batch, in the printed layers or due to a deviation in the tool path (i.e. the path the nozzle follows), e.a. [17].

Gravity will probably put the most restrictions on the 3D printing process, especially considering the rate of vertical construction (increase of height in time). These restrictions

translate into optimisation of 3D design, mix properties and processing (equipment) with respect to each other. Lately there has been some research into so-called travelling formwork to support fresh filaments just after extrusion [10].

Widely accepted to be the most important influencer, however, is the interlayer bonding strength. This is also the most difficult to design for, since so many aspects need to be considered and so little room for error is allowed. Due to its importance, the interlayer bonding strength gets a whole paragraph of its own: § 2.1.4.3.

2.1.2.4. Printability

Often, in literature the expression 'printability' is used for 3DPC as analogy to 'workability' when casting concrete. Printability encompasses all three of the above definitions: pump-, extrude- and buildability. A printable material is then one with reasonable properties in all three aspects [18].

Time is a major stakeholder for printability. The time frame over which a mixture is printable is called 'open time' [7]. The open time is usually not very long (due to slump loss in time) and poses as such additional problems for the desired continuous process. Conventional batching of paste is being questioned and researchers are yet to find out whether micro-batching or instantaneous mixing is the way forward in 3DPC [17].

2.1.3. Establishing printability

Since 3DPC is such a novel technique, no standard testing procedures for its specific characteristics (e.g. printability) are defined yet. Usually, researchers turn to workability assessments and give a twist to the standard methods.

Many sources use workability tests to evaluate printability:

- the mini slump test (ASTM C1437) [5];
- the slump test (GB/T 14902-2012) [20][44];
- the flow table test (EN 1015-3:1999) [19];
- the V-funnel test (JGJ/T283-2012) [20][44];
- the vibrate (or jump) table test (GB/T 2419-2005) [18][20].

Other (electrical) rheometer tests are also possible, but they require more expensive equipment and all of the above-mentioned sources indicated best results for the five cited tests.

Papachristoforou et al. [19] examined different ways of workability assessment including the flow table test. They found that the flow table test was the most consistent of all in deriving a printability quotation according to their criteria given in Table 1. Many different mixture designs were tested, e.g. changing the amount of superplasticiser (SP) which greatly influenced buildability criterion 4 in Table 1. They also tested the mixtures at different stages in time: i.e. at 0, 15 and 30 minutes after mixing. An obvious observation was the reduction in workability (and printability for that matter) over time. However, the most important finding was the printability

range of the expanded diameter (flow table test; EN 1015-3:1999): minimally 18 cm and maximally 24 cm.

Table 1: Criteria for accepting concrete mixture as printable [19]

Characteristics of 3DPC	Criteria
(Pump- and) Extrudability	1. The mixture is extruded through the nozzle 2. Good printing quality: no voids and no dimensional variations
Buildability	3. Five layers can be printed without collapse 4. A unity ratio of height of the first and last filament

Li et al. [20] included viscosity modifying agents (VMAs) in concrete mixtures to control their rheological characteristics. Proper addition of the right VMAs can improve water retention and hence stimulate internal curing, reduce bleeding and improve interlayer bonding strength. In that way they do resemble the effect of adding superabsorbent polymers. Again, the samples were printability tested at different times after mixing: 15 min, 30 min and 45 min. The results with respect to mechanical properties will be discussed in § 2.1.4. The vibrate table test [20] was applied to assess prior workability and led to some general, important conclusions:

- the higher the VMA content, the more viscous the paste;
- the diameter range (from a vibrate table test) for optimal printability lies between 17.4 cm and 21.0 cm;
- with paste age, printability reduces.

Obviously, the diameter ranges that allow for good printability depend on testing method and mix design. Simply concluding that these are generally valid, would be wrong. However, it is reassuring to conclude at this point that the 'simple' (i.e. easy, mechanical, non-electrical) workability tests are an adequate way of assessing printability as well. It is clear from § 2.1.2 that there is a lot more to be checked, especially with respect to extrude- and buildability. Judging these properties is still greatly operator-dependent.

2.1.4. Mechanical properties

The mechanical properties of the printed concrete (and the resulting element) change in time, as already acknowledged in § 2.1.2.3 by the thixotropy.

2.1.4.1. During construction

Cementitious materials at rest become stronger and more rigid in time. This build up in yield stress and elastic modulus is known as structuration. Microscopically, structuration develops in three stages: flocculation, nucleation and percolation. These stages are schematically shown in Figure 5.

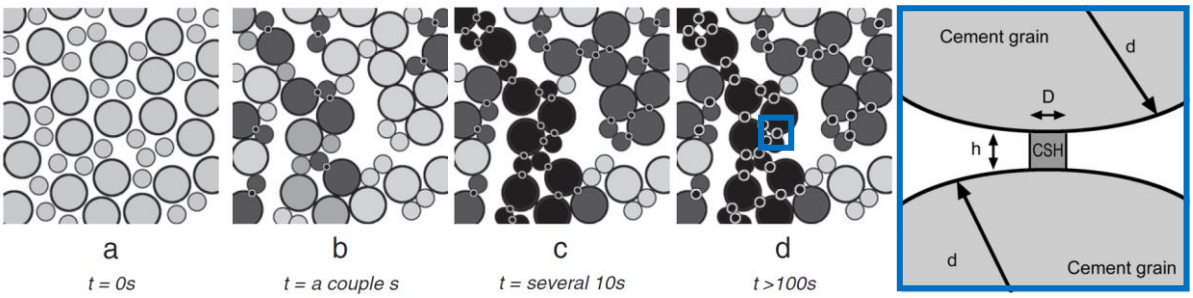

Figure 5: Stages of structuration in cementitious mixtures [21]

In Figure 5 time t increases (in orders of magnitude) from left to right (a to d):

a) at the end of mixing ($t = 0\ s$), all cement particles are dispersed over the volume;
b) **flocculation** ($t \leq 20\ s$): colloidal attractive forces on the cement grains make them move together (i.e. flocculate), while they push out interstitial water in between them. These flocculated (but not yet bonded) grains already show an initial yield stress τ_{c0} and shear modulus G_0. Flocculation keeps on going until all particles are bonded or can no longer move. It is important to emphasise that no calcium silicate hydrate (CSH) bridges are formed during flocculation. Initial strength and rigidity solely come from a balance in colloidal forces: (strongly) attractive van der Waals forces between (close) cement particles in suspension; small attractive or repulsive electrostatic forces, originating from adsorbed ions and relatively strong steric hindrance by the presence of additive polymers;
c) **nucleation** ($t \geq 20\ s$): at the same time as flocculation manifests, some hydration bonds begin to form between particles, at certain nuclei. These hydration bridges, with mainly CSH connections, are considerably stronger than the colloidal attraction that exists from flocculation. In time, more CSH bridges are formed and the yield strength and moduli G and E noticeably increase;
percolation ($t \geq 20\ s$): with more and more CSH bridges formed, also more and more cement particles get strongly connected (i.e. percolate) and form longer chains. At this point in time the cementitious material would still be remixable without much effort;
d) **structuration** ($t \geq 100\ s$): the chain length of percolated particles as well as the number of strong hydrate bonds keep increasing and so do $\tau_c(t)$, G(t) and E(t). At microscopic level, the chemical bonds are irreversible, however macroscopically the paste can still be remixed when applying sufficient energy to break some of the connections [10][21].

Hydration (i.e. the formation of cementitious bonds, such as CSH) is what makes workability reduce in time. Sometimes, flocculation and nucleation are aided by adding (nano-)particles or accelerating the chemical reaction [10].

Roussel [21] concluded after extensive comparison of other research that the structuration rate A_{thix} [Pa/s], i.e. the rate at which $\tau_c(t)$ increases in time is more or less constant, giving rise to the relationship (Equation (1)):

$$\tau_c(t) = \tau_{c0} + A_{thix} \cdot t \qquad (1)$$

This expression is valid in the structuration phase (d). Figure 6 shows the evolution of yield stress in time. Just after deposition of the new filament, flocculation will lead to the initial value τ_{c0}. From then on, nucleation and initial percolation will not alter the elasticity (i.e. the plateau in Figure 6). Continued percolation and structuration will enhance the strength conform Equation (1), during elevation, i.e. new layers being added on top.

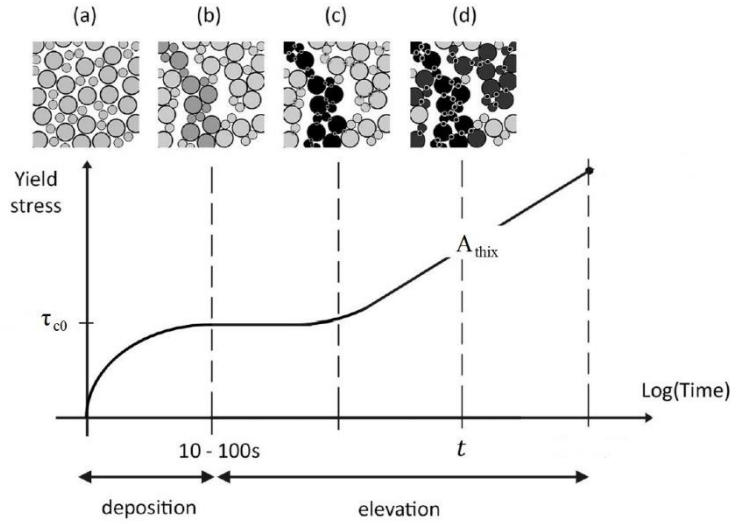

Figure 6: Evolution of yield stress in time [10]

Usually the printed layer thickness (of one filament) h_0 lies between 1 mm and 100 mm. In that case, gravitational action (its self-weight by means of hydrostatic pressure, cf. § 2.1.2.3) will be the first major loading that has to be overcome by the initial strength values (τ_{c0} and G_0). However, for smaller layer thicknesses other phenomena rule. From thick to thin, the stability criteria state:

- $1\ mm < h_0 < 100\ mm$: the gravity induced stress approximately equals $\rho g h_0$, with ρ the mass density of the paste and g the gravitational acceleration. Due to the small thickness and the flat shape of the filament, it is considered to be predominantly a shear stress. As such, τ_{c0} will need to meet the criterion:
$$\tau_{c0} > \rho g h_0 \quad (2)$$
which is generally the case: both are in the order of tens to thousands Pa.
- $h_0 < 1\ mm$: at the nozzle, the displacement velocity and acceleration might become too high for the thin layer, at which case inertia stresses become more critical than the gravitational ones. With V, the nozzle displacement velocity, up to a couple tens cm/s, the basic stability criterion becomes:
$$\tau_{c0} > \rho V^2 \quad (3)$$
- $h_0 <<< 1\ mm$: for extremely thin layers, the surface tension might become critical.

During elevation (Figure 6), additional layers are put upon existing ones, and hydrostatic pressure increases in the lower element. For the printing contour perimeter P [m], the rising rate of the element $\dot{H}$ [m/s] becomes $h_0 V/P$. For a final element height H, the maximum yield stress in the bottom equals $\rho g H/\sqrt{3}$ (obtained from the Mohr-Coulomb relation between normal

and shear stress). This is then the maximal value in Figure 6, and from that Figure, the stability criterion for the structuration rate is extracted:

$$A_{thix} > \dot{H}\left(\frac{\rho g}{\sqrt{3}} - \frac{\tau_{c0}}{H}\right) \quad (4)$$

When a certain element height H_c is reached, failure by buckling (cf. § 2.1.2.3) is more critical than by gravity. Self-buckling is expected to occur in slender vertical elements, only subjected to their own weight from a critical height of:

$$H_c(t) \approx \sqrt[3]{\frac{8E(t)I}{\rho g A}} \quad (5)$$

in which:

- E(t) is the time dependent elastic modulus: $E(t) = 2G(t) \cdot (1 + \nu)$, with ν the Poisson coefficient;
- I is the quadratic moment of inertia with respect to a horizontal axis around which buckling is inspected;
- A is the horizontal rectangular cross-sectional area.

The buckling-critical modulus of elasticity E_c is then given by:

$$E_c \approx \frac{H^3 \rho g A}{8I} \quad (6)$$

Figure 7 plots the required modulus of elasticity for both prevention of failure by gravitational load and by buckling. The dotted line shows the gravity criterion, above which buckling will be critical. The continuous curved lines represent the buckling criteria for different widths of the filaments (respectively from left to right: 5, 10, 15, 20, 25 and 30 cm). A critical flow-onset shear strain γ_c of 2 % is chosen, from which $G = \tau_c/\gamma_c$ and E follow, using $\tau_c = \rho g H/\sqrt{3}$.

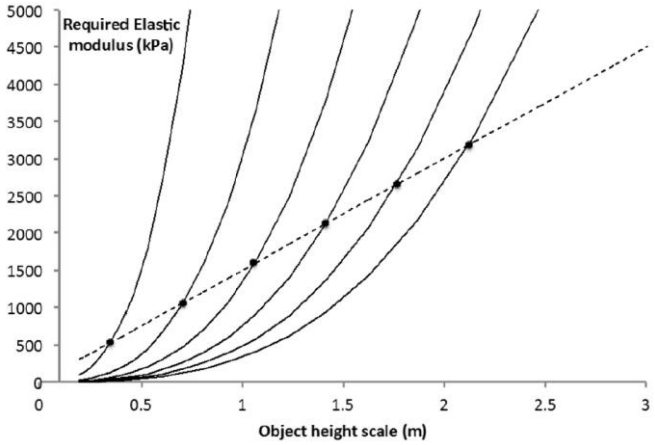

Figure 7: Required modulus of elasticity E as a function of total element height H [10]

Both failure states are very much dependent on time since resistance properties (e.g. the elasticity modulus) change in time. Figure 8 clearly illustrates the importance of knowing the optimal open time of the mix design, i.e. the duration over which it is printable. Up until about an hour after mixing, buildability still is not sufficient, while pump- and extrudability suffice. The open time in this would roughly be half an hour (between 55 min and 85 min after mixing).

When the mixture in the container is at rest too long, printability will decrease again. This might be due to inadequacies in one of the three aspects: pump-, extrude- or buildability or combination of them.

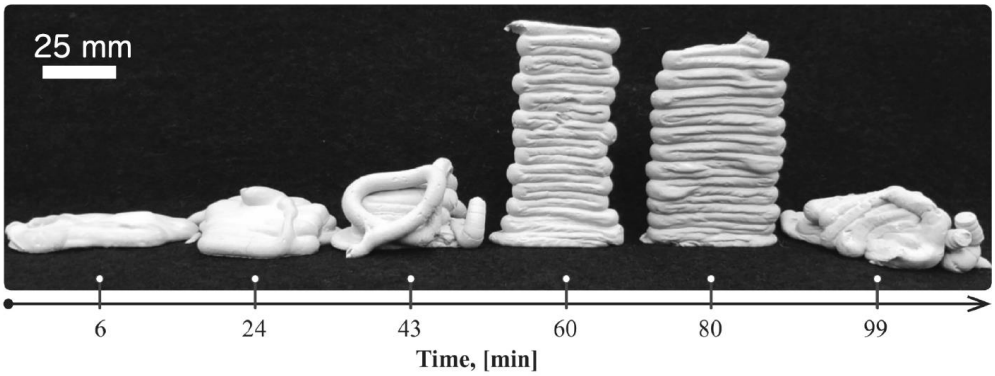

Figure 8: Illustration of the open time concept [17]

2.1.4.2. Hardened properties

While stability during construction of the element is important, its hardened properties are more important for they directly influence the structural lifetime. Of course, defects during construction will ultimately reduce the hardened properties and hence lifetime as well.

The typical construction method of 3DPC results in mechanical anisotropy (usually orthotropy for straight contour elements) [5][6][20][23][24][25].

Marchment et al. [6] tested layered elements made of basic concrete mixes in compressive and flexural strength (for both the perpendicular and lateral loading directions in Figure 9). The tests were repeated for different cycle times, of 10, 20 and 30 min. For all cycle times, the compressive strength was more than 30 % higher in the perpendicular direction, than in lateral direction. The same conclusion was made for the flexural strength, with differences ranging from 13 % to 55 % depending on the cycle time. The latter seemed of great influence on the hardened mechanical properties: a cycle time of 20 min consistently gave rise to lower compressive and flexural strength than cycle times of 10 and 30 minutes. An inverted bell curve pattern in strength vs. cycle time was proposed. This pattern was however not what was expected: e.g. Le et al. [23] reported that an increase in cycle time leads to a reduction in interlayer bonding strength, which might cause an overall decrease in compressive and flexural strength. The increase in strength after 30 minutes of cycle time could not yet be explained. Further research proved the correlation between the surface moisture content and strength in (cycle) time. The surface after 20 min was more than 40 % less moist than at 10 and 30 min [6]. The initial (10 min) humidity can be explained by the freshness of the mortar and the outer edge of the filament that contained more water for lubrication during printing [5][11][28]. The minimal surface moisture at 20 min is due to drying. And the increase again at 30 min was linked to the intensified bleeding rate that countered the loss of water due to drying [5].

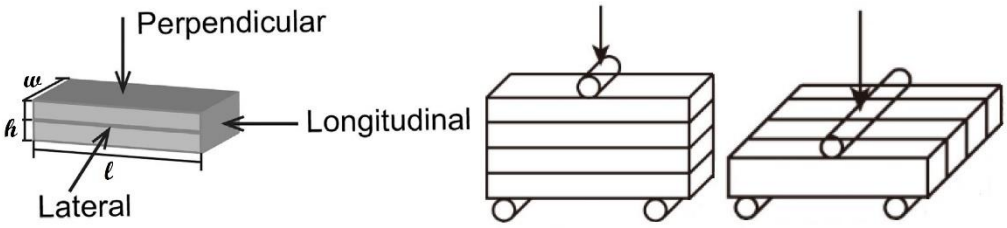

Figure 9: Loading directions for compressive and flexural strength measurement [5] [6]

Le et al. [23] printed larger slab elements (e.g. 350 mm x 350 mm x 120 mm) by building the slender wall elements close to each other. Instead of only printing in perpendicular direction, also in lateral direction the slab element grew (Figure 9). By doing so, void inclusion between neighbouring filaments is a risk (Figure 10) that might (and will) alter the mechanical properties. The researchers took samples for mechanical strength testing from straight and curved printing directions and compared them to mould casted specimens.

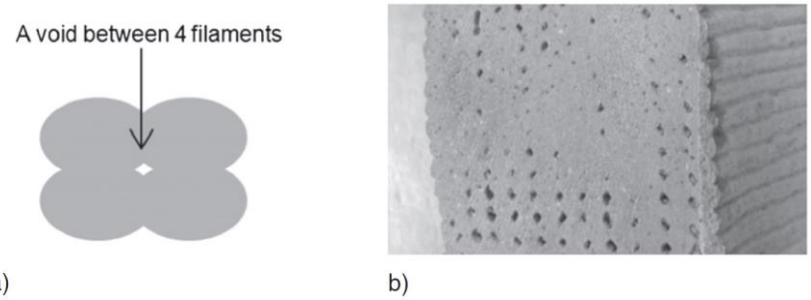

Figure 10: a) Voids formed between neighbouring filaments; b) Bad example [23]

For the straight printed elements, the compressive strengths in perpendicular and longitudinal direction are similar to those of mould-cast concrete, but in lateral compression there is a strength reduction in 3DPC of 15 %. Le et al. [23] assigned this to possible induced shear by flaws at the filament boundaries. However, more likely is the explanation of Sanjayan et al. [5] who observed similar mechanical properties. The longitudinal compressive strength was maximal in their findings, and the lateral minimal. According to them, the pressure exerted in each direction of Figure 9 during printing, defines the according compressive strength in the element. Since the highest pressure in the filament is created through extrusion in the longitudinal direction, this orientation has the best compressive strength. In perpendicular and lateral direction, the paste is more or less free to flow and experiences little to no pressure. However, since filaments are stacked vertically, the hydrostatic pressure will gradually increase in perpendicular direction, and hence result in a higher compressive strength compared to the lateral direction. Temporary or moving formwork might increase the lateral compressive strength [5]. The curved elements show an overall reduction in compressive strength in all directions of around 30 %. In detail observations of the tested specimens revealed voids between the curved filaments (cf. Figure 10) that globally reduced the compressive strength.

Printed flexural strengths in perpendicular and longitudinal direction are higher than those in mould-cast specimens. This is valid for both straight and curved elements. This is probably due to a good compaction in those directions due to the printing procedure: longitudinal extrusion and vertical stacking. These lead to local densification of the mortar and possibly even a lower

water-cement (w/c) ratio due to expulsion of water under pressure. In lateral bending, the printed elements had reduced strength, which is blamed on the presence of imperfections at the boundary of the filaments. The interlayer bonding strength is one of the most important parameters in 3DPC, which will be discussed in the next paragraph.

Paul et al. [24] tend to agree with the above observations, however they mentioned new research by Nerella et al. [54] and Feng et al. [55] in which even higher (> 10 %) compressive strengths were obtained in perpendicular and longitudinal direction. They themselves found the longitudinal compressive (and flexural) strength to be minimal, however [24]. These kinds of contradicting observations remind one that much of the test results will depend on the printing procedure. As such, one has to remain critical and not draw hasty conclusions.

When optimally processed, 3D printed concrete can have a higher density than ordinary concrete elements [23]. The reduction of air voids was already mentioned in § 2.1.2.1. This is however not always the case in 3DPC. The inclusion of voids, such as shown in Figure 10 (i.e. underfilling), or due to improper mix design and rheological characteristics will limit the densifying tendency [17].

To conclude this paragraph, another noteworthy observation is cited. That is, superplasticisers and retarders will generally reduce the early-age mechanical properties (roughly in the first week) but may have a stimulating effect on longer term (especially SPs) [23].

2.1.4.3. Interlayer bonding strength

Commonly referred to as the most important property in 3DPC, interlayer bonding strength gets a lot of academic interest. A good connection between old and newly printed filament is crucial for mechanical properties (cf. supra) and element integrity: failure between two layers will generate failure of the whole [23]. The bonding strength is influenced by a lot of variables, which complicates attributing the respective effect to its rightful cause.

A good starting point is the formation of a cold joint between layers when the cycle time is too long [23]. This happens when the lower layer's surface has hardened already or is too dry or has too many rough defects [10]. The cycle time does indeed depend on the outline of the printed element but should be designed for a good lower surface as well. In § 2.1.4.2 the surface moisture was already indicated to be an important influencer. Ideally the lower filament should still be fresh and moist to be able to optimally bond with the next layer [6]. However, a too moist surface, with possibly even free water, will reduce the bonding strength. Yet again, a precise optimal surface condition needs to be found, keeping in mind that many studies have juxtaposing conclusions [5]. Cold joints may also prove to be temporary, when hydration can start and continue between the layers [17].
Roussel et al. [10] concluded that a high structuration rate is at the origin of cold joints. Besides a longer cycle time, also a higher thixotropy (as defined in § 2.1.2.3) lead to weaker interfaces. In [26] he proposed the following maximum cycle time t_{max} that still allows for good interlayer bonding (Equation (7)):

$$t_{max} = \frac{\sqrt{\frac{(\rho g h_0)^2}{12} + \left(\frac{2\mu_p V}{h_0}\right)^2}}{A_{thix}} \quad (7)$$

in which all parameters are as defined in § 2.1.4 and μ_p is the plastic viscosity of the paste [27]. Splitting tests for the assessment of interlayer bonding strength showed that drying should be prevented since it made the interface strength drop by more than 50 % [10]. The so-called printing environment (temperature, convection, humidity, etc.) is hereby added to the list of stakeholders of proper 3DPC.

The interlayer bonding strength is a type of adhesion, combining both mechanical and chemical linkage. At microscale the chemical forces (attractive or repulsive) rule, while at macroscale surface roughness and interlocking gain importance. With the formation of CSH, other products are formed as well, such as $Ca(OH)_2$. This rather weak hydroxide is found at a relatively higher concentration at the interface between two printed layers. Towards the cores of both layers, strong CSH are more abundant. Needless to say that a longer cycle time will not be beneficial with respect to the amount of $Ca(OH)_2$ found at the interface; hence weakening the connection [29].

The above insights are just few of many to be studied for a complete understanding of the interlayer bond strength. There does not yet exist one source that covers all aspects of the matter, but new research is slowly but steadily realising this goal. This paragraph is concluded with a hodgepodge of recently (being) studied influencers of interface bonding strength:

- A difference in (autogenous) shrinkage rate of two stacked filaments might cause a weak (or young) bond to be broken [17]. (See § 2.2 Shrinkage.)
- Carbonation (i.e. the chemical reaction between CO_2 from air and Ca^{2+} in the concrete to form calcite ($CaCO_3$)) happens at the edges of the filament and spreads inwardly. This might reduce the surface's tendency to bond with the new layer. Carbonation is also a cause of shrinkage [17][37]. (See § 2.2.5 Carbonation shrinkage.)
- Though curing may increase mechanical properties, some curing methods (e.g. membrane forming compounds, molecular films, adhesion promotion, …) might also reduce the interface bonding strength between layers [24]. For connections between mould-cast concrete of different ages, the curing method can be checked with requirements in ASTM C1315. It is yet to find out whether the same criteria apply for 3DPC [30].
- The optimal printing speed depends on the flow characteristics of the paste as well as on geometrical requirements for the filament (a higher speed tends to give smaller filaments). A higher speed has a tendency to generate micro voids in the layers which could possibly affect hardened properties. However, a comparative study has shown that the tensile bond strength was not really affected by the choice of printing speed. Though it was noted that in general a large variance exists in bonding strength values [28].
- The nozzle standoff distance will affect bond strength and surface quality. Smaller standoff distances lead to stronger bonds. Of course, the nozzle should not be too close to the print-on layer. A closer standoff distance allows the new layer too be pressed on the

former one (but not too much with respect to deformation), creating better bonding conditions [28].

2.1.4.4. Tolerances

The main theme throughout this first chapter has been optimisation: quite literally all parameters involved in a 3D printing process will influence each other. Each construction will be unique, with specially optimised mix design, tool path and equipment to meet each other's needs. Therefore, from the start of the optimal process design, priorities and tolerances need to be defined [17].

2.2. Shrinkage

Shrinkage is one of the major obstacles for concrete elements. It will lead to unwanted deformations that affect the geometry as well as mechanical properties. Especially when the deformations are restrained, shrinkage may lead to (tensile) stresses and cracking that degrade the quality of the printed element. Shrinkage can be categorised according to two characteristics: (1) time (and duration) and (2) chemical and/or physical cause. In this chapter, an overview of the six most commonly known (and acknowledged) types of shrinkage is given. By theoretical definition these do not intertwine, but in practice it is rather hard to distinguish each of them properly: especially since measurements are arduous and susceptible to errors; and since different types of shrinkage coexist [31].

2.2.1. Plastic shrinkage

Plastic shrinkage is thusly called because it happens in the concrete's plastic state, i.e. very early on; just after deposition and up until setting [31]. The paste is still fresh and can be considered as solid particles suspended in cement-water (state A in Figure 11). The printing environment (e.g. wind, high temperature, low humidity, …) might cause rapid loss of water to the surroundings (cf. drying shrinkage, but especially in plastic state) by evaporation. First, shrinkage is simply due to the volumetric loss of water. After a while however, the loss can no longer be replenished fast enough and not all solid surfaces are enveloped in water anymore. As such, menisci start to form between the inter-solid pores, giving rise to capillary pressure (state B in Figure 11). This pressure is a result of the adhesive forces between water and solids, as well as the surface tension in the menisci. Both will literally try to pull the solids closer, ending up in settlement and a reduction in volume, known as plastic shrinkage (Figure 11, C). When evaporation continues, the menisci will break due to a continued loss of water and as such, the capillary pressure build-up will drop as well (Figure 11, D). This last state is especially detrimental because it will limit hydration too. When the shrinkage deformation is restrained, cracks will occur [32]. A possible solution to plastic shrinkage is curing. Both external and internal curing are adequate [30]. The internal curing by including superabsorbent polymers (SAPs) in the mix design is one of the main topics of this research and will be subject in chapter 2.3.

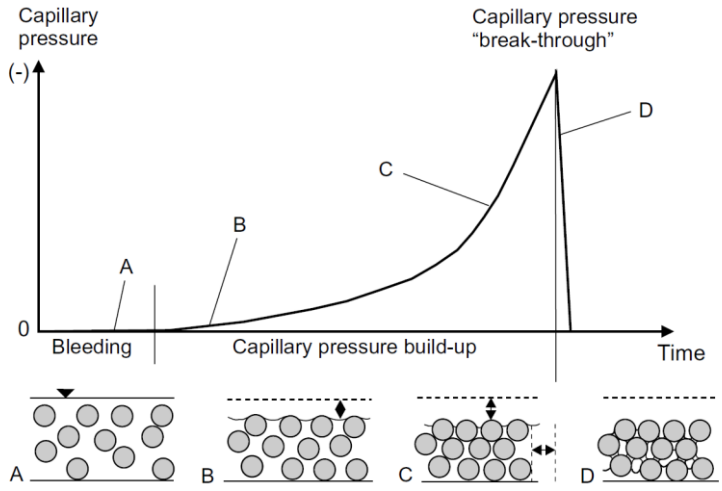

Figure 11: Plastic shrinkage caused by the capillary pressure build-up [32]

2.2.2. Chemical shrinkage

Chemical shrinkage is the loss of volume due to denser hydration products than their reactants. The volume reduction will induce autogenous shrinkage on its part. Enabling a clearer distinction between the two types of shrinkage, the definitions of absolute and apparent volume are in order. The absolute volume is the sum of volumes of solids and liquids, while the apparent also includes the internal voids and gases. The whole external volume of the specimen corresponds to its apparent volume. By definition, chemical shrinkage acts on the absolute volume, while autogenous shrinkage will change the whole apparent volume. Approximately 10 % of the fresh volume is lost due to chemical densification during hydration. The relative amount of solids will increase over time, at the expense of water volume. Chemical shrinkage cannot be omitted, since it is inherent to the hardening process of concrete [31].

Baroghel-Bouny et al. [68] investigated different types of shrinkage for plain ordinary Portland cement (OPC) pastes having various water-cement factors ($0.25 \leq w/c \leq 0.60$). They came to the following conclusions with respect to chemical shrinkage (in the first 24 hours after mixing):

- Below 30 °C of surrounding temperature, the chemical shrinkage will increase with increasing temperature. Above 30 °C, the effect of temperature can be disregarded.
- At low w/c, i.e. $w/c < 0.30$, the initial rate of chemical shrinkage will be up to 20 % higher than at greater ratios of water to cement. Above $w/c = 0.30$, the (initial) rate of chemical shrinkage is similar for all water-cement factors and increases quasi-linearly with increasing temperature. This effect is ascribed to two causes, respectively physical and chemical in nature: (1) at low w/c, more contact points exist between solid particles, enhancing nucleation (cf. stage c in Figure 5), hydration and as such chemical shrinkage; (2) at low w/c, there is a denser packing of cement particles, creating a greater ionic concentration and hindering of diffusion, resulting in a faster precipitation of hydrates such as $Ca(OH)_2$, which are reactants of carbonation processes (see § 2.2.5).

2.2.3. Autogenous shrinkage

Autogenous shrinkage requires an elaborate explanation. It was defined by Jensen & Hansen as the bulk deformation of a closed, isothermal, cementitious material system not subjected to external forces [33]. The words in this definition were not lightly chosen:

- bulk, meaning the apparent volume, rather than the absolute;
- closed, meaning no exchange of matter (i.e. water) with the environment takes place (i.e. there is no change in mass);
- isothermal: the temperature of the element does not change (much) or is at least considered to be constant for the observed effect of autogenous shrinkage solely.

Autogenous shrinkage acts by two different methods, depending on the stage in time: before or after structuration has commenced (cf. Figure 5 in § 2.1.4.1). During hydration but before gaining much rigidity, chemical shrinkage will use up water in the production of CSH. Since percolation is not yet fully developed, the voids created will collapse under self-weight. As such, the absolute volume change is equal to the apparent deformation. This means that before structuration, autogenous and chemical shrinkage cannot be distinguished from each other. After some time however, percolation will lead to structuration and the chemical loss of water manifests as voids supported by a skeleton of hydration products. From then on, the absolute and apparent volume changes will no longer be alike. Microscopically a lot of fine pores and voids are created due to chemical removal of water. This is to be called chemical shrinkage, since it affects the absolute volume. Macroscopically, however, not much volume change is noticed since the voids can be upheld by the gain in structure. From the start of structuration on, autogenous shrinkage is also known as self-desiccation. The apparent volume change is then caused by capillary pore water pressure build-up, as explained for plastic shrinkage. Water in the pores form menisci and might be able to draw them closer together, resulting in overall shrinkage [31][33].

In ordinary concrete applications, autogenous shrinkage has a marginal effect compared to drying shrinkage (see § 2.2.4). This is because a good workability requires a larger w/c than chemically needed for hydration. Water will therefore be amply present, even during structuration – be it that the pores are fully saturated or at least with a relative humidity of around 100 % –, so that capillary pressure build-up will not be very high and as such, self-desiccation almost non-existent. Autogenous shrinkage (especially self-desiccation) is therefore most often prominent for mixture designs with a low water-cement ratio (see infra) [31][35].

Baroghel-Bouny et al. [68] came to the following general conclusions in their research on autogenous shrinkage of plain OPC pastes:

- The (volumetric) autogenous shrinkage is greatly dependent on the temperature of the environment: peaking at around 40 °C (above which it tends to decline again).
- The magnitude of (linear) autogenous shrinkage quasi-linearly increases with decreasing w/c, at any given age. Mixtures with low water-cement ratios encounter the greatest portion of their long-term (~ one year) autogenous shrinkage in the first 24

hours after mixing: 42 % in the case of $w/c = 0.25$, 23 % in the case of $w/c = 0.30$ and almost none at all for $w/c \geq 0.35$.

- Sometimes swelling due to crystal growth (as a result of hydration) is measured at early ages (< 48 hours). This is especially the case for $w/c > 0.40$, where swelling can even continue for several days. For $0.35 < w/c < 0.40$, swelling was practically non-existent and for $w/c < 0.35$, only shrinkage was measured at whatever age.
- The choice of the reference age for relevant shrinkage comparison is primordial. In the study by Baroghel-Bouny et al. [68] the Vicat setting time as well as the so called 'knee-point' (see Mounanga et al. [71] for more details) were used as onset of deformation comparison, with clearly varying results. The knee-point marks the change of chemical-autogenous shrinkage to self-desiccation, and shows by a sudden lower shrinkage rate.
- The internal relative humidity (RH_i) shows a good correlation to the autogenous shrinkage and its mitigation: the ultimate autogenous shrinkage (~ one year) decreases linearly with increasing RH_i (and increasing initial w/c) [68]. Snoeck et al. [57] used sensitive RH_i sensors to observe the effect of superabsorbent polymers on the mitigation of autogenous shrinkage, which resulted in the same conclusion: the higher the internal relative humidity, the better autogenous shrinkage is mitigated.

Supra, the distinction between volumetric and linear deformation measurements was already subtly noted. Studies by Charron et al. [69] and Boivin [70] showed that linear measuring techniques tend to underestimate the early age shrinkage. The exact reasons are still subject for future research, but the authors already mention three possible ones: the temperature is controlled better in volumetric tests as in linear tests the cementitious material is enclosed by a rather thick and stiff membrane; this enclosing membrane might also induce reabsorption of bleeding water in the linearly tested material; and the elastic (latex) membrane used in volumetric tests might already increase internal pressure in the paste and as such induce an additional shrinkage, absent in the linear tests.
In order to compare the results from both types of measurement, Boivin [70] suggested the hypotheses in (8):

$$\frac{\Delta V}{3V} = \frac{\Delta L}{L} \tag{8}$$

which simply divides the volumetric strain ($\Delta V/V$), with V the original volume and ΔV the change in volume, by three to get an equivalent linear strain that can be compared to the one obtained in linear shrinkage testing ($\Delta L/L$). This suggestion follows from the assumption of isotropic shrinkage behaviour. However, this isotropic behaviour is questioned by Boivin as the equivalent linear measurement (from volumetric testing) still is about three to five times bigger than the one from linear testing. In fact, Boivin recommends further research into the possible anisotropic shrinkage behaviour of cementitious materials (at early age) [70].

2.2.4. Drying shrinkage

Drying shrinkage is volume loss, continued over the whole lifetime, caused by evaporation of internal water in hardened concrete (e.g. gel water between sheets of CSH [42]). The water loss

will give rise to capillary tensile stresses that may lead to cracking (especially in combination with external loading) [34]. Its effect is usually bigger than that of other types of shrinkage and therefore deemed more important [31]. A possible curing method (or suitable environment) will have to remain actively present over the complete lifetime of the element. The amount of internal (and unbound) water is the most important parameter.

2.2.5. Carbonation shrinkage

A lot of research is currently being performed on the effects of carbonation. Not every aspect is yet fully understood, and it is generally believed that more observations could be assigned to carbonation, than those already known. Carbonation is the chemical transformation of cement hydration products and CO_2 (from air) into calcium carbonate (and water). Portlandite or calcium hydroxide $Ca(OH)_2$ is assumed to react fastest with CO_2 from the surroundings according to Equation (9):

$$Ca(OH)_2 + CO_2 \rightarrow CaCO_3 + H_2O \quad (9)$$

The rate of reaction diminishes in time due to the formation of a $CaCO_3$-layer covering the $Ca(OH)_2$ crystals. The transformation of CSH will then amount to the most carbonation, via:

$$(CaO)_x(SiO_2)(H_2O)_{y+z} + xCO_2 \rightarrow xCaCO_3 + (SiO_2)(H_2O)_y + (H_2O)_z \quad (10)$$

Other Ca^{2+} bearing phases present in the mortar are also susceptible to carbonation, but (9) and (10) are the most important processes. The intrusion of CO_2 and the subsequent carbonation reactions make the acidity of the pore fluid rise (i.e. the pH value drops). This change in acidity is used to visualise the carbonation front, that will gradually move inward, by means of colour indicators (e.g. phenolphthalein) [58]. It is already noticed that the change in acidity might also change the behaviour of certain additives, such as superabsorbent polymers, discussed in § 2.3.

These chemical reactions have two main consequences: dehydration and decalcification. Both are causes of carbonation shrinkage. The dehydration, or loss of bound H_2O, triggers the same mechanism as in drying shrinkage. Water that was once bound (or held under the form of hydroxide) is freed and can now be lost to the element environment and thusly add to drying shrinkage. Decalcification reduces the Ca/Si ratio in the remaining hydrates, causing a morphology change into a more sheet-like structure [37]. This structural reorganisation leads to the shrinkage of the overall volume (due to a collapse of voids), while paradoxically the transformation of $Ca(OH)_2$ into $CaCO_3$ is volume expanding (3 % to 19 %, depending on the crystal form taken) [36].

2.2.6. Thermal shrinkage

The cement hydration reaction is exothermic and thus heat producing. This will heat up the setting concrete as well as unbound water, which might evaporate to the environment [38]. Thermal shrinkage happens during plastic or autogenous shrinkage, though independently.

The contraction of hardened concrete due to a decrease in temperature is also a type of thermally induced shrinkage. It is well known and omnipresent for all matter.

2.2.7. Measuring shrinkage

There exist many different measurement techniques for shrinkage, each most suited to a specific type. Not as many have been standardised yet, since they mostly depend on the ingenuity of the researcher and the testing facilities of his/her institution [31].

Charron et al. [69] investigated the effect of specimen size on external shrinkage measurements. They used prismatic specimens with a square base of 50 mm x 50 mm and lengths of 250 mm and 1,000 mm. However, neither the rate nor the magnitude of deformation at 26 hours after mixing differed substantially for different specimen lengths.

2.3. Superabsorbent polymers

Quite recently, superabsorbent polymers (SAPs) are being tested for applications in construction materials such as concrete (cf. Magnel Laboratory for Concrete Research). The possibilities seem endless, creating so called smart materials. But Rome was not built in one day, rather reshaped over the years and always brick by brick. This chapter deals with the general characteristics of SAPs as well as their effect on printability, mechanical properties and shrinkage.

2.3.1. In general

2.3.1.1. Definition and application

Superabsorbent polymers are three-dimensional cross-linked poly-electrolytes that can absorb up to 1,500 times their own weight in water (or aqueous solutions), forming hydrogels. Developed in the 80s, their first application was found in hygiene industry and more specifically in diapers. Since then the demand has been steadily growing, opening up new markets in, amongst others, the construction industry. The largest production share still goes to consumer goods in health care, with up to a million tonnes each year. The chemical demands of SAPs vary for each industry and even for each application, giving rise to many different types of cross-linked synthetic polymers, with different chemical backbones:

- polyacrylic acid (PAA), sometimes neutralised with hydroxides of alkali metals (e.g. $Na^+(OH)^-$), especially used in hygiene applications;
- polylactic acid (PLA);
- polymethacrylate (PMA);
- polyethylene oxide (PEO);
- polyethylene glycol (PEG);
- …

The last two are mainly used in non-hygiene applications and are called technical SAPs. Technical SAPs are generally based on monomers of acrylamide, acrylic acid or vinyl acetate. Some producers are BASF, Evonik Industries, Nippon Shokubai, Sumitomo Seika, Technical Absorbents, Arkema and NSF Floerger e.a. Natural polymers with swelling capacity exist as well (e.g. polysaccharides), they have the advantage of being biocompatible and biodegradable,

however suffer from low mechanical strength (compared to synthetic SAPs) and batch variation [40][41][42].

The main function of SAPs in concrete technology is controlling the water and as such controlling the rheological properties in fresh concrete and curing abilities in hardened concrete [39].
In [47] a list is given by Cusson, Mechtcherine and Lura, with all possible improvements of concrete properties by means of SAP introduction in the mix design:

- shrinkage reduction: SAPs provide internal curing and maximise cement hydration; they can mitigate plastic, autogenous and drying shrinkage [56][57];
- frost resistance: during cement hydration (and water loss in general), the polymers will shrink and provide water. This leads to a pore system that can be optimised to increase the freeze-thaw resistance [42];
- rheology modification: including SAPs will alter the effective w/c. Part of the total amount of water ($(w/c)_{tot}$) is absorbed by the polymers (i.e. additional w/c or $(w/c)_{add}$)) and as such reduces the amount of water left in the concrete ($(w/c)_{eff}$)). The effective water is used for hydration and workability. A reduction in effective water-cement ratio ($(w/c)_{eff}$) may lead to a stronger concrete but also a more viscous one during printing (see § 2.1.3 as well);
- controlled water release: SAPs of different chemical characteristics may be combined to control the release of water (or other absorbed substances) in time (since some polymers may take longer to desorb). The (un)swelling depends on the acidity and salinity of the concrete and this dependency could be used to engineer the wanted reaction of SAPs in time [61];
- waterproofing: (most) SAPs are able to absorb and desorb cyclically without reduction of swelling capacity. This makes them act as sealing agents when cracks and intruding fluids would appear along their path [59];
- crack healing: the waterproofing ability aids in crack healing of concrete as well [42][59][60];
- surface curing: especially plastic shrinkage may cause cracking of and slower strength development in the concrete surface. This was stated to be an important influencer of interlayer bonding strength. SAPs are able to cure the surface from within the concrete and improve bonding capacity;
- fire protection: SAPs can be soaked in certain chemicals (e.g. $CaCl_2$) to obtain a fire-resistant mortar [62];
- removal of contaminants: SAPs can be applied to the contaminated surface, and with proper designing the contaminants can be absorbed and irreversibly bound to the polymers, after which they can be removed again, leaving behind little to no contamination [47];
- and many more, such as application in: shotcrete (cf. § 2.3.2), water-blocking construction filler as backfill material in tunnel construction, smart paints, sensors, …

2.3.1.2. Geometrical and molecular characteristics

Superabsorbent polymers are mass produced by chemical polymerisation. The most often used technique of polymerisation involves the use of free radicals (i.e. free radical polymerisation (FRP)). The process consists of three main phases: initiation, propagation and termination. During initiation, the free radical initiator is added to a multitude of stable monomers. The initiator then bonds (after activation by heat, valency, ultra-violet light, …) with the first monomer, breaking up a double (or triple) chemical bond in it. The initiator has as such shifted the radicality towards the other side of the monomer, where it has not connected to. From then on propagation commences as the new radical is able to react with other monomers to form polymer chains. Termination can happen in many ways, which are not all discussed here. Generally, polymerisation will end up in two chains binding, or by chemical connection to impurities (whether or not added on purpose). The production process is defining for the geometrical characteristics of the polymers. Bulk polymerisation (i.e. pure, liquid monomer + initiator) will usually end up in a large batch of polymer gel, that can be kneaded, extruded, dried, cut, broken, grinded, … These polymers tend to be of an irregular, edged shape (cf. SAPs A, G, P and M in Figure 14). Suspension polymerisation (i.e. liquid monomers in heterogenous suspension) will lead to spherical polymers (cf. SAPs D and H in Figure 14). By extruding the batch, fibres can be formed and cut to length (cf. SAP F in Figure 14). The important thing is that the chemical process will influence the shape; meaning not only the chemistry needs to be engineered properly, but the process as well. The mean diameter of SAP particles ranges from tens to thousands of micrometres.

SAPs are natural or synthetic, three-dimensional networks of polymer chains that are chemically (covalently) or physically (electrostatically) cross-linked and have hydrophilic functional groups in them. These functional groups are usually: -OH, -CONH, -$CONH_2$ and -COOH. They are chemically charged, or polar and tend to bond with ions present in the neighbourhood (e.g. Ca^{2+} and Al^{3+} present in cement-water). Some of these bonds can be very strong due to di- or tri-valency (i.e. complexation) and can cause additional cross-linking or charge screening in the polymer chains. These chemical changes in time are not always for the good of practical use. Some SAPs more than others are susceptible to physical, chemical and biochemical stimuli (e.g. oxidation from air, temperature, light, acidity, salinity, …) that can reduce their shelf-life, or in other words: the features they were designed for [41][42][63].

2.3.1.3. Swelling capacity

The main driving force for the (water) absorption capacity of SAPs is their internal osmotic pressure. The polymer links keep the electrically charged or polar functional groups close together, resulting in a high osmotic pressure on the inside. Absorbing water reduces this pressure by dilution of the electrically opposing charges (Figure 12). The SAP literally grows by taking in the (dipolar) water and as such the distance between the functional groups increases [41][48]. The water molecules that are actually bound to the hydrophilic groups are called as such: bond water, while the term ‘free water’ is used for water that simply takes up space in the expanding polymer [42].

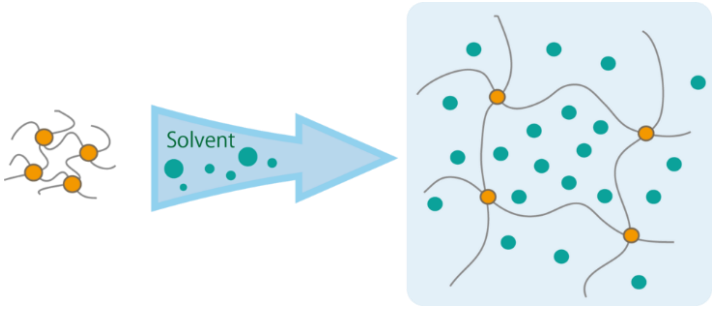

Figure 12: Illustration of swelling of a SAP [48]

The swelling capacity is limited by three opposing forces until a state of equilibrium is met and the SAP is fully saturated. The first opposing force comes from the elastic restraint in the polymer links. They are elongated under volumetric expansion due to water uptake but reach a limit in elasticity. Secondly, a difference in osmotic pressure from the surroundings might cause water to flow back and out of the SAP. Thirdly, the hydrogels might be subjected to external mechanical loading, e.g. under the hydrostatic pressure of cement paste. The polymers are then literally squeezed due to which they may lose water.

Not so much opposing, but rather hindering the swelling capacity are di- and trivalent ions present in the cement-water (e.g. Ca^{2+} and Al^{3+}, § 2.3.1.2) that react with the hydrophilic groups and form additional cross-linking. They go into strong complexation with or form a shield around the functional molecules, depriving H_2O of any chance of attraction [41]. The extra cross-linking will improve their mechanical properties as well, reducing the swelling capacity [42].

The swelling capacity (SC) of SAPs can be measured in several ways, mostly based on mass or volume changes. It is usually defined as weight (or mass) of fluid absorbed, divided by the original dry weight of the particles (w_{dry}), and expressed in g/g (Equation (11)):

$$SC = \frac{w_{sat} - w_{dry}}{w_{dry}} \tag{11}$$

in which w_{sat} is the total weight after (sufficient time for) absorption. The two most common techniques are the teabag method and the filtration method, both gravimetrical (i.e. by measurement of a difference in weight). In the first method, a sealed teabag is filled with a measured amount of dry SAP particles (w_{dry}) and put in the test solution. After absorption, the teabag is hung up to remove excess liquid and weighed again (w_{sat}). In the filtration method a filter paper is soaked in the test liquid before it is used to drain the swollen SAPs (with measured dry and saturated weight). A lid is placed on top of the conical shaped filter paper to avert evaporation. Due to capillary fluid between the swollen polymer particles, that cannot be removed, both methods might lead to a small but negligible overestimation of SC [42]. The detailed description can be found in the recommendation by the technical committee 260-RC of Réunion Internationale des Laboratoires et Experts des Matériaux (RILEM) [64].

To conclude this paragraph some issues are highlighted that are specifically apt when mixing SAPs into cementitious materials [43]:

1) SAP particle size does matter. Very large particles ($\varnothing \gtrsim 150$ µm) have reduced efficiency due to insufficient time for water absorption during mixing. They are capable of absorbing more liquid than smaller particles, purely due to their bigger volume, but they also need longer to reach full saturation. Very small particles ($\varnothing < 100$ µm) achieve full absorption capacity quickly but are geometrically limited in the volume of liquid they can contain [53][65]. In that sense, they too have limited efficiency per gram of added polymer. Figure 13 shows the influence of the initial (dry) particle size on the final grown particle diameter and on the absorption rate (i.e. saturation) in time. Both are valid for the absorption of (synthetic) cementitious pore fluid [65].
2) Jensen & Hansen [53] concluded that the outer surface zone of superabsorbent polymers is less active than the inner bulk. Since small particles, compared to bigger particles, have a relatively large outer surface and less active bulk, they will also absorb less liquid per gram of SAP added.
3) SAP swelling in cement paste is considerably more difficult than in plain water. This has both to do with the presence of shielding ions as well as with the short time frame in which they can 'freely' absorb water/liquid, as hydration follows quickly after mixing [43].
4) Desorption of swollen polymers is caused by the capillary pressure in the surrounding concrete after loss of water. Mönnig [49] showed there is a correlation between the desorption rate and the relative humidity (RH) of the (printing) environment. High relative humidity leads to a prolonged desorption rate, and as such, a longer period of internal curing [49][57].
5) In the closest proximity of a SAP particle the w/c is higher than on average. This will locally add to the hydration percentage [49].

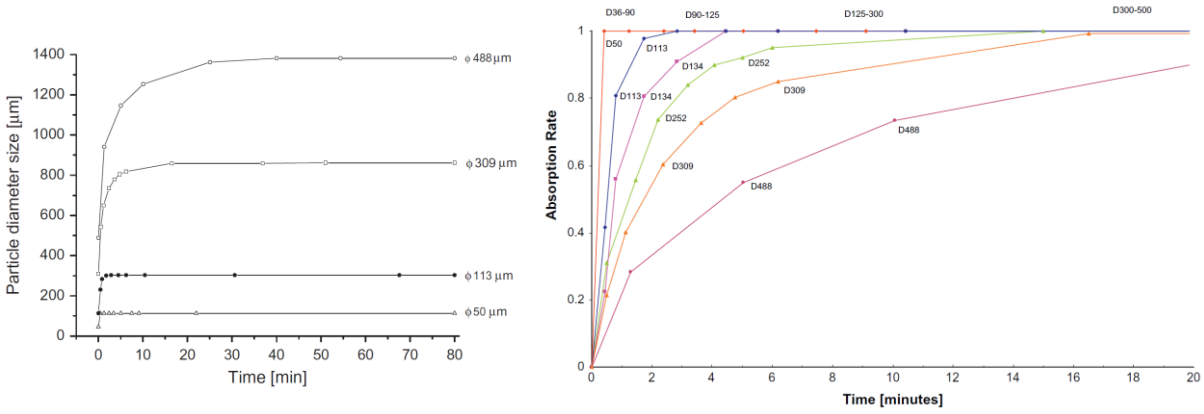

Figure 13: Effect of initial SAP particle size on (left) particle growth and (right) absorption rate, in time [65]

2.3.2. Effect on printability

The addition of SAPs to a cementitious mix design, without additional water to compensate their absorption, is comparable to simply removing water from the mixture. In that case, the workability will diminish, and with it pump- and extrudability as well. On the other hand, the increase in yield stress and higher plastic viscosity that result from a reduction of (effective)

w/c, improve buildability [44]. From a certain high amount of SAPs on, they will start to physically show as swollen particles at the surface, which is unwanted [51].
The thickening effect of SAP addition can be mitigated through the use of plasticising admixtures. These will induce flaws of their own, especially in mechanical properties at young age. However, the thickening should not always be regarded as negative when it comes to pumpability. In case of shotcrete (i.e. concrete that is 'shot' under pressure and has to adhere to almost vertical structures or even ceilings), this thickening might show advantageous. The main reasons for a high slump (and thus workability) in shotcrete technology lie in the risk of sudden rebound in the pumping tubes and in the requirement of proper thickness build-up (in thin layers). The advantages of SAP addition, on the other hand, lie in the reduction of set-accelerators, that reduce long-term strength properties and in freeze-thaw resistance, which is very poor due to a lack in control of air-entrainment [51]. The analogy with shotcrete may seem farfetched, but this literature review has shown that in order to obtain the big picture, one may have to borrow ideas from other technologies.

2.3.3. Effect on hardened properties

2.3.3.1. Structure

Concrete has a continuous three-dimensional network of pores and capillaries, that will tend to change in time due to ongoing hydration and (drying) shrinkage. Since SAPs have shown to stimulate hydration over a longer period of time, they will influence the pore structure as well. One gram of cement will chemically bind with 0.23 g water and adhere to 0.19 g of gel water. As such, complete hydration is only possible for an effective water-cement ratio of 0.42 [53].
Pores are classified as: gel pores when they are smaller than 10 nm; voids for sizes above 10 µm; and capillary pores for everything in between. Three types of water are distinguished depending on their location in the matrix: gel water between CSH sheets (bound or adsorbed), water in capillary pores and chemically bound water in hydration products. IUPAC uses another classification of pores: micropores smaller than 2 nm, macropores larger than 50 nm and mesopores in between [42].

The size and amount of SAPs, the original and effective w/c and the way of addition of SAPs (i.e. saturated or dry) are the three most important influencers of the hardened structure. SAPs filled with water will act as soft aggregate; when they are empty, they act as voids. Their dispersion rate (uniform, flocculated, …) will influence mechanical properties (see infra). And due to the internal curing effect, hydration is stimulated locally and globally [49]. Study has shown that especially at later ages ($\geq$ 2 weeks) the hydration degree of concrete specimens with SAPs was higher than that of ordinary samples [67]. At later ages even (8 weeks), a hydration increase of up to 10 % was noticeable [50]. When no additional water was added to compensate the swelling, little to no difference in overall porosity was measured compared to reference samples without SAPs [49][66]. However, when extra water was used, the total porosity did increase a couple of percentage points [50]. The overall porosity is of course made up out of micro-, meso- and macropores. While especially microporosity is reduced by addition of SAPs (due to prolonged hydration and mitigation of autogenous shrinkage cracking); meso- and

macroporosity are larger since SAPs are in essence water reservoirs (i.e. voids). Permeability is mostly dependent on the network of micropores and is indeed reduced by SAP addition. The polymers also tend to retain possibly intruding fluids by absorbing them (cf. self-sealing concrete technology) [42].

2.3.3.2. Interlayer bonding

The fundamental requirement for a good interface bonding strength is a good surface moisture (see chapter 2.1). SAPs mitigate drying and autogenous shrinkage through internal curing, from which the surface benefits as it remains hydrated longer. This will enhance the bonding capacity with a superposed filament [5]. However, as mentioned in § 2.3.2, some SAPs might show at the interface surface and as such reduce the bonding strength since they have rather negligible mechanical strength themselves [50]. Yet again is optimisation key.

2.3.3.3. Compressive and flexural strength

SAPs will clearly influence the structure of the hardened concrete. This will have its effect on the strength properties as well. In [45] it is shown by Kovler that a lot of researches have juxtaposing conclusions, however a general trend can be found. It reads: “No pronounced negative effects on compressive strength are found upon adding SAP, if a right amount of extra water is added for the purpose of internal curing [45].” It should be noted however, that the compressive strength results are more differing than those of flexural tests. Generally, there is a (small) reduction of compressive strength with respect to reference samples. Especially at early ages, where it accounts for a reduction of circa 20 %, while after 28 days this has been decreased to around (and below) 10 %. A higher SAP or entrained water content leads to lower compressive strength. Similar observations hold for the flexural strength. But, the reduction in bending capacity (or generally, in tension) is not so high as the one for compressive strength. This is assigned to the decrease in microcracks as internal curing mitigates self-desiccation, and to a higher rate of hydration. These positive effects cannot always counter the weakening effect of more macropore formation. Lastly, the elastic modulus is comparable for both samples with and without SAPs. The shape of the SAP plays a role too: irregular ones lead to more stress concentration than spherical ones (for particles of the same size) [53].

2.3.3.4. Durability

SAPs have a positive effect on durability, as has become obvious throughout this literature review. They reduce permeability, may absorb harmful intruders, create a good void structure that is frost-thaw resistant, etc. [42][46][50].
The applications mentioned in § 2.3.1.1 also add to durability but need more research.

2.3.4. Effect on shrinkage

One of the primary reasons of using SAPs in concrete is the mitigation of (autogenous) shrinkage [44]. Over the last years a lot of research has been done specifically in this field. However, not all types of shrinkage are covered as much as others. Except for carbonation shrinkage, effects of SAP addition have been observed in [31]:

- plastic shrinkage:
  Only limited study has been done so far, but early results prove that SAP addition reduces (even halves) the amount of plastic deformation in the first hours after casting/printing, i.e. in the time span of plastic shrinkage [31]. Near the drying surface, free water is lost to the environment first, being gradually replenished by the water stored in the SAPs, mitigating plastic shrinkage as such [56]. There has been noted a reduction in heat formation in the first (24) hours for samples containing SAPs. It is assumed that, though an overall increase of hydration will result, it is delayed a bit at first: spreading out the heat production of the exothermic reaction over a longer period. The thermal shrinkage influence, happening parallel to plastic shrinkage is thus diminished. Another influencer was the reduced capillary pressure that showed when using SAPs [31].
- chemical shrinkage:
  The cement hydration reaction is at the heart of chemical shrinkage. Since SAPs improve the rate of hydration, they will increase the rate of chemical shrinkage as well. Indeed, the highest loss ($-$ 25 %) of volume by hydration was observed in mixtures with SAPs instead of in reference mixtures. Especially the chemical activity of the first 2 days seemed a driving factor. Not all studies tend to agree: it has been observed in some that there is no difference in deformation, whether or not SAPs are used [31].
- autogenous shrinkage:
  The Powers' model for the phase distribution of a hardening cement paste was used by Jensen & Hansen [53] to derive the optimal amount of additional water content to improve internal curing, complete hydration and mitigate autogenous shrinkage. In § 2.3.3.1 it was already stated that the minimal w/c to reach full hydration was 0.42. This water is either available in the mix itself or as water entrained ($(w/c)_{entr}$) in the SAPs and 'free' to be used for hydration. For a mix design, initially without water entrainment, and given original w/c, Jensen & Hansen formulated:

$$\begin{cases} (w/c)_{entr} = 0.18 \cdot \text{w/c} & \text{w/c} \leq 0.36 \\ (w/c)_{entr} = 0.42 - w/c & 0.36 < w/c < 0.42 \end{cases} \quad (12)$$

  in order to stimulate internal curing. This $(w/c)_{entr}$ can then be used to design for the ideal amount of SAPs included in the mix design: $(w/c)_{entr} = (w/c)_{add}$ [42]. In [45] Kovler started the design of the mixture assuming half of the absorbed water in cement filtrate (CF) to be added for swelling of the SAPs in the cementitious material.
  Extensive research by many institutions have come to the same conclusion: SAPs lead to a reduction of autogenous shrinkage and sometimes even a volume expansion [31]. Interesting observations have been done with respect to: (1) size and amount of SAPs, (2) distribution of SAPs over the volume and (3) presence of other (larger) aggregates (i.e. difference between paste and concrete). (1) Small-sized polymers released curing

water more gradually leading to longer controlled internal curing (and less evaporation). This meant a better mitigation of autogenous shrinkage and less volume reduction or even expansion. When the amount of SAPs increases, the difference between small and large particles diminishes [31][42]. (2) A uniform distribution of SAPs is paramount for a good mitigation of self-desiccation [31]. The mixing procedure is obviously an important stakeholder. Rough mixing leads to breaking up of (swollen) SAPs which might be detrimental (cf. 'active surface' in § 2.3.1.3). (3) Autogenous shrinkage is best mitigated in concrete mixes, i.e. cement pastes with larger granulates [31]. It should be noted however, that a relatively larger amount of big granulates inevitably leads to a better reduction in shrinkage as granulates will not shrink at all. In that respect, the measurement of shrinkage (and its mitigation) will therefore be more convenient in mixtures with small granulates.

- drying shrinkage:
  SAPs have a positive (lowering) effect on drying shrinkage but would not seem able to completely avert shrinking over longer time (except possibly for a SAP-to-cement ratio of over 0.4 mass percentage points (m%)) [31].

2.4. Final remarks and research objectives

This literature review has proven very helpful in laying the foundation of knowledge needed for efficient further (laboratory) research. Some valuable general conclusions drawn above will steer the mix design and explain observations.

The laboratory research, outlined in the next chapters, starts off with the optimisation of mix designs according to their printability characteristics. The obtained mixtures are then tested for their early age shrinkage behaviour and mechanical properties, focussing on the interlayer bonding strength. As no normative methods exist for neither of these topics in 3DPC, newly developed procedures are followed, based on international standards on normal concrete testing. The results as well as the adequacy of some of the preceding practices will be discussed in detail and statistically analysed for their significance.

In the hope that this research amounts to new and useful insights into the influence of SAP addition on concrete behaviour, as well as to new and effective testing procedures of printed specimens, in the end of this dissertation conclusions and recommendations to future work are drawn.

MATERIALS

Marmor non eodem genere omnibus regionibus procreatur.

MARCUS VITRUVIUS POLLIO

DE ARCHITECTURA | LIBER SEPTIMUS | CAPUT SEXTUM

Marble is not alike
in all countries.

3. Materials

This chapter treats the materials used in the laboratory research.

3.1. Cement

Ordinary Portland cement CEM I 52.5 N Strong (Holcim Belgium) was used in all mixtures. Its indicative chemical composition, as listed in the manufacturer's product sheet, is given in Table 2. It has a normal structuration development and a mass density ρ_{cem} of 3,160 kg/m^3.

Table 2: Chemical composition of CEM I 52.5 N Strong

Component	Fraction [m%]
CaO	64.30
SiO_2	18.30
Al_2O_3	5.20
Fe_2O_3	4.00
MgO	1.40
Na_2O	0.32
K_2O	0.43
SO_3	3.50
Cl^-	0.06

3.2. Sand

Standardised sand (Normensand Germany) with grain sizes ranging from 0.08 mm to 2.00 mm was used in all mixtures. These conform to the requirements of the Comité Européen de Normalisation (CEN) and those stated in NBN EN 196-1. The moisture content is guaranteed to be below 0.2 % and the mass density ρ_{sand} equals 1,241 kg/m^3.

3.3. Water

Except stated otherwise, local tap water at a temperature of 20 °C was used for executing all tests. The tap water is potable and complies to the requirements of the Flemish government provided in BVR(1)13.12.2002. The mass density used in calculations is $\rho_{water} = 1{,}000$ kg/m^3.

3.4. Superplasticiser

As superplasticiser (SP) MasterGlenium 51 con. 35 % (BASF The Netherlands) was used in all mixtures. The dry particle fraction of this polycarboxylate ether is 35.0 % according to NBN EN 480-8. Its acidity ranges from 5 pH to 8 pH and it has maximally 0.1 m% and 2.0 m% of Cl^- and Na_2O in it respectively. Its mass density ρ_{SP} equals 1,075 kg/m^3.

3.5. Superabsorbent polymers

Table 3 and Figure 14 hold the details of the superabsorbent polymers (SAPs) that were available for this research, as defined by Snoeck [42]. The terminology introduced in Table 3 is elucidated below.

Table 3: SAPs used in this research [42]

SAP	Type	Production	Company	Size [µm]	SC [g/g]		ST	MU [%]
					DW	CF	[s]	
A	copolymer of acrylamide and sodium acrylate	Bulk	BASF	100±22	305±4	61±1	10	26|83|394
D	cross-linked sodium salt	Suspension	Sumitomo Seiko	492±79	351±5	52±2	55	37|105|306
F	cross-linked acrylate polymer	Extrusion	Technical Absorbents	L 5.2±0.3 mm Ø 27±3 µm	165±3	47±1	8	30|89|389
G	cross-linked acrylate polymer	Bulk	SNF Floerger	157±82	332±6	47±2	22	25|79|392
H	cross-linked acrylate polymer	Suspension	SNF Floerger	70±34	281±6	40±5	36	31|93|264
M	cross-linked potassium salt polyacrylate	Bulk	Evonik Industries	486±141	285±2	59±1	65	26|75|186
P	cross-linked potassium salt polyacrylate	Bulk	Evonik Industries	190±61	286±1	58±2	14	30|86|219

- The type of SAP refers to its chemical backbone (cf. § 2.3).
- The production method and producing company of each is tabulated as well, for the sake of completeness.
- The size refers to the SAP mean particle diameter, under the assumption of it having a spherical shape. The regularity of form of each can be assessed from Figure 14.
- The swelling capacity (SC [g/g]) of the polymer as defined in Equation (11) is given for absorption of demineralised water (DW) and cement filtrate (CF). The cement filtrate was obtained by mixing 10 g of ordinary Portland cement CEM I 52.5 N in 100 g of demineralised water, followed by filtration [42] [64].
- The swelling time (ST [s]) is the time needed for a SAP to reach maximum saturation (in the test liquid). SC and ST depend among others on the shape of the particles [52] and on the chemical type as well as production method [72] (see § 2.3.1.3 Swelling capacity).
- The moisture uptake (MU [%]) in a humid climate, defined as the percentage of saturated mass (or weight w_{sat} [g]) divided by the original dry mass (or weight w_{dry} [g]) (Equation (13)):

$$MU = \frac{w_{sat}}{w_{dry}} 100\ \% \tag{13}$$

  The MUs are given for a RH of respectively 60 %, 90 % and 98 % as determined by means of water vapour sorption testing, separated in that order by vertical lines in Table 3.

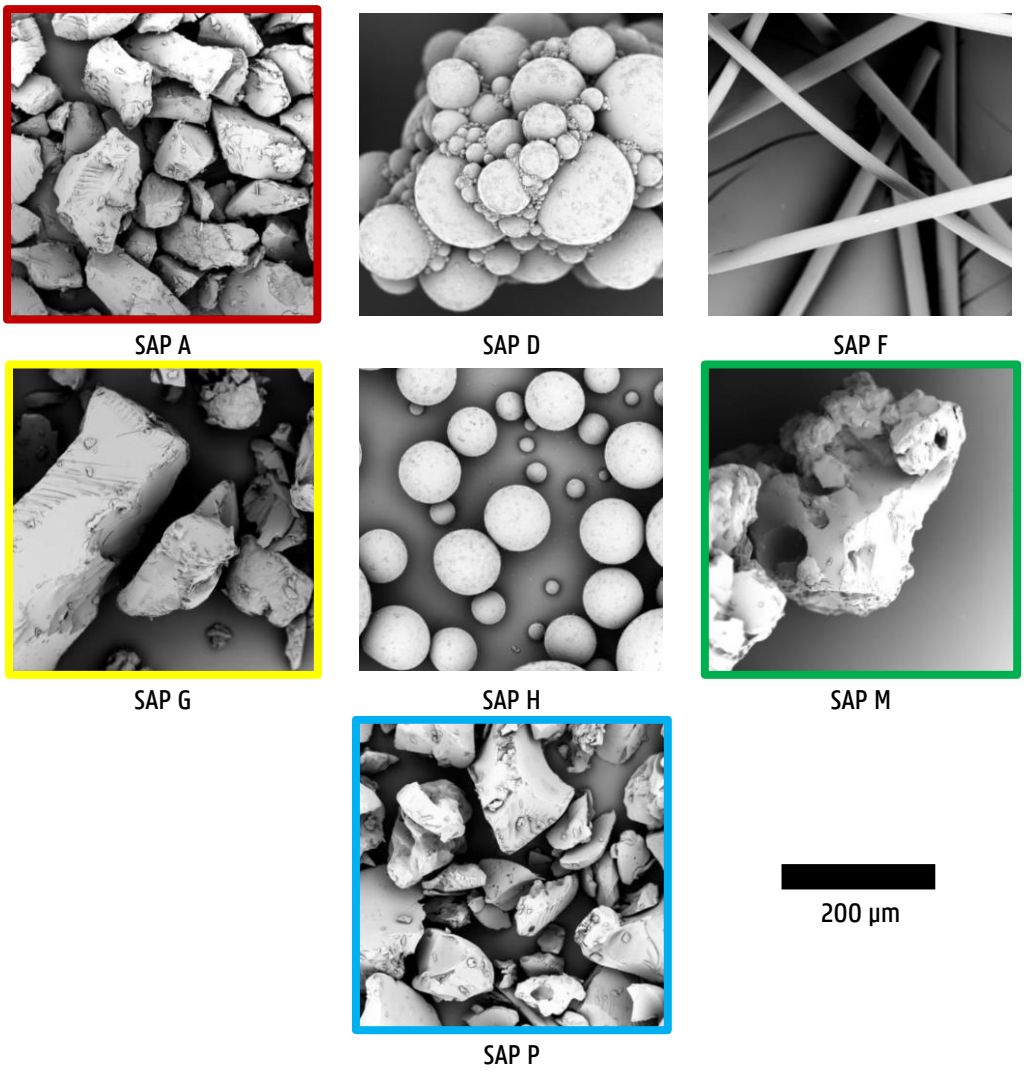

Figure 14: SAPs used in this research [42]

It is noted that only the highlighted polymer types will be used after printability optimisation in § 5.1 as SAPs D, F and H deemed inadequate. SAPs A, G, M and P all have bulk densities of around 700 kg/m^3 and true densities of ca. 1,400 kg/m^3 [42].

3.6. Reference mixture

During the experimental research, a mix design based on the work of Khalil et al. [73] was used as reference for developing new mixes with superabsorbent polymers. The reference mixture (denoted REF) has a total water-cement ratio of 0.365, equal to the effective water-cement ratio, as no additional water is used in absence of SAPs. The mix consists of all basic components as discussed above (except for SAPs), in portions as tabulated in Table 4.

Table 4: Mix design of reference mixture REF

Component	Mass [g]	m% of cement
CEM I 52.5 N Strong	675.00	N.A.
CEN standard sand	1350.00	N.A.
Water	246.38	36.50
MasterGlenium 51 con. 35 %	1.01	0.15

This reference mixture was chosen for its good 2D printability (see next chapter) as well as for the extensive research that had already been done or was carried out at the moment by other researchers.

In the mixtures with superabsorbent polymers, an additional mass of 37.125 g water is added to obtain a total w/c of 0.42, following from Powers' model. The amount of SAPs is then determined by trial and error to compensate the additional mixing water and reduce the effective w/c to 0.365, in accordance with REF. The exact optimisation process is explained in detail in chapter 5.

3.7. Storage conditions

All dry materials including SAPs, and the SP were stored in sealed containers at a temperature of 20 °C and deprived of light. Tap water at a temperature of 20 °C was used during testing.

METHODS

Decor autem est emendatus operis aspectus probatis rebus compositi cum auctoritate. Is perficitur statione, seu consuetudine aut natura.

MARCUS VITRUVIUS POLLIO

DE ARCHITECTURA | LIBER PRIMUS | CAPUT SECUNDUM

Consistency is found in that work whose whole and detail are suitable to the occasion. It arises from circumstance, custom and nature.

4. Methods

This chapter deals with all mixture preparation and testing procedures.
As more than fifteen different experimental setups were employed throughout this research, they are subdivided according to the main subject they will evaluate (cf. § 1.2 The goal):

1) Preparation;
2) Characterisation;
3) **Printability**;
4) **Early age shrinkage**;
5) **Mechanical properties**;
6) Statistical analysis.

4.1. Preparation

In this section the mixing and printing procedures to produce test specimens, are clarified.

4.1.1. Mixing procedure

All components were weighed, and the SP is shaken in its container for about 20 s and left to rest for 60 s prior to extracting 1 ml from the whole using a syringe. The superplasticiser was then added to the measured amount of water by drawing water in the syringe and expulsing it again, repeating this three times. SAPs were weighed accurately up to 0.1 mg.

The stainless-steel mixing bowl and stirrer were always soaked in fresh water in between mixing processes. Just before they were put to use, they were each swung ten times to remove excessive water and leave them surface-moist.

Two slightly different mixing procedures were followed in this research. The first one is according to NBN EN 196-1, as presented in Table 5.

Table 5: Mixing procedure 1

Step	Duration [s]	Speed [rpm]	Description
1	30	140	Mixing of cement + SAP
2	30	140	Immediately adding water + SP and mixing the whole
3	30	140	Gradually adding sand
4	30	285	Increased rotational speed
5	30	0	Scraping off material from the sides of the bowl
6	60	0	Rest
7	60	285	Increased rotational speed
+	270	N.A.	Total mixing time

The second procedure is a slightly adapted version of the above-mentioned mixing procedure and is applied in 2D printing experiments in the Magnel Laboratory for Concrete Research (Table 6).

Table 6: Mixing procedure 2

Step	Duration [s]	Speed [rpm]	Description
1	30	140	Mixing of sand + cement + SAP
2	30	140	Immediately adding water + SP and mixing the whole
3	30	285	Increased rotational speed
4	30	0	Scraping off material from the sides of the bowl
5	60	0	Rest
6	60	285	Increased rotational speed
+	240	N.A.	Total mixing time

It is important to note that in mixing procedure 2 sand is added first to the surface-moist bowl, after which cement and SAP are respectively added on top.

Unless stated otherwise, mixing procedure 2 was followed. At the end of this procedure, the time passed since first contact of water and cement amounted to 3 minutes and 30 seconds.

4.1.2. Printing procedure

2D printing of mortar was done by means of a Quikpoint mortar gun with a Black & Decker 5.2 Amp drill built in (Figure 15) [81].

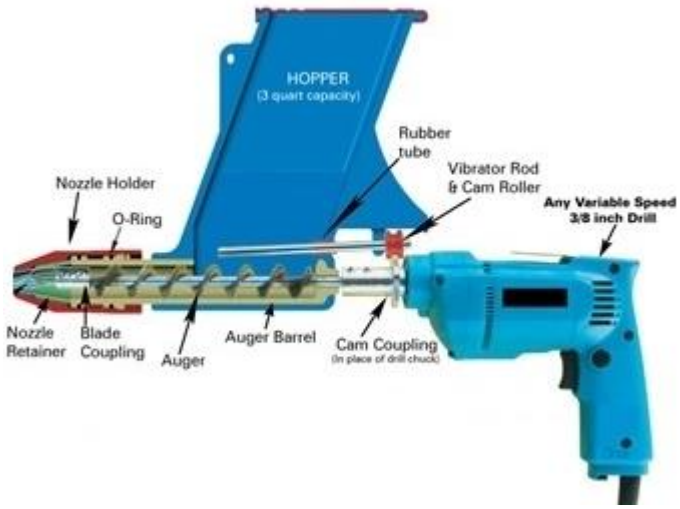

Figure 15: Quikpoint mortar gun [81]

During the 2D printing experiments, the mortar gun was mounted vertically on a fixed steel frame, in turn fixed to a rigid printing table. The printing table was provided with a sliding steel carrier in which the printing substrate (see next paragraph) could be placed. The mortar gun could be altered in height for the nozzle to have the required clearance above the printing

substrate. The carrier was moved by means of a rotating stainless-steel rod, of which the rotational speed was varied in a complementary software program. The rotational motion of the rod was then transformed into a smooth translational motion of the carrier. The rotational speed of the auger (Figure 15) could be influenced by manually changing the voltage input of the drill.

The carrier is about 30 cm long, 10 cm wide and has a raised edge of 2 cm. It is able to move over its whole length under the nozzle. The latter has an elliptical opening of 3 cm x 1.5 cm and a height of 6 cm.

For all experiments, the printing procedure was consistently carried out as follows:

- The hopper's internal surface was wetted by means of a water spray bottle providing an even mist twice.
- A sufficient amount of the mortar mixture (i.e. one third of a batch) was fed to the hopper and the mass was gently pushed towards the opening at the auger and vibratory rod.
- The drill voltage was set to the required value (e.g. 45 V for the reference mixture) and left as such for the remainder of the procedure.
- A test run, to establish a good mortar flow, was done by switching on the mortar gun but leaving the carrier stationary. By doing so the auger barrel and nozzle filled up with mortar. The extruded quantity was captured and disposed.
- The printing substrate (infra) was placed in the carrier and the latter was moved to the starting position, i.e. with one end right under the nozzle.
- The mortar gun was moved in height, providing a clearance of 1.5 cm between the nozzle and the substrate (or previously printed layer).
- The rotational frequency of the carrier rod was set to 750 Hz, which corresponded to a translational speed of the carrier of 1.7 cm/s.
- Next, the mortar gun and carrier were switched on simultaneously and the hopper mass was manually gently pushed towards the auger to maintain a smooth flow.
- In case a layer had to be printed upon another layer, the same printing direction was adopted.
- After each printing operation (of one mixture), the mortar gun was cleaned extensively.

The flow rate of the reference mixture provided by the mortar gun in the conditions described above, amounted to 8.4 cm^3/s: that is 1.7 cm/s translational speed times 1.5 cm of layer height times 3.3 cm of layer width. It was intended to keep the width of the extruded layer within 10 % deviation on the nozzle width for all mix designs.

Generally speaking, the time gap between two superposed layers was negligible. When a time gap of 15 or 30 min was demanded, the gun was cleaned after every mortar batch so that no old material could contaminate the new. The second layer was always printed from a new batch with the same initial workability as the underlying layer.

4.1.3. Printing substrate

As some of the experiments require the filaments to shrink (or expand) unrestrained, a proper printing substrate treatment was needed that allowed them to move as freely as possible on the supportive surface. Therefore, the standard substrates (clear glass plates) were manipulated consistently for all experiments in the following way (Figure 16):

- A layer of talcum powder (ca. 0.05 g/cm^2) was applied on the entire plate surface.
- Cling film was cut transversely to the width of a glass plate and put on top of it.
- Both ends of the cling film were taped to the bottom of the plate.
- After printing the filament, the cling film was cut just in front and after the layer(s) with a sharp knife, freeing the movement of the specimen in time. This was done carefully as to not move the filament or introduce shear stress in it.

Figure 16: Printing substrates

4.1.4. Laboratory conditions

All mixing and printing procedures as well as most experiments were carried out in a climatized room, where a temperature of 20 °C ± 3 °C and relative humidity of 65 % ± 5 % were upheld throughout. All samples were stored in this room until the day of testing.

4.2. Characterisation

In this section all testing procedures characterising SAPs and the optimal mix designs of the mixtures with SAPs are discussed.

4.2.1. Swelling capacity

The swelling capacity of the available SAPs, as tabulated in the previous chapter (Table 3), was evaluated by means of a filtration method based upon the recommendations by RILEM [64]. The purpose of this test lay solely in ascertaining the SAPs still possessed the same swelling characteristics as defined by Snoeck in [42], as they might have lost some of their initial SC under the influence of time and UV light. This test was only to be indicative of consistent behaviour, and therefore a less comprehensive variant of the complete method sufficed.

The swelling capacity was established for all available SAPs in both demineralised water and cement filtrate (only stirred for 4 hours instead of 24 hours). The tests were executed in singular and for an allowed swelling period of only 5 minutes.

4.2.2. Surface moisture

The evolution of the surface moisture of printed filaments in one hour was observed by gently pressing blotting paper strips on top of it every 15 min and measuring their change in mass. The Aurora ref. 10 blotting paper with an areal density of 125 g/m^2 was cut to strips of approximately 7.5 cm x 2.5 cm, to allow three of them to fit on the surface of one filament (cf. § 4.1.2).

The mass of absorbed surface fluid per unit area κ [g/cm^2] of one paper strip is obtained by going through the subsequent steps:

- The paper strip is weighed with a precision of 0.1 mg (m_{dry} [g]).
- The strip is placed on the surface of a printed layer at the predefined time and pressed onto it by means of a plastic weight for a duration of 60 seconds. The weight exerts a uniform pressure on the strip of 77.5 Pa $\pm$ 0.1 Pa.
- The paper is carefully yet swiftly removed from the surface using metal tweezers and put into a closed petri dish to prevent evaporation.
- Immediately after, the strip is weighed again (m_{sat} [g]) to find its mass after possible absorption.
- The mass of the amount of fluid absorbed from the filament surface m_{abs} [g] is then obtained by subtracting m_{dry} from m_{sat}.
- The exact surface of the paper strip A_{strip} [cm^2] was obtained by reverse calculation knowing the areal paper density and the initial dry weight of the strip.
- The mass of absorbed surface fluid per unit area of the paper strip is found by dividing m_{abs} by A_{strip}.

The maximum areal mass of absorbed water κ_{max} was obtained by spraying water on the paper strips until fully saturated. It is used as a reference value which cannot be exceeded by the ones resulting from the above testing procedure.

4.2.3. Setting times

A MATEST Vicatronic served in the automatic Vicat testing of all studied mortars according to NBN EN 196-3. The device automatically measures the penetration depth of its probing needle (⌀ 1 mm) every 15 min over a period of 21.5 hours. The results of the Vicat tests were analysed according to NBN EN 196-3 to obtain the initial and final setting times of each mixture. The initial setting time was determined when the penetration depth read 6 mm $\pm$ 3 mm and the final setting time when it first dropped below 0.5 mm. Each mix design was only tested once, reducing the statistical value of its result.

4.2.4. Microscopy

The sizes of dry and swollen SAPs as well as the pores in longitudinal sections of hardened double-layered specimens (cf. § 4.2.5, Figure 17) were visually inspected and photographed by means of a Leica DFC295 digital microscope colour camera. The acquired images were then analysed making use of the software ImageJ. A multitude of similar subjects (ranging from 9 to 90 depending on the test case) was measured in two perpendicular directions. The average of these measurements was taken as diameter of the equivalent spherical object.

4.2.5. Air content

The air content of hardened double-layered specimens was analysed according to the linear traverse method as described in ASTM C457 by means of a fully automated Concrete Experts International RapidAir 457 device. The printed filaments are longitudinally sawn in half at an age of 28 days and both sides (hatched facade in Figure 17) are polished with variable grading and dried afterwards at 35 °C for one hour. After polishing, the surface of the samples was treated with black ink and barium sulphate ($BaSO_4$) to increase the contrast between the air void and cementitious matrix. In case white spots that were not caused by air or SAP inclusion, but by a clear granulate section, showed on the surface, they were marked black as to remove them from the analysis.

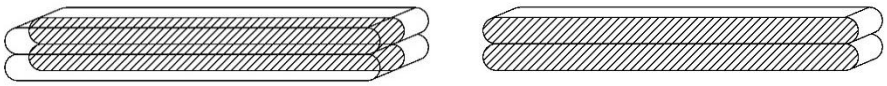

Figure 17: Longitudinal section of a double-layered specimen

Figure 18 shows the path the camera of the device takes starting in the upper left corner and following the red and green arrows. The camera moves stepwise, taking overlapping pictures about 1 cm^2 of surface at a time. In these images, three parallel lines (called chords) are drawn in the direction of the measurement. The total lengths of these chords as well as the lengths and number of segments that encounter a white background (coloured red in Figure 18) are used to determine the air void percentage [74].

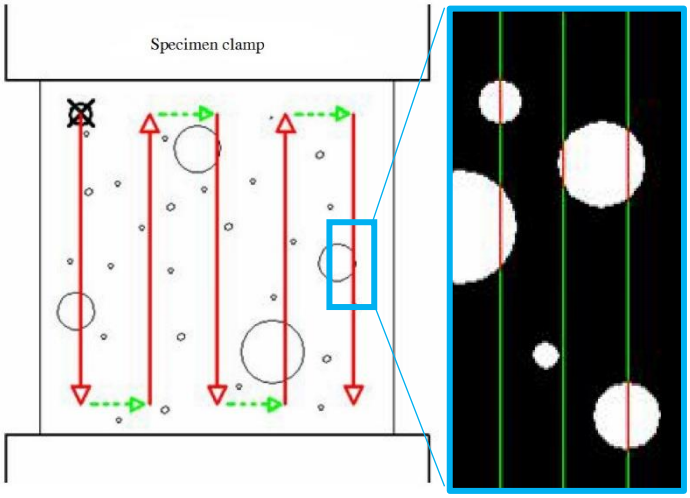

Figure 18: RapidAir 457 air content measurement method [74]

ASTM C457 recommends a total chord length of at least 2,413 mm in case the granulates in the hardened mortar have a maximum diameter smaller than 25 mm, which was the case for all mix designs. However, as the length of complete double-layered specimen neared 30 cm, which was too big to secure between the clamps (Figure 18), it was halved transversely as well. In that way, four longitudinal sections were tested for each mix design, with a total chord length of at least 2,200 mm.

The RapidAir 457 is limited to a range of void sizes between 8 µm and 10 mm [74]. Smaller pores can be studied by means of mercury intrusion porosimetry, as discussed in the next paragraph.

The most important characteristics obtained during air void analysis include:

- histograms and (cumulative) distributions;
- the total chord length Λ [mm];
- the total length of chord segments intersecting voids λ [mm];
- the air content λ/Λ, usually expressed as percentage;
- the total number of voids encountered N_{voids};
- the mean void diameter Φ [mm], assuming spherical volumes (Equation (14)):

$$\Phi = \frac{3\lambda}{2N_{voids}} \tag{14}$$

4.2.6. Mercury intrusion porosimetry

Capillary pores, having a diameter between 10 nm and 10 µm, were studied with mercury intrusion porosimetry (MIP) measurements (PASCAL series 140 and 440, Thermo Fisher Scientific Inc). Gel pores with a diameter smaller than 10 nm can be examined by means of adsorption tests, but were not considered in this research as the focus lay on the influence of SAP addition.

The contact angle θ [°] of mercury on concrete equals 140°, giving mercury a spherical head when flowing through a small concrete pore. However, the metal still needs to be pressurised in order to enter the pore network as it has a surface tension ζ of 0.483 N/m (in laboratory conditions) [42]. The relationship between applied pressure p [Pa] and the capillary pore radius r [m] entered, is given by Washburn in function of θ and ζ (Equation (15)):

$$p = \frac{-2\zeta\cos(\theta)}{r} \tag{15}$$

This equation assumes a regular, cylindrical and continuously connected pore network, which is not the case in reality. Figure 19 shows a representation of different pore types: a) continuous pore; b) continuous ink bottle pore; c) dead-end ink bottle pore; d) isolated pore [74].

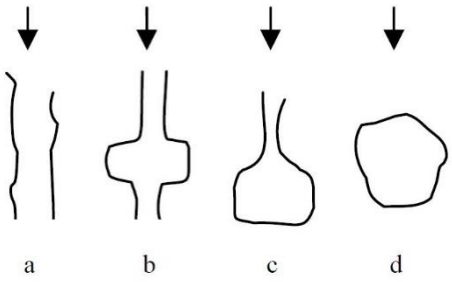

Figure 19: Schematic of different pore types [74]

The amount of mercury that is able to enter the pore network is a measure for the porosity of the concrete specimen. However, as illustrated in Figure 19, some pore types do not participate in the distribution of mercury. Only continuous pore types do, and even then will the ink bottle pores account for a measurement of only the smallest opening diameters, as they require a larger pressure on the metal (which gradually increases during the test). The presence of dead-end and isolated pores can lead to an underestimation of the complete void volume.

Cylinders with a diameter of 14 mm were bored out of hardened double-layered filaments and freeze-dried at an age of 28 days (Figure 20). Such a cylinder was then put in a cylindrical testing cell of 19.0 mm diameter and 22.2 mm height, after which the mercury intrusion porosimetry was commenced. For each mix design only one MIP test was executed.

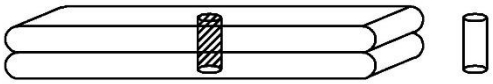

Figure 20: 14 mm diameter test cylinder for MIP

The most important results obtained from MIP measurements include:

- the cumulative intrusion curve which plots the specific pore volume per mass of test cylinder Y [mm^3/g] in function of the pore diameter $d = 2r$ [mm] (or radius);
- the derivative intrusion curve $dY/dlog(d)$, being the cumulative one derived to the logarithm of the diameter;
- the median pore diameter d_m [mm].

4.3. Printability

In § 2.1.3 it became clear that defining the printability is not straight forward. For one, it is a combination of pumpability, extrudability and buildability and no standardised tests exist for these yet. One typical workability test was executed in this research as well as a descriptive qualification of the general printability.

4.3.1. Workability

The workability of all mix designs was evaluated according to the flow table test (NBN EN 12350-5) performed at 3, 10, 15, 20, 25 and 30 min after finalising the mixing process. It was executed for both mixing procedures 1 and 2 (cf. § 4.1.1) as it would seem that the result

is dependent on that choice. Apart from the double diameter reading that was performed with half a centimetre accuracy, contrary to the 10 mm recommended in the norm, the latter was followed to the letter.

The mix design optimisation in this research was based on these workability results, applying mixing procedure 2, and keeping the flow diameter in the range of $\pm$ 0.5 cm of that of REF by means of trial and error.

4.3.2. Printability qualification

The overall printability was qualitatively evaluated, based on criteria proposed by Papachristoforou [19] in Table 1 and own findings during the printing process. The qualification only holds for the first five minutes after finishing mixing procedure 2.

The following properties are observed to evaluate the printability of the mortar mixtures:

A) the flow table workability, three minutes after mixing as a measure for immediate pumpability;
B) the drill voltage needed for a flow rate of 8.4 cm^3/s (cf. § 4.1.2) as a measure for the viscosity of the mixture and its associated pumpability too;
C) the surface smoothness and absence of tears in the filament as a measure for extrudability;
D) the dimensional stability of a single layer as a measure for its buildability;
E) the dimensional stability of the lower layer when a new one is printed on top, as a measure for its buildability.

The last three criteria are evaluated in comparison to the reference mixture with the scores shown in Table 7. The numerical scores were used in comparative graphs to show the results more comprehensibly.

Table 7: Scores for printability properties

Emoticon	Score	Description
☺	+2	"This mix design performs best."
🙂	+1	"This mix design performs better than REF but worse than the best."
😐	0	"This mix design performs as good as REF."
😕	-1	"This mix design performs worse than REF but better than the worst."
☹	-2	"This mix design performs worst."

4.4. Early age shrinkage

As no standardised techniques to measure the (early age) shrinkage of printed specimens exist yet, new methods were devised making use of test equipment available.

4.4.1. Unprotected shrinkage in height via automated laser measurement

The in-house developed automated laser measurement (ALM) table was used to measure the height evolution of single printed filaments in time. The table is fitted with a high precision laser beam sensor ILD 1800-50 and optoNCDT 1800 interface, manufactured by Micro-Epsilon Messtechnik. It is mounted on a carrier with two stepping motors in both main directions of the table. The laser has a resolution of 5 µm, translated into a measurement precision of 0.3 ‰ for filaments of around 15 mm height.

Single layers of about 15 cm length (Figure 21) were printed and the substrate was fixed to the ALM table. By doing so, consistently the same 3 parallel laser paths over the length of the specimen could be followed to measure their height at different ages. The evolution was monitored over 24 hours, starting the first measurement at 6 min and 30 s after printing, with at least one more survey until the final one a day later at the exact hour. Each time about 2 cm of fixed wood was measured as well to act as reference level.

Figure 21: ALM test specimen

The measured data was edited and analysed as follows:

- The laser dot coordinates were transformed into layer heights using the reference level.
- The outer two centimetres of the path were cut off from the analysed data, to discard outliers associated with the uneven ends of the filaments.
- The remaining segments were averaged in height as the number and exact longitudinal position along the path length of the laser dots was different each time.
- This average specimen height was then compared to those at other ages but over the same laser path.
- The shrinkage was calculated with respect to the first measurement.

4.4.2. Autogenous shrinkage by means of corrugated tube measurements

The autogenous shrinkage of all studied mortars was monitored on corrugated tubes with digital dilatometers according to ASTM C1698 (Figure 22).

Figure 22: Auto-Shrink dilatometry (ASTM C1698)

A polyethylene normative corrugated mould was filled with the test mixture, making use of the mortar gun as to minimise the amount of entrapped air. In between filling steps (3 in total), the tube was shaken on a vibration table for 30 s to make the air float up and the mortar fill the corrugations. The sealed mould was ensured to have an end-to-end length of 420 mm $\pm$ 5 mm. The exact initial length was recorded manually (Figure 22) and used to accurately obtain the lengths at older ages. Afterwards, the tube was placed in an automatic continuous measuring frame with digital dilatometers with a deformation range of 5 mm. Each mix design was observed in triplicate for 7 days, recording the movement every 10 minutes.

The linear autogenous strain ε_{auto} [µm/m] is obtained as follows (Equation (16)):

$$\varepsilon_{auto} = \frac{L(t) - L(t_{ref})}{L(t_{ref})} \cdot 10^6 \text{ µm/m} \quad (16)$$

with:

- $L(t)$ [mm], the length of solely the concrete element inside the mould, at time t;
- t [s], the time instant, starting at $t = t_0 = 0$ s, i.e. the moment of first contact of water and cement;
- t_{ref} [s], the reference time instant, at which ε_{auto} is zeroed out. According to ASTM C1698, t_{ref} should be taken equal to t_{fs}, the final setting time according to the Vicat test. However, other ages will be used as reference instant as well, in comparison to results of other measurement techniques (cf. infra).

This results in graphs of $\varepsilon_{auto}(t)$, which were visually inspected to find the knee-point: a distinctive bending point which implies the transition of the element in a suspension to a solid state [35]. Usually the knee-point comes after the final setting time as determined in Vicat testing, which indicates that the latter might not reflect the real microstructural change accurately [75]. Therefore, graphs with $\varepsilon_{auto}(t)$ zeroed out at t_{kn}, the time at knee-point, and at final setting as determined by means of the Vicat testing, were used for analysis. Both times then served as time zero. The derivative $d\varepsilon_{auto}/dt$ was studied as well, to quantify the change in rate of shrinkage over time. According to ASTM C1698, the standard deviation in shrinkage of the studied mortars equals 28 µm/m.

4.4.3. Unprotected shrinkage in the horizontal plane by means of photographic image digital analysis

Auto-Shrink dilatometry allows assessment of the (chemically driven) autogenous and self-desiccative shrinkage in time, as it seals off the concrete from the environment. Consequently, plastic shrinkage is therefore not accounted for in the previous technique. But since it has a considerable share in the overall unprotected shrinkage it was deemed paramount for this research to be quantified (cf. § 2.2).

In order to do so, single-layer printed filaments were photographed with 5-minute intervals, taking the first picture 6 min and 30 s after finishing mixing procedure 2, or equivalently 10 min after the first contact of water and cement. Figure 23 shows the setup of the Logitech C920 Full HD 1080p webcam and underlying object.

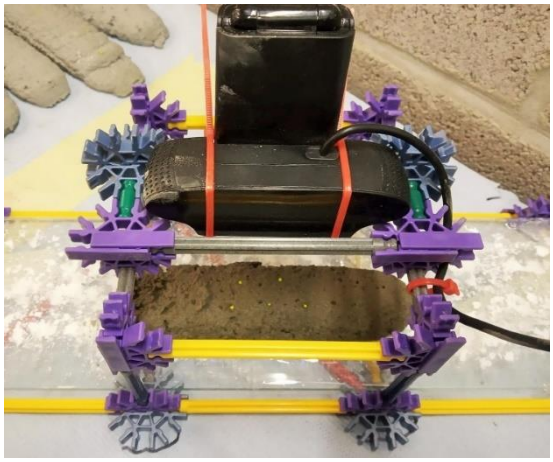

Figure 23: Camera setup for photographic image digital analysis

The object is a mortar filament of about 15 cm long that has 5 fluorescent yellow focussing points randomly placed on its surface. The focussing points are made of 0.5 mm thick iron wire, cut to a length of 1 to 2 mm and covered in metallic paint. They serve to aid the digital image analysis software GOM Correlate to register the changes in time of the same surface of interest. That measures about 33 mm x 72 mm or respectively 285 x 622 pixels at a focal length of around 6 cm. As such, one pixel accounts for ca. 0.116 mm or a possible strain error of about 1.6 ‰ longitudinally and 3.5 ‰ transversally. According to NBN B15-002 an estimated unprotected shrinkage of about 4 ‰ is expected at the age of 7 days and in the laboratory conditions as defined in § 4.1.4 [78]. This suggests that the proposed testing procedure might overestimate the shrinkage, and that a higher precision camera would be more reliable. However, prior testing has proven the procedure to be fairly accurate for the overall measured two-dimensional shrinkage lay in the range of one percentage point.

For the first 24 hours the pictures were analysed 20 at a time, with a digital mesh of 15 x 15 pixels applied to the surface of interest. The following 6 days of recorded material was analysed at 30-minute intervals, 30 images at a time and with the same mesh size implemented. The earliest photograph was taken reference for all others, to which the mean technical strain ε_{cam} was calculated in both the longitudinal (x) and transverse (y) direction (Equation (17)):

$$\varepsilon_{cam,i} = \left(\frac{\Delta l}{l_0}\right)_i \tag{17}$$

in which:

- i [-] denotes the strain direction: x or y;
- Δl [mm] equals the difference in directional length of the complete surface of interest: negative in the case of contraction; positive in the case of extension;
- l_0 [mm] is the initial directional length of the surface of interest.

By overlapping each set of m images (20, respectively 30) with one picture, the strains could be referenced to the very first image at 6 min 30 s after mixing. Let $\varepsilon_{cam,k,1}$ be the first strain, calculated according to Equation (17), of a total of $(m-1)$ strains going with set k and $\varepsilon_{cam,k-1,m-1}$ be the last strain of set $(k-1)$, then $\varepsilon_{cam,k,1}$ can be expressed in reference to the first image of set $(k-1)$ by the following expression (Equation (18)):

$$\varepsilon_{cam,k,1} + \varepsilon_{cam,k-1,m-1} + \varepsilon_{cam,k,1} \cdot \varepsilon_{cam,k-1,m-1} \tag{18}$$

This procedure can be followed for all strains 2 to $(m-1)$ of set k and in expansion for all strains of successive sets.

For the sake of adequate comparison to ε_{auto}, the obtained array of strains $\varepsilon_{cam,i}$ was reverse calculated to equivalent instantaneous lengths, after which Equation (16) was used. In the reverse calculation the initial sample length and width were assumed, i.e. 72 mm and 33 mm respectively. The factor (100 % $-$ $\varepsilon_{cam,i}$ [%]) at each predefined time allowed to find the instantaneous length (and width) of the surface of interest, by multiplication to the initial dimensions.

The test was executed in triplicate for each mix design during 24 hours and only once for each mix design over a period of 7 days (with the exception of REF, that was monitored twice).

4.5. Mechanical properties

In this chapter the testing procedures to evaluate the mechanical properties of double-layered specimens are explained, focussing on the strength of the interlayer. In all of the following tests, drilled cylindrical samples with a diameter of 25 mm are used (Figure 24) and test results show the properties of these samples at an age of 28 days.

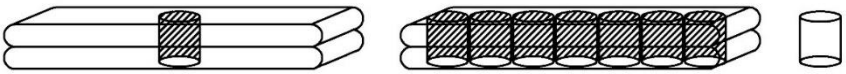

Figure 24: 25 mm diameter cylinders used in mechanical property tests

4.5.1. Compressive strength

The compressive strength perpendicular to the printing plane, f_c [N/mm^2] was determined by means of a Walter+Bai Series DBC testing machine. The cylindrical samples represented in Figure 24 were sawn to a height of approximately 25 mm, by removing top and bottom layer. As such the prisms obtained even bases required for a good result of the testing procedure, being a failure state as shown in the middle of Figure 25 [76]. To compensate the possible unparallelism of both bases during testing, 3 mm thick high-density fibreboard plates were put in between the

bases and the hydraulic press stamps. This also reduces the spread in test results, especially for specimens with a small height.

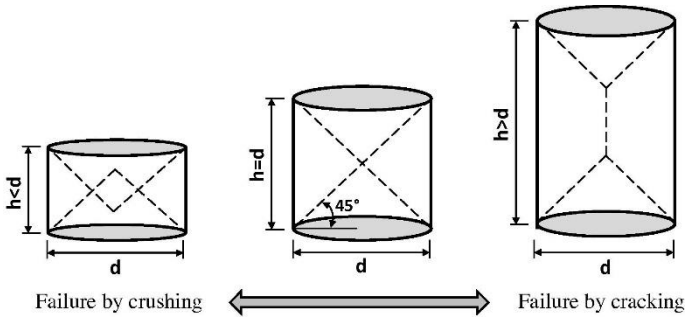

Figure 25: Failure states of concrete cylinders subjected to compression [76]

The mean diameter and height of each element were measured with a precision of 0.01 mm, and the weight was noted in centigrams. The procedure happened in accordance with recommendations stated in NBN EN 12390-3 under load control conditions with an incremental rate of 100 N/s. The number of test specimens for each mix design ranged from a minimum of 3 to a maximum of 5.

4.5.2. Interlayer bonding strength

The drilled cylindrical specimens (Figure 24) were sawn to a height of approximately 10 mm, making sure the interlayer was positioned right at the centre of the piece. The top and bottom bases were then coated in Sikadur 30 two-component epoxy and glued to circular or rectangular prismatic steel dollies (Figure 26, left). The epoxy glue had, at the moment of testing, an internal tensile strength of 21 MPa and adhesive strengths of 8 MPa to concrete and 21 MPa to steel. These values clearly exceeded the tensile strengths of the interlayers tested.

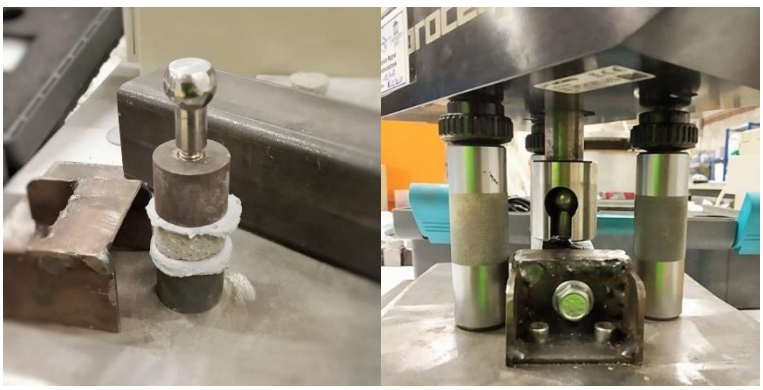

Figure 26: Interlayer tensile strength test setup

One of the steel mounts was then anchored to a rigid table, while the other one was connected to the testing knob of a Proceq DY-2 pull-off device (Figure 26, left and right). The tensile test was executed according to NBN EN 1542, however with the following alterations:

- the tested specimens have different measurements;
- the test was carried out load controlled at an incremental rate of 50 N/s;
- the deformation rate was monitored instantaneously and limited at 78 µm/s.

The tensile force at failure F_t [N] was recorded and divided by $\pi(25/2)^2$ mm^2 to obtain the tensile strength f_t [N/mm^2]. It is important to note here that only results of failures that clearly happened at the interlayer were taken into account. At least 3 cylindrical specimens were tested for each mix design.

4.5.3. Interlayer shear strength

The same procedure as defined in the previous section was followed to assess the ultimate shear force F_s [N] and equivalent shear strength f_s [N/mm^2] of the interlayer. This time however, the setup was slightly altered to the one shown in Figure 27.

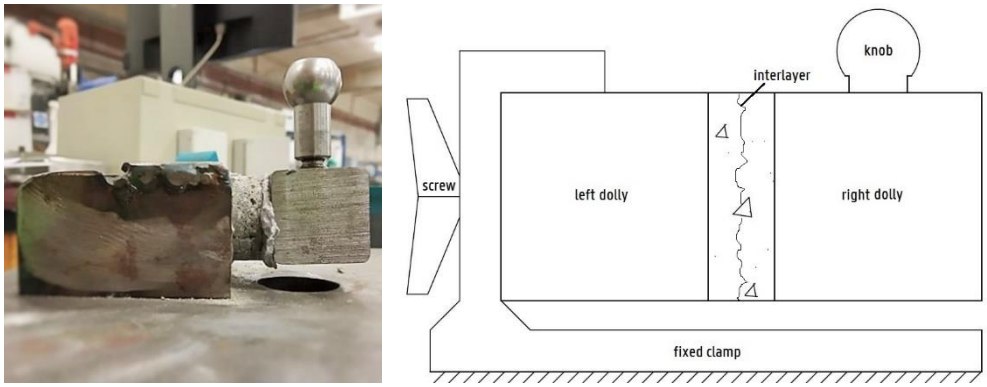

Figure 27: Interlayer shear strength test setup

The test setup will inevitably induce bending tension in the specimen as well, though deemed of minor importance to the result at failure given the rigidity and small dimensions of the steel dollies. To minimise the influence of bending even more, the concrete cylinders were sawn to a height of only 8 mm, keeping the interlayer centred. The success rate of testing was considerably lower than for other mechanical tests, as such at least 9 specimens were tested for each mix design (with the exception of those printed with a 30 minute time gap that always failed at the interlayer: then only 4 specimens were tested).

4.6. Statistical analysis

The goal of this research lies in analysing the potential influence of SAP addition on printability, early age shrinkage and mechanical properties (of the interlayer). As all available polymers had different chemical and physical characteristics, it is essential to take these into account by comparing the test results statistically and establishing their level of significant difference. The software program SPSS Statistics 25 was used to perform the following analyses:

- An independent-samples t-test was executed for the comparison of two means. It was reasonably assumed in this research that the tested specimens of different mix designs were indeed independent from each other.
- Multiple means are compared by doing a (one-way) analysis of variance (ANOVA) as t-tests will suffer more type-I errors due to multiplicity. ANOVA only concludes whether there is a significant difference between at least one set of two means, but it does not reveal which means mutually differ. Additional tests are required to do so.

- In case of homogeneity of variances (verified by means of a Levene's test), the Student-Newman-Keuls (SNK), Bonferoni and Tukey multiple comparison tests were performed. With respect to efficiency and conservativeness this test scores moderately compared to other comparison tests available.
- In case of inhomogeneity of variances, a Dunnett's T3 test was carried out.
- Linear regression curves were plotted to evaluate the correlation between 2 variables, when thought valuable. In that case the coefficient of determination was checked to draw a substantiated conclusion.

Whenever deemed important in the next chapter (Results and discussions) the exact statistical method as well as its outcome are explained in detail. In general (and if not stated otherwise), a significance level α of 5 % was implemented, but for some analyses it was more relevant to obtain the effective significance α_{eff}. In all statistics a sample size n of at least 3 was available.

RESULTS & DISCUSSIONS

Item si umor occupavit corporum venas inparesque eas fecit, cetera principia ut a liquido corrupta diluuntur, et dissolvuntur conpositionibus virtutes.

MARCUS VITRUVIUS POLLIO

DE ARCHITECTURA | LIBER PRIMUS | CAPUT QUARTUM

Bodies which contain a greater proportion of water than is necessary to balance the other elements, are speedily corrupted, and lose their virtues and properties.

5. Results and discussions

The laboratory work started off with the optimisation of mix designs with superabsorbent polymers based on the flow table test. In the remainder of this essay, the notation X123 is used in which X denotes the SAP type: A, D, F, G, H, M or P and 1, 2, 3 denote the amount of X added in units of 1 m%, 0.1 m% and 0.01 m% of cement.

5.1. Printability

5.1.1. Flow optimised mix designs

The reference mixture, as defined in § 3.6, serves as standard for and basis of the new mix designs. As it has a water-cement ratio of 0.365, there is room for improvement with respect to full hydration optimisation. According to Equation (12) the additional amount of water w_{add} required to this end is then 37.125 g:

$$\begin{aligned} & w_{add} = (w/c)_{add} \cdot c \\ \overset{(12)}{\Longleftarrow} & (w/c)_{add} = 0.42 - w/c = 0.42 - 0.365 = 0.055 \end{aligned} \tag{19}$$

in which $c = 675$ g is the mass of cement in a normal testing batch of mortar (cf. Table 4). The reference mixture with additional water is denoted REF* and has a total w/c of 0.42, enabling complete cement hydration. REF* is the basic mix design to which a varying amount of SAPs is added, evaluated regarding their workability and optimised by trial and error.

As such the amount of SAPs added needs to compensate w_{add} by short time absorption during the mixing procedure (cf. § 5.2.1). The swelling times of the SAPs as determined by means of Vortex measurements, are sufficient to ensure complete swelling during mixing. Initial masses for the experimental iteration were based on the swelling capacities in cement filtrate as recorded in Table 3 [42] and halving those as recommended by Kovler [45].

The resulting optimal mass percentages of additional SAPs, by allowing a deviation of $\pm$ 0.5 cm on the flow table diameter of REF are tabulated in Table 8 for both mixing procedures. The initial iteration value in m% of cement, as derived from the reasoning above is also given. Percentages between brackets denote that the optimisation happened with respect to A015 instead of REF, as discussed below.

Table 8: Optimised mass percentages of additional SAPs
Values between brackets denote an optimisation with respect to A015 instead of REF

SAP	Initial estimate	Mixing procedure 1	Mixing procedure 2
A	0.18 m%	0.17 m%	0.17 m%
D	0.21 m%	(1.25 m%)	(0.78 m%)
F	0.23 m%	0.30 m%	(0.30 m%)
G	0.23 m%	0.25 m%	0.25 m%
H	0.28 m%	(1.50 m%)	(0.92 m%)
M	0.19 m%	0.22 m%	0.22 m%
P	0.19 m%	0.15 m%	0.15 m%

At the start of the experiments, A015 was considered a valid reference mixture with similar printability as REF. However, as Figure 28 shows for the evolution of flow table diameter after mixing procedure 1, the curves of A015 and REF diverge over time (< 30 min).

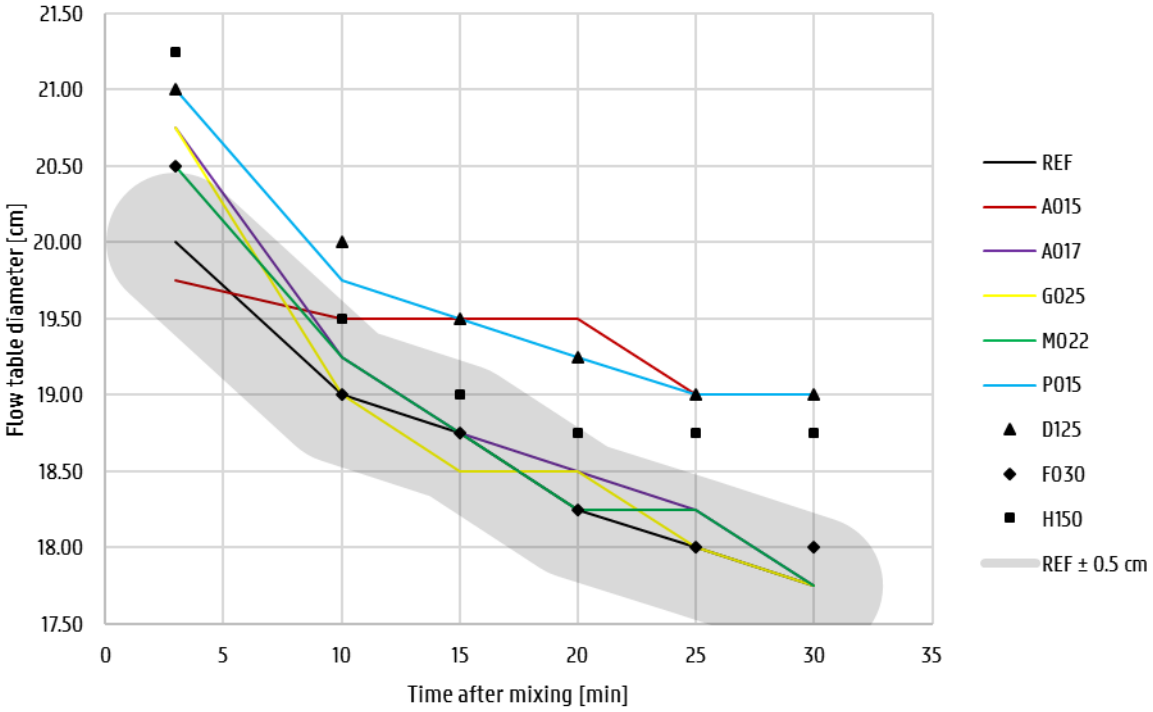

Figure 28: Flow table diameter in function of time, after mixing procedure 1 (n = 1)

Initially, the mixture with SAP A was not optimised to resemble the curve of REF, as A015 was regarded as an equally good printable and well-studied reference. Therefore, other mix designs that iteratively resulted in flow evolutions within the diameter range of A015 $\pm$ 0.5 cm were allowed as well and believed optimised.

When the actual printing tests were due and mixing procedure 2 was applied (as is standard at the laboratory), it was immediately noted that A015 had a very different flow behaviour, as did the mixtures with SAPs D, H and P. The printing tests were put on hold as to allow the flow table test to be repeated, however this time after mixing procedure 2.

Another curious observation was consistently made when mixing with SAPs D and F: during steps 4, 5 and 6 of mixing procedure 1, the substance was very dry and incoherent, but after the final step at an increased rotational speed, the mixture was rather moist and quite liquidlike. Furthermore, it was concluded that:

- the optimal mass percentage of D was too high, preventing it ever being used in large scale concrete construction practice;
- the swollen SAP F fibres were being broken by the mixing procedure (more specifically during the final step) due to their low strength in swollen state;
- the same holds for SAP D, with its grapes-like polymer structure that gets broken into single grapes, so to speak. However, this would increase the specific surface of the whole

and theoretically the swelling tendency as such (after adsorption to the surface). The reason of insufficient swelling capacity therefore lies in the swelling kinetics of SAP D rather than in it breaking up during mixing;

- for those reasons, SAPs D and F were to be disregarded in further research.

In the literature review the importance of the mixing procedure with respect to possible crushing of superabsorbent polymers was already put in mind.

When optimising the mix design with SAP H, it was remarked that a polymer addition below 0.6 m% induced little to no change in the overall workability. A relatively large and uneconomic amount of SAP H was needed to establish a flow like REF. This is ascribed to the fact that SAP H is the smallest of all being examined, comparatively quite slow in swelling, and has a quasi-exact spherical shape and a diameter of only 70 µm ± 34 µm. Therefore, being dry, it lies in the size range of CEM I 52.5 N particles with a mean diameter of about 10 µm [78] as shown in Figure 29 of the boundaries of the cumulative particle size distribution of ASTM Type 1 OPC [77]. It would seem that the mixing water attraction by the superabsorbent polymer is not sufficient enough to overcome the adhesion and almost immediate chemical binding of water to cement (cf. § 2.1.4.1). This was in a way already stated by Jensen & Hansen in [53] by concluding that the outer surface of a superabsorbent polymer is less active than the inner bulk (§ 2.3.1.3). And since a sphere holds the most volume for the least outer surface, the observation can be explained. Another possible explanation is that the H particles, assuming they would absorb mixing water, still have a spherical shape and as such do not influence the workability that much. However, since that influence was only marginally noted from addition of more than 0.6 m%, which is twice the amount estimated in Table 8, it cannot solely be ascribed to the positive effect of the spherical shape of swollen particles, but to a lack of swelling capacity as well. Polymer fibres sometimes suffer from a balling effect, by which they cling together and reduce the overall outer surface area and the combined swelling capacity as well. Microscopic study of hardened specimens of a SAP H mixture would be recommended to substantiate the above reasoning. On that basis, SAP H was ruled out of further research as well.

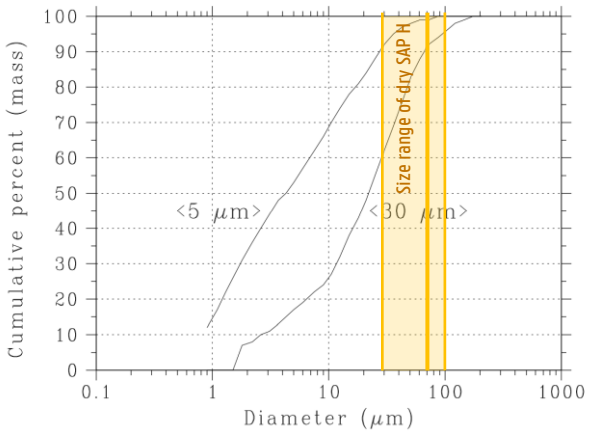

Figure 29: Boundaries of cumulative particle size distribution for ASTM Type 1 cement [77]

As such, only bulk-produced SAPs remained for further investigation as both extrusion (F) and suspension (D and H) polymers deemed uneconomic, vulnerable or too feeble for purpose.

Figure 30 shows the flow evolution over the first 30 minutes after mixing procedure 2. During this recapitulation of the flow table test, A017 was designed in answer to the diverging curves of A015 and REF. For the sake of completeness, A017 was also tested after mixing procedure 1 as shown in Figure 28.

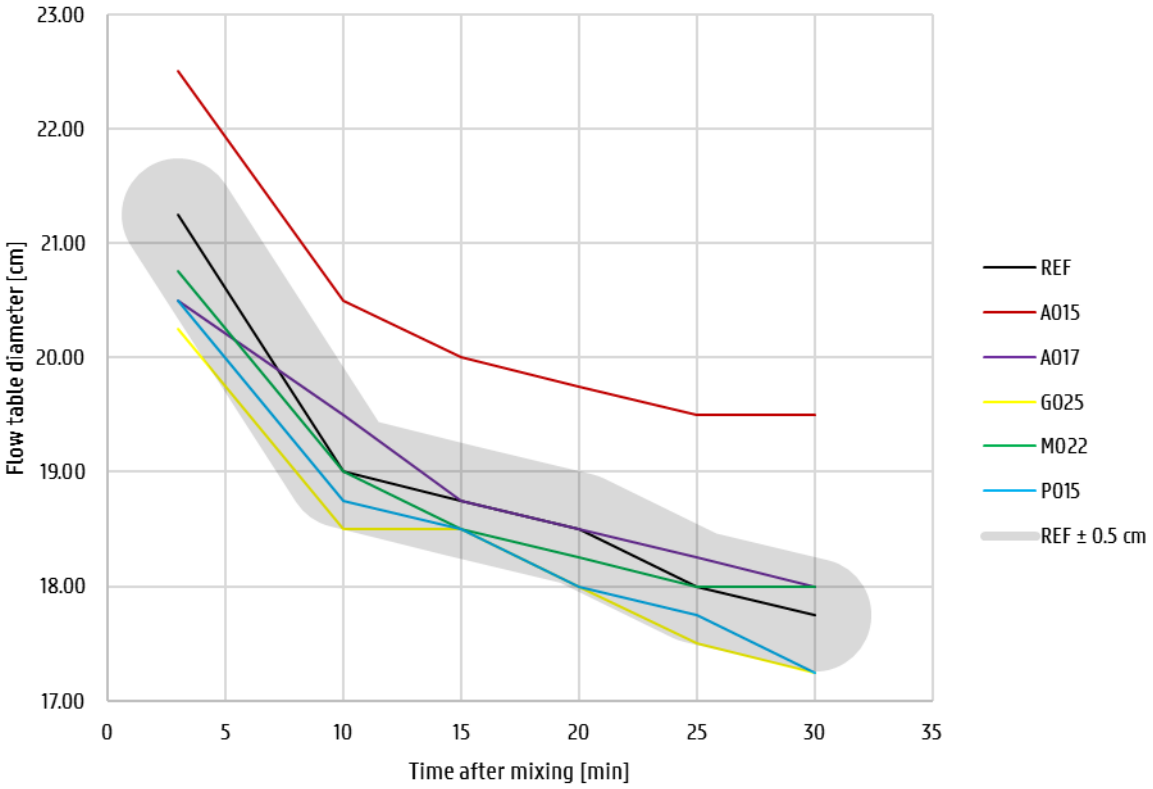

Figure 30: Flow table diameter in function of time, after mixing procedure 2 (n = 1)

Figure 30 shows the curve of A015 differing quite substantially from the other mix designs that were clearly optimised to resemble the workability of REF. As explained before, A015 will still be considered in coming tests, regardless of its flow table outcome.

Figure 31 compares the flow table diameters in time of all remaining optimised mix designs, for both mixing procedures (suffixes -1, respectively -2). A very important conclusion can be drawn from it: the flow table test result is dependent on the preceding mixing procedure:

1) REF shows similar curves for both mixing procedures, with curve 1 (for the respective mixing procedure 1) negligibly lower than curve 2 from 10 minutes on. Only immediately after mixing, procedure 2 results in a more flowable substance. It is believed of importance that the cement is put in a surface moist mixing bowl first in procedure 1, while in procedure 2 the cement is put on top of the sand mass keeping it from early contact with water. However, this early inequality of hydration rate is so marginal, it is disregarded. The exact reason why the initial flowabilities differ so much, remains unknown.

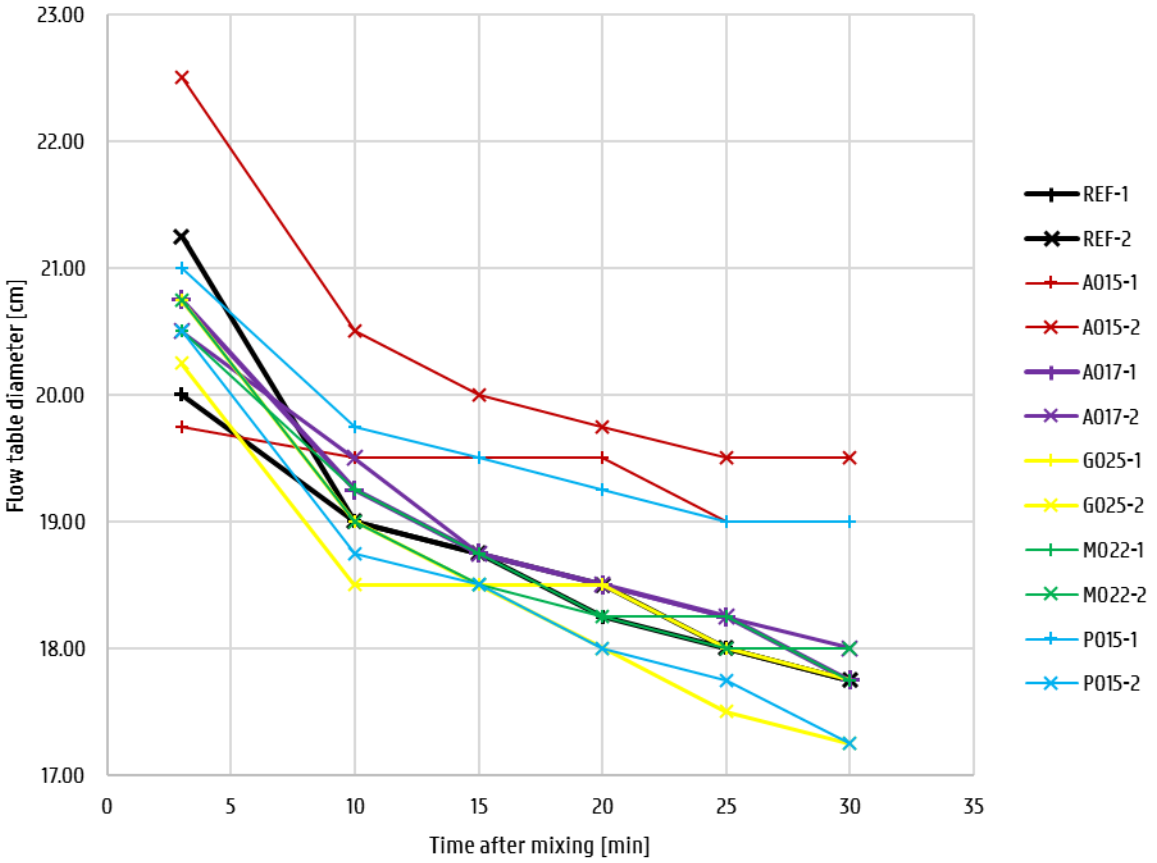

Figure 31: Flow table diameter in function of time, after mixing procedure 1 vs. 2

2) A015 shows a rather large difference in workability between the two mixing procedures, while A017 shows a similar trend, i.e. curve 2 above curve 1, but not as distinguishable. The general trend for SAP A is explained as follows. SAP A has a relatively large surface per mass added as it is about half the size of SAPs G and P and as small as one fifth of an M particle, and has a short swelling time of only 10 seconds. When mixing procedure 1 is applied, the SAP has sufficient time in step 2 to absorb all the mixing water it can, before the sand is added. Sand is known to have a hindering and sometimes destructive effect on the working of superabsorbent polymers [67]. When it is dryly added to the paste at step 3, however, the swollen polymer A seems not to yield that much under its presence. In fact, it is believed SAP A loses little to none of its absorbed water to the sand as the mixture is relatively dry compared to procedure 2. When mixing according to the latter, SAPA is put in the bowl together with the sand and cement and blended through before the addition of liquids. As such its early swelling capacity is compromised by the presence of sand particles from the start, contrary to procedure 1. In short, mixing A according to procedure 1 has the same effect to the sand as to reduce the effective w/c. The difference between both curves is negligible in the case of A017, which is accounted to the fact that the addition of 0.17 m% A is the optimal amount needed to compensate w_{add}. This means that the polymer is able (i.e. sufficiently abundant) to absorb all the water it is designed for, regardless of sand slowing it down.
3) A015 naturally shows a better flowability than A017 as 0.15 m% of A is not enough to compensate the additional water. In that way, the polymer leaves a part of w_{add} behind

it cannot absorb. That amount increases the effective water-cement ratio and consequently also the workability of the mixture.

4) M022 has similar flow curves for both procedures, with minor differences ascribed to the variation in execution of the experiment and in measuring the diameters. It is the biggest SAP in comparison, with a diameter of 486 µm ± 141 µm. Therefore, being dry, it fits the particle range of the smallest sand granulates as shown in the sieving curve for standard sand (Figure 32). Associated with its size, it has a longer swelling time of about 65 seconds in comparison to the other studied SAPs. Both explain the graphs in Figure 31: being big and slow (in comparison), the polymers have insufficient time and surface per mass added to swell substantially in step 2 of mixing procedure 1. Therefore, the head start in absorption, as described previously, is only minor and as it happens insignificant to the results of both mixing procedures.

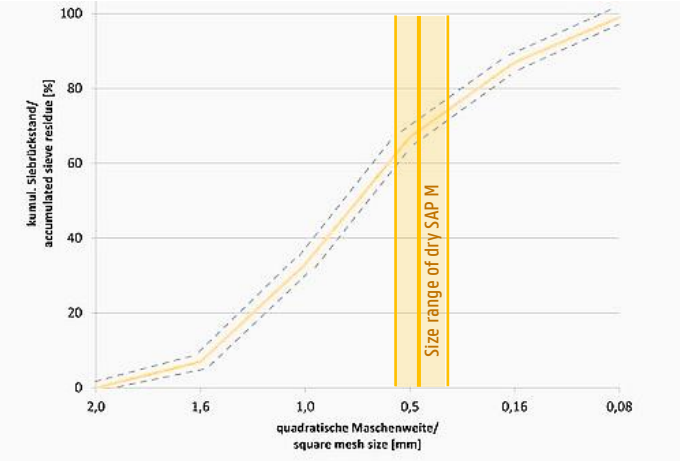

Figure 32: Sieving curve for standard sand

5) For both G025 and P015, curve 2 lies below curve 1. These SAPs have intermediate properties compared to A and M: G has a size of 157 µm ± 82 µm, a ST of 22 s and swelling capacity in CF of 47 g/g; P scores slightly better, with a size of 190 µm ± 61 µm, a swelling time of only 14 seconds and a SC in CF of 58 g/g. Their size is comparable to the smallest 20 % of sand granulates (cf. Figure 32) and this fact lies at the basis of the divergence in Figure 31. In step 2 of mixing procedure 1, it is assumed that both G and P reach their swollen state, be it slightly slower than recorded for CF. When sand is added in step 3, the swollen polymers are believed to be attacked more by the sand granulates than their comparison types A and M. The latter are respectively smaller and bigger than SAPs G and P and seem due to their size less vulnerable for sand. SAPs G and P are thought to lose absorption water in step 3 of mixing procedure 1 and have a hard time recapturing their losses as they are elastically weakened by their swollen state. In mixing procedure 2 they have the benefit of being more rigid since unsaturated and being blended through the sand before swelling can occur. All of this leads to an overshoot in the designed amount of effective water, resulting in a more flowable mix. The fact that the difference between both curves is bigger for P015 than for G025, lies in the masses of each added to the mixture, as well as in the small variation of properties. SAP G is on average smaller, making it less targetable for sand; more abundant, making its presence

more redundant; and also needs more swelling time, reducing the influence of duration between both mixing procedures. As a result, curves G025-1 and G025-2 will lie closer together. The exact same reasoning, though with the opposite outcome can be made for P015.

In the previous discussion, the focus lay on the geometrical properties and the basic chemical differences, translated into swelling behaviour parameters. No doubt, the exact chemical structure is of paramount importance to the overall behaviour of the polymers as well. But since the exact formulation of each was not known, nor the exact kinetics of the absorption process, they were not taken into consideration. However, they should be taken into account, in order to correctly describe their behaviour in fresh mortar. For example, SAP A is a (cross-linked) copolymer of acrylamide and sodium acrylate while the other studied polymers have a cross-linked polyacrylate backbone, with different active groups to them. These chemical differences might especially explain the different swelling and desorbing characteristics in time.

In conclusion, the geometrical aspects are influential to the behaviour of SAPs in fresh mortar, as the chemical environment in which the polymers act is the same and the basic swelling parameters do not differ much. SAPs F and D are extreme examples of the influence of geometry. But, the specific kinetics of each superabsorbent polymer are influential too and need to be studied more in order to correctly describe the observations.

In the remainder of this research only the following mix designs will be considered: REF, (REF*,) A015, A017, G025, M022 and P015.

5.1.2. Printability qualification

The printability of each mix design was evaluated by five criteria, A to E, as defined in § 4.3.2. Analogously to criteria C, D and E, the scalar values of A [cm] and B [V] are translated into scores [-] as well. Table 9 holds all evaluations.

Table 9: Printability qualification of mix designs

Criterion	REF	A015	A017	G025	M022	P015
A [cm]	21.25	22.50	20.50	20.25	20.75	20.50
A [-]	0	+2	-1	-2	-1	-1
B [V]	45	44	46	49	42	43
B [-]	0	+1	-1	-2	+2	+1
C [-]	0	-2	0	-1	+2	-1
D [-]	0	0	0	0	0	0
E [-]	0	0	0	+2	-2	0

The obtained qualification is more comprehensibly plotted in the spider chart of Figure 33. The discussion is held criterion per criterion:

A) The first qualification is based on the flow diameters 3 minutes after mixing, as a measure for immediate pumpability. The flow table workability was discussed in detail in the previous paragraph. At the earliest measurement, the flow diameters still differed the most from REF, but over time the evolutions clearly align (Figure 30).

B) The higher the drill voltage had to be placed in order to get the reference mortar flow rate of 8.4 cm^3/s, the more energy was lost to overcome the internal viscous shear stress. A positive score denotes a less viscous mixture than REF. It is quite remarkable that M022 shows a lower workability than REF and yet has the lowest viscosity. A similar but less distinct observation can be made for P015. The smaller viscosity is in those cases ascribed to the larger swollen particle sizes which create sand-size water compartments that tend to reduce the internal shear stress and friction with the auger and barrel surfaces. The mix design with SAP G shows the worst results for both workability and viscosity. As its curve already flirted with the lower bound of the allowed interval around REF (Figure 30), the high viscosity is ascribed to a relatively dry mixture. Future research could perhaps include a mix with a lower mass percentage of G, as at this point it is assumed that the polymers take a little too much of the additional water in, reducing the early effective w/c.

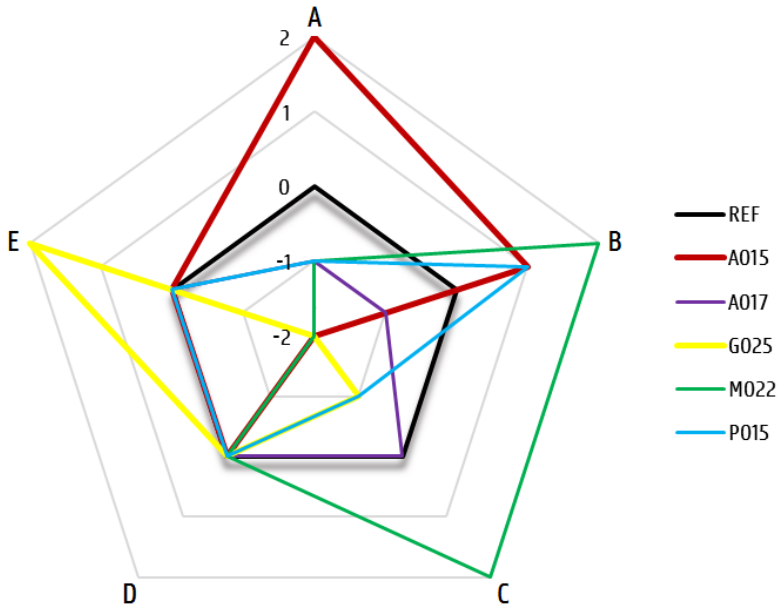

Figure 33: Spider chart of printability qualification

C) None of the printed filaments showed tears nor rough surfaces, so this qualification does not show as much deviation between the mixtures, with respect to the other criteria. It was however noticed that M022 shows an exceptionally smooth surface, which is attributed to its low viscosity.

To substantiate the surface qualification in C), the ALM measurements of three longitudinal laser paths (for each mixture) were used to calculate the surface roughness R [mm], according to Equation (20):

$$R = \frac{1}{L}\int_0^L |z(x) - \bar{z}| \cdot dx \qquad (20)$$

in which:

- L [mm] is the total longitudinal path length measured, i.e. 100 mm;
- x [mm], the location along the length: $0 < x < L$;
- $z(x)$ [mm] is the measured surface level at location x;
- $\bar{z}$ [mm] is the average level of the surface over L.

The three paths are spread evenly over the width of the filament and cover the full length. They were measured 6:30 min after mixing procedure 2, which is within 5 minutes after printing. A measurement of A017 was not available as at that point in time ALM was deemed inadequate to evaluate the unprotected shrinkage in height (cf. § 5.3.2). Table 10 holds the mean roughness and standard deviation for each mix design ($n = 3$). Statistically these values do not significantly differ. The scores in Table 9 are based upon these results.

Table 10: Surface roughness of single-layer printed specimens (n = 3)

Mix	Mean roughness [mm]	Standard deviation [mm]
REF	0.30	0.02
A015	0.43	0.10
G025	0.41	0.10
M022	0.27	0.13
P015	0.35	0.12

D) All printed singular filaments are dimensionally stable: they do not deform under their own weight.

E) When a second layer is printed on top of a first one, all mixtures show good buildability and do not deform noticeably more than REF, except for mortars containing SAPs G and M. G025 (Figure 34, right) shows 'no' deformation when a new layer is printed on top, while the first layer of M022 (Figure 34, left) is compressed considerably under a second layer. Both are ascribed to their respective viscosities. The evaluation was done by visual inspection as only these two mix designs showed a noticeable difference.

Figure 34: Visual inspection of the stability of the first layer when a second one is superposed

5.2. Characterisation

In this chapter the results of the characterisation tests are discussed. They will be used to interpret the results of the shrinkage and strength experiments in chapters 5.3 and 5.4.

5.2.1. Short time swelling behaviour

Figure 35 shows the result of the initial swelling capacity test for all studied SAPs. Brightly coloured bars represent the experimental values; faded bars the expected values as given in Table 3 [42].

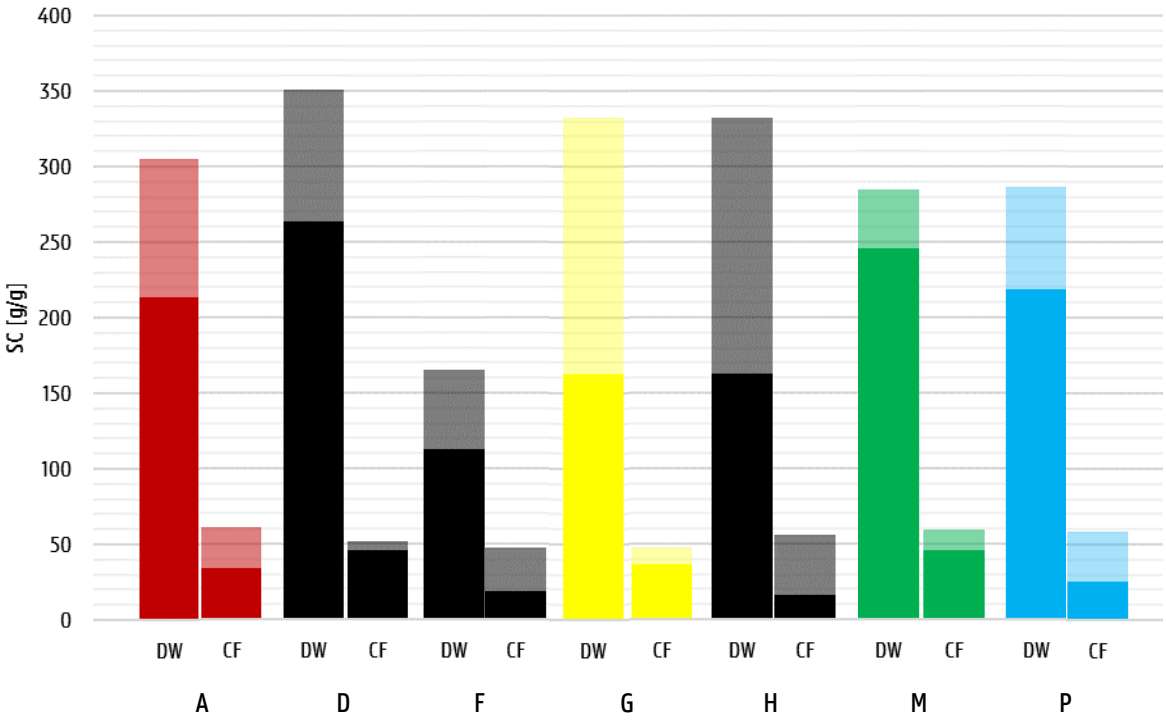

Figure 35: Swelling capacities of studied SAPs (n = 1)

The lower SC was due to a saturated demineralising filtration system, resulting in an incomplete purification. Snoeck [42] established the swelling capacity of A in tap water to be 163 g/g $\pm$ 1 g/g versus 305 g/g $\pm$ 4 g/g in demineralised water. As such, almost a difference in SC of 50 % arises between the two. Using that analogy, it could be said that the DW used in the current tests was contaminated for about 35 % of its volume with regular tap water. It is assumed that this explains all reduced SCs in the tested DW.

As to the difference in swelling capacity in CF, it is noted that not the same CF recipe was followed, as the one in literature used demineralised water and stirred for 24 hours, when the current procedure employed tap water and stirred the mixture for only four hours before filtering.

5.2.2. Setting characteristics

Figure 36 shows the Vicat needle penetration in time for all studied mix designs (in singular). The starting penetration was set to the maximal depth encountered during the test.

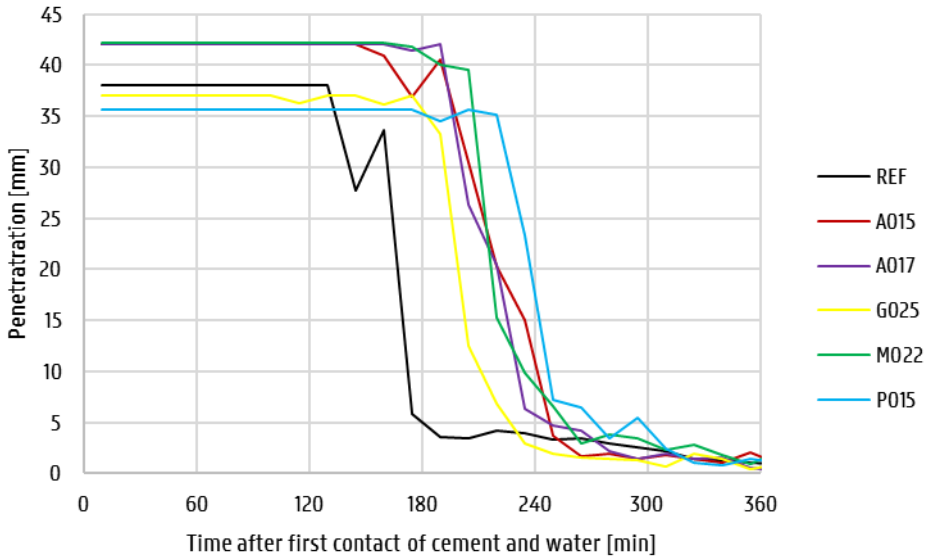

Figure 36: Vicat needle penetration in time (n = 1)

Table 11 shows the obtained Vicat setting times. The initial setting time was taken at the first recording of a distance between the base plate and needle point of more than 3 mm (i.e. the lower bound of 6 mm $\pm$ 3 mm). The final setting time was taken at the instant the difference between two subsequently monitored penetrations fell below 0.5 mm. This procedure is in accordance with the norm cited in § 4.2.3. The peaks after initial falls in the graphs of REF and A015 are ascribed to a local hard particle (e.g. sand) blocking the needle penetration.

Table 11: Vicat setting times (n = 1)

Mix design	Initial [min]	Final [min]	Duration [min]
REF	145	220	75
A015	175	280	105
A017	205	310	105
G025	190	295	105
M022	205	310	105
P015	235	340	105

From these results two early conclusions can be drawn:

- The reference mixture sets first, or in other words: the SAPs tend to delay the setting times. This conforms to conclusions drawn by Justs et al. [82] and Dudziak et al. [83] that internal curing retards the setting behaviour of cement mixtures.
- The mix designs with SAPs take about half an hour longer to complete the setting process: i.e. the difference between final and initial setting times. This is also associated with the retarding effect of internal curing on the setting process [83].

Other tests (such as the corrugated tubes test and photographic image analysis) will show indications of initial and final setting times as well. The Vicat setting times are compared to these values in the next sections. Since the Vicat test was only executed in singular for each mix design, its statistical significance substantially reduces, and care should be taken in drawing general conclusions. Moreover, the setting times recorded in Table 11, might have been influenced by the surface dryness as it is unprotected to the environment and subject to evaporation [31]. The SAPs tend to maintain the surface moisture (cf. literature and the next paragraph) and as such seem to prolong the setting process more than in the reference mixture.

With respect to the difference in setting times of different mixes, the following thoughts came to mind:

- A015 results in a higher effective w/c, and less swollen polymers to gradually release their absorbed water. As such the earlier initial setting compared to other SAP mixtures, can be explained. More effective water is initially present (i.e. not absorbed by polymers) and immediately available cement hydration. The mixture is also likely to lose more water to the surroundings and have a drier outer surface as such. It is remarkable that the difference of only 2 m% less SAPs added with respect to A017 has a relatively big influence on the setting process: slowing the onset down with half an hour. This difference is mostly accounted to the test sample size of one. Additional Vicat tests are required to make a conclusive statement.
- In some way the results resemble the outcome of the flow table test in Figure 31: A017 and M022 show a similar trend (i.e. least influence of mixing procedure and same setting times), while G025 and P015 differ and the former respectively less than the latter (i.e. more influenced by the mixing procedure and faster respectively slower setting). However, as these data are obtained from singular mixture testing, not much importance should be given to this thought: more testing is crucial to confirm the theory.

5.2.3. Surface moisture evolution

Figure 37 shows the mean surface moisture evolution κ [g/m^2] in time after printing. Statistical analysis concluded there was only a significant difference ($\alpha = 0.05$) between REF and A015, G025 and P015 at 0 and 30 minutes after printing. However, it is quite clear that REF will result in a lower surface moisture and generally about half of those of other mix designs. Statistically M022 and A017 are identical: $(1 - \alpha) \leq 0.02$, which seems to be the recurring theme in all characterisation tests so far. Though not of great significance, the difference between A015 and A017 might be attributed to the higher $(w/c)_{eff}$ in A015 and as such a more humid surface. All mixtures show a declining surface moisture in time, ascribed to the chemical consumption of water and its evaporation to the environment.

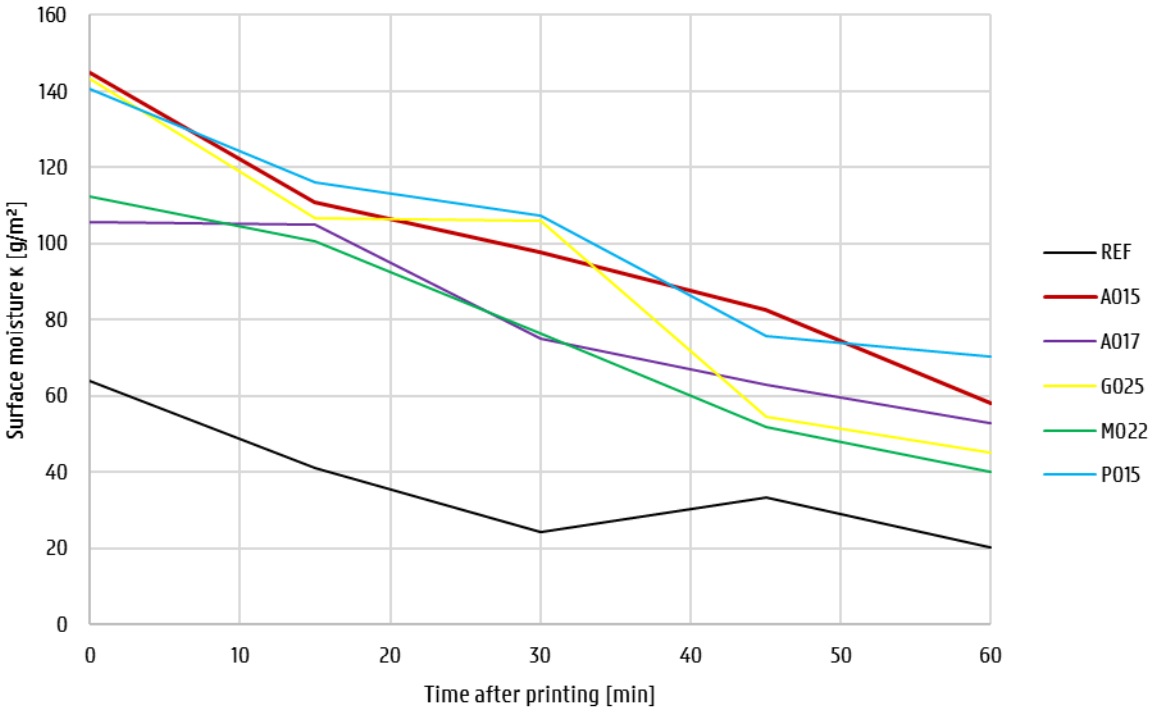

Figure 37: Surface moisture evolution (n = 3; σ ≤ 0.57μ; no error bars for the sake of clarity)

Unlike the findings of Marchement et al. [6], the mixtures do not show a pronounced inverted bell curve pattern with a minimum around 20 min after printing. Instead, the mixtures with SAPs show a more or less linear reduction of surface moisture. REF on the other hand has a minimum of κ around 30 min after printing. In [5] Sanjayan et al. ascribed the initial higher surface moisture to the fresh state and a later increase to intensified bleeding, which might explain the evolution for REF. The mixtures with SAPs are believed to show less bleeding as they control the flow of water by gradually releasing it, in thermodynamic equilibrium (cf. § 2.3.1.3).

5.2.4. Porosity

5.2.4.1. Macro- and microporosity

Table 12 and Figure 38 show the statistically analysed results of the microscopic study of dry and saturated SAPs as well as the voids they leave behind in 28-day old samples of respectively A015, G025, M022 and P015. The air voids in hardened specimens of REF were studied as well. All 'set void' data was obtained from longitudinal cross-sections of double-layered filaments. Dry SAPs were studied lying loosely on the microscopic plate; saturated particles were obtained by precisely adding semi-demineralised water (i.e. the same as in § 5.2.1) using a ml-syringe until the SAPs were fully swollen.

Both also include expected diameters $E(d)$ [mm] respectively calculated:

- in dry state as the ones tabulated in Table 3;
- in saturated state, as the equivalent spherical diameter obtained after swelling in demineralised water, based on the SCs in Table 3 and assuming proportionality between mass and volume (as the mass density of water equals 1 g/ml);

- in set state, as the equivalent spherical diameter obtained after swelling in CF, based on half of the SCs in Table 3 (cf. § 5.1.1, recommendation by Kovler [45]) and assuming proportionality between mass and volume as well;
- the set void diameter in the reference mixture is solely due to generally entrapped air and is estimated as the mean diameter obtained from the RapidAir test (cf. infra).

Table 12: Statistical analysis of particle diameters [mm]

Variable		REF	SAP A	SAP G	SAP M	SAP P
dry	n	N.A.	75	63	31	84
	μ	N.A.	0.083	0.137	0.416	0.167
	σ	N.A.	0.020	0.073	0.149	0.051
	E(d)	N.A.	0.100	0.157	0.486	0.190
saturated	n	N.A.	9	6	9	18
	μ	N.A.	0.479	0.812	2.145	0.953
	σ	N.A.	0.160	0.152	1.242	0.400
	E(d)	N.A.	0.673	1.087	3.198	1.252
set void	n	572	84	118	74	230
	μ	0.156	0.308	0.522	1.010	0.646
	σ	0.106	0.185	0.271	0.657	0.325
	E(d)	0.186	0.312	0.450	1.502	0.584

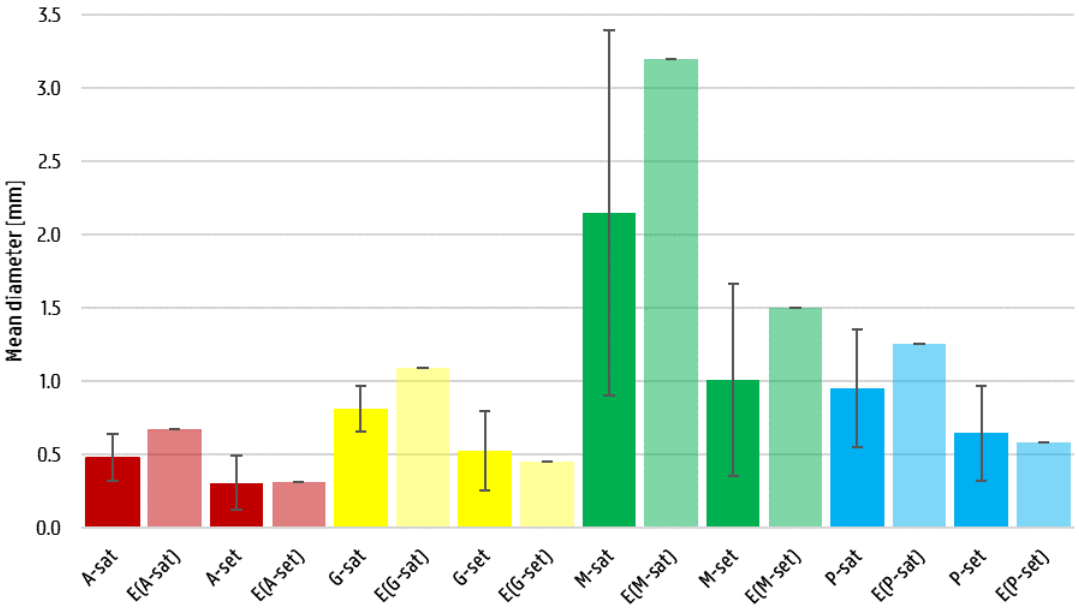

Figure 38: Swollen particle (DW) and set void diameters (mortar) (n > 5)

All dry particle and set void diameters are significantly different ($\alpha_{eff} = 0.00$) whereas all swollen sizes differ significantly too except for SAPs G and P ($\alpha_{eff} = 0.76$). T-testing showed that all dry particle sizes were statistically equal to those tabulated in Table 3, which justifies the use of the latter to characterise the polymers.

In Table 13 the following quantities are presented for comparison:

- d_i [mm], diameter with i: dry, sat, set or air in accordance to the particle state or void (see Table 12);
- V_i [mm^3], volume with i the same index, obtained by assuming the particles to be spherical;
- the ratios of d and V of different particle states.

Table 13: Comparison of particle diameters and volumes (microscopy)

SAP	d_{sat}/d_{dry}	d_{set}/d_{dry}	V_{sat}/V_{dry}	V_{set}/V_{dry}	V_{set}/V_{sat} [%]
A	5.8	3.7	192.0	50.9	26.5
G	5.9	3.8	206.2	54.9	26.6
M	5.2	2.4	137.0	14.3	10.4
P	5.5	3.7	165.0	51.3	31.1

The following reasonable conclusions are drawn from the microscopy tests.
The diameter of a swollen particle (in semi-pure DW, cf. § 5.2.1) is about 5 to 6 times that of a dry particle. It is believed this will be more, respectively less in pure DW and tap water.
The diameters obtained from testing are about 20 % to 30 % smaller than the ones theoretically estimated (Figure 38), which is ascribed to the testing DW which had impurities (cf. § 5.2.1).
The diameter of the void one polymer leaves behind in hardened specimens is about 3 to 4 times that of a dry particle. A considerably lower value (i.e. 2.4) is found for SAP M, which is ascribed to the visual measuring technique (2D section versus 3D volume of an irregular-shaped particle). Also, the set void volume an M particle leaves behind lies in the same size range as sand particles. During mixing, they are more resistant to desorption under sand attack, but they seem to be hindered to reach their maximum capacity as well. In comparison, SAPs G and P appear to lose water again during mixing (especially at an increased rotational speed), but once at rest (e.g. in a printed specimen), they are able to reach their full swelling capacity, as theoretically estimated. This reasoning needs to be substantiated with the kinetic properties of the SAPs.
The ratio of the swollen volume (semi-DW) and dry particle volume is comparable to the swelling capacity in the same testing liquid, obtained in § 5.2.1. These quantities can reasonably be compared as the mass density of water equals 1 g/ml and since the change in volume of SAP is solely accounted to the uptake of mixing water. SAP M has the lowest ratio of 137 (cf. Figure 38) which is ascribed to the measuring technique (2D visualisation of a 3D volume) and the small sample size ($n = 9$).
The ratio of the set void volume and dry particle volume is comparable to the swelling capacity in cement filtrate in Table 3. The sole exception is again SAP M (Figure 38), which seems unable to obtain the estimated volume in a specimen at rest (cf. supra).
The ratio of the set void volume and swollen particle volume (in semi-DW) is comparable to the ratio of the respective swelling capacities obtained in previous testing (§ 5.2.1), which lie around 20 %. M is excluded from this comparison again for the main reason that its set volume does not reach its estimated capacity. In comparison, the value of V_{set}/V_{dry} for SAP M is 14.3 versus 54.9 for SAP G (or 26.0 %) while V_{sat}/V_{dry} is 137.0 for SAP M and 206.2 for SAP G (or 66.4 %).

Figure 39 shows the cumulative air content obtained by the RapidAir test. The most important results, being the air contents and void frequency in mm^{-1} are given in Table 14.

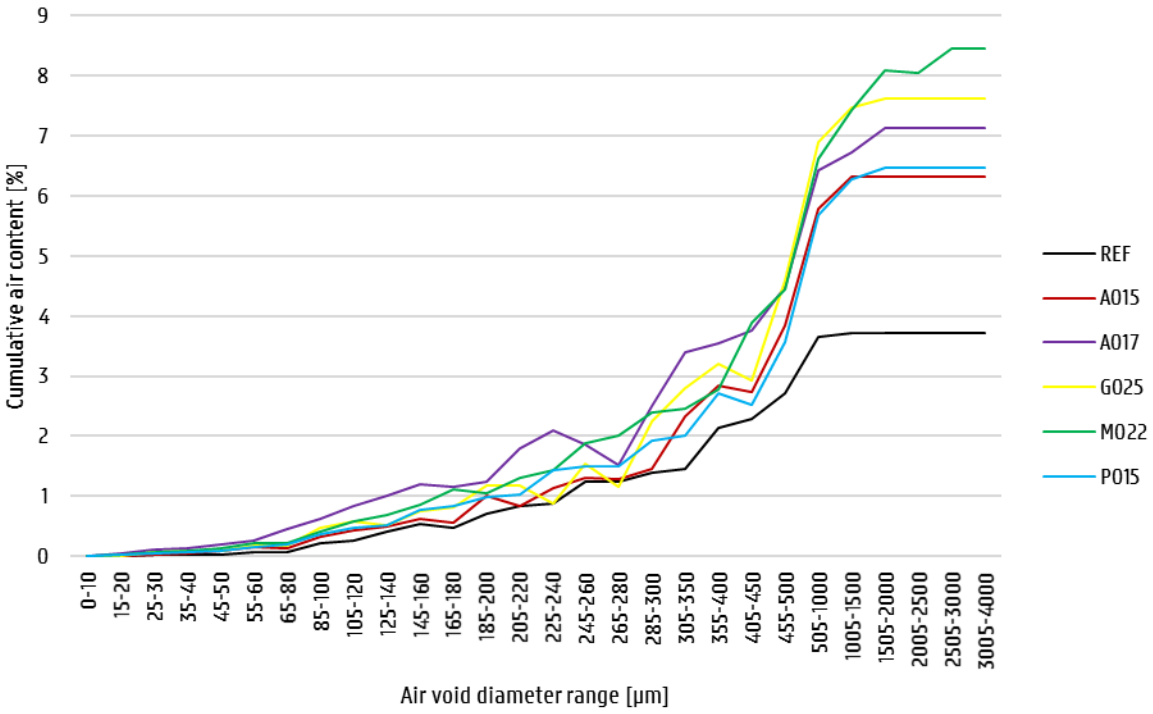

Figure 39: Cumulative air content in hardened specimens (n = 1)

Table 14: Air content in hardened specimens (n = 1)

Sample	Total air content [%]	Void frequency [mm^{-1}]	Void period [mm]
REF	3.72	0.202	4.95
A015	6.31	0.294	3.40
A017	7.06	0.387	2.57
G025	7.62	0.365	2.74
M022	8.45	0.383	2.61
P015	6.48	0.312	3.21

The total air content and void frequency in hardened specimens increase with SAP addition and the exact increase is more or less proportional to the amount of SAPs added, or equivalently the amount of dry volume added (as the true densities are equal and around 1,400 kg/m^3). If the mass percentages of added SAPs are translated into their true dry volume and the latter is multiplied with V_{set}/V_{dry} (Table 13), a linear relation exists between the result and the air content with a coefficient of determination of 0.84. The calculation is summarised in Table 15. $E(\#)$ [-] denotes the estimate number of dry particles added, based on previous calculations (cf. Table 13).

Table 15: Calculation of total set volume according to Table 12

Sample	m%	$V_{dry,tot}$ [mm³]	E(#)	V_{set}/V_{dry}	$V_{set,tot}$ [mm³]	Total air content [%]
A015	0.15	723	8,708	50.9	$36.8 \cdot 10^3$	6.31
A017	0.17	820	9,869	54.9	$41.7 \cdot 10^3$	7.06
G025	0.25	1,205	8,769	14.3	$66.1 \cdot 10^3$	7.62
M022	0.22	1,061	2,549	51.3	$15.2 \cdot 10^3$	8.45
P015	0.15	723	4,160	50.9	$37.1 \cdot 10^3$	6.48

The exception to this rule is M022 which shows the largest air content while its estimated set volume is smallest. This is ascribed to an increased count of voids around its interlayer, compared to other studied samples (Figure 40). The reason why M022 is likely to suffer more from entrapped air at the interface between two superposed printed layers is accounted to its relatively dry surface (Figure 37) even at zero time gap in combination with its relatively worst dimensional stability (cf. Table 9). One of four test specimens of G025 suffered from a larger entrapped air content at the interface as well. As the voids are visibly smaller than those in M022, they are ascribed to the relatively best stability of both its first and second layer which might as such entrap small air pockets between their rigid and relatively rough surfaces (Table 10).

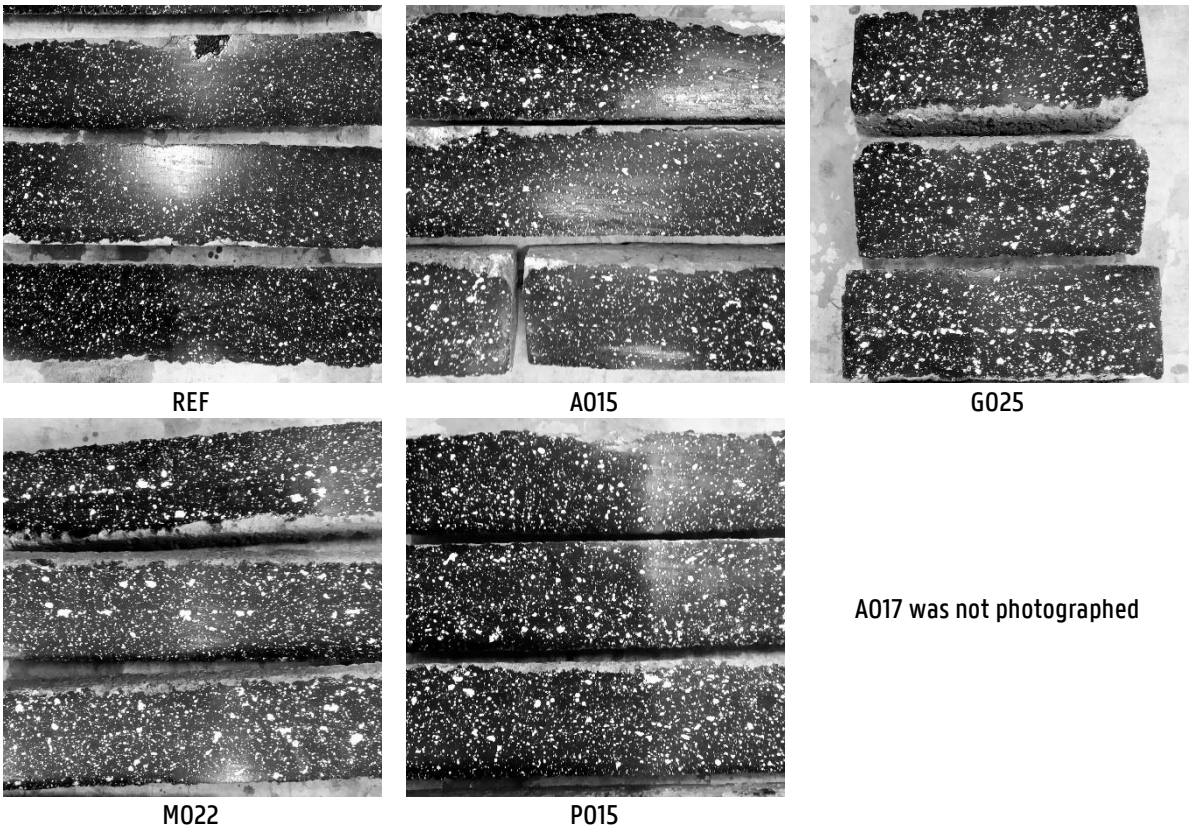

Figure 40: Studied specimens in RapidAir test

The printing procedure might also lead to entrapped air at the interface of two layers, due to a change in standoff distance between nozzle and sublayer (cf. § 2.1.4.3), for example. Also, larger swollen SAP particles (e.g. SAPs P and M), about which in § 5.2.1 was said that they might have a lubricating effect when pumped, could migrate to the outer edges of the mixture under

pressurisation (i.e. segregation) [8]. As such, the swollen polymers would likely be found at the outer surface of a printed filament and end up at the interface of two. In this research, the printing process was carried out consistently, reducing the effect of the nozzle standoff distance or printing speed for that matter. The possibility of swollen SAP particles segregating and migrating to the outer edges of the cementitious mixture was not actively studied in this research. Though the photograph of M022 specimens in Figure 40 might prove it interesting for future research.

The inclinations in the cumulative air content of Figure 39 show a good resemblance to the set void volumes obtained from the microscopic analysis: SAP A has a clear peak in the interval of 305 µm to 350 µm; G in the range of 455 µm to 500 µm; P above 505 µm and M especially in the range of 1 mm to 3 mm. Care should be taken to make the right comparison: e.g. all SAPs show a peak in the diameter range of 505 µm to 1,000 µm, while these clearly cannot be accounted to swollen SAP A particles. In general, even for the REF series, the fraction of total air voids in that range is about 8 % no matter what sample is investigated. Only for SAP P is there a distinct increase of $\gtrsim 1$ %, due to the presence of swollen polymers.

Snoeck [42] determined the total air content (of macro- and micropore sizes) to be 3.4 % in hardened reference mortar (R0.35) without SAPs and $w/c = 0.35$. The mixture has a chemical composition of 1 part CEM I 52.5 N OPC, 3 parts silica sand 0/2, 0.35 parts water and 0.0234 parts SP (MasterGlenium 51). In the mixtures A0.5a (1 x cement, 3 x sand, 0.64 x water, 0.5 m% SAP A, 0 x SP) and A1a (1 x cement, 3 x sand, 0.77 x water, 1.0 m% SAP A, 0 x SP) the air content was respectively 6.0 % and 9.2 %. The mixtures were casted in moulds and compacted by jolting 60 times. Though the mixtures are not the same as the ones used in this research, a trend can be noticed. REF has a larger air content (3.7 %) compared to 3.4 % while it was concluded by Snoeck in [42] that a lower w/c leads to a higher amount of entrapped air (micro-scale). Comparing the mixtures A015 and A017 to A0.5a and A1a, the latter two having a considerably larger amount of SAPs and water added to them, it is remarked that the air contents lie in the same range (A0.5a $<$ A015 $<$ A017 $<$ A1a). It would however be reasonable to expect that the mixtures with a lower amount of SAPs and water added to them, have a lower air content as well. It is therefore believed that the process of sample preparation plays a large role in the result: printing could induce additional air in the mixture, or at least not remove the air already present after mixing. Jolting on the other hand, densifies the matrix by driving the air upwards through vibrational motion. It is recommended to include in future research some investigation into the influence of sample preparation, e.g. by mould casting without densifying the matrix and comparing the results to the ones obtained in Table 14.

5.2.4.2. Nanoporosity

Mercury intrusion porosimetry led to the findings in Table 16 and Figure 41 ($n = 1$). The affixes -supra, -inter and -infra respectively denote the top, inter- and bottom layer.

Table 16: Nanoporosity (n = 1)

Sample	Total porosity < 10 µm [%]				Median diameter [nm]		
	Top layer	Interlayer	Bottom layer	Overall	Top layer	Interlayer	Bottom layer
REF	15.2	16.2	15.9	16.2	255.6	273.2	246.6
A015	19.1	18.4	18.4	18.6	384.4	336.1	327.5
G025	18.0	16.5	17.1	17.2	255.3	141.0	183.9
M022	19.0	18.3	16.7	18.0	391.8	311.3	227.0
P015	17.4	19.9	17.6	18.3	355.1	388.3	299.4

In general, only few conclusions can be drawn with reasonable significance as the sample size of each mixture and each layer was only one.
Mixtures with SAPs tend to increase the total nanoporosity in all layers of hardened specimens by 5 % to 25 % with respect to the reference. This conforms with the conclusion stated by Baroghel-Bouny in [68]: when the (total) w/c decreases, the nanoporosity decreases as well. This is associated to the denser matrix that results from a reduction in total amount of mixing water.
No conclusive statement can be made about which layer (top, interface or bottom) has the largest total nanoporosity, however there is a clear difference in continuous pore network as suggested by the distinct variations in derivative intrusion curves (Figure 41). From the median diameters in Table 16 it is concluded that in general the bottom layer has the network with the smallest continuous pore diameter. This is ascribed to the densification under additional hydrostatic pressure in fresh state, exerted by the top layer. G025 does not follow this trend as it is believed that due to its relatively best dimensional stability (Table 9) the added weight of a second layer will have a smaller effect. The pore network with the largest continuous diameter is found in either the top layer or interlayer. It is generally true that the top layer is less dense than the underlying layer as it is subject to only its own hydrostatic pressure. At the interface on the other hand, air can get trapped as new layer is printed on top of an older one. The pore network in the interlayer (micro-scale) is believed to be influenced by the surface roughness (with sufficient rigidity) of one or both meeting layers, and their outer surface moisture, as larger water voids will after hydration have a wider connection of pores (nano-scale). No conclusive statement follows from comparison of the MIP results to the results from printability and surface moisture testing, however. M022 is a good example of this theory: it has the smoothest surface and one of the driest surfaces in combination with the largest difference in median diameters of the pore networks, 391.8 nm in the top layer versus 311.3 nm in the interlayer.

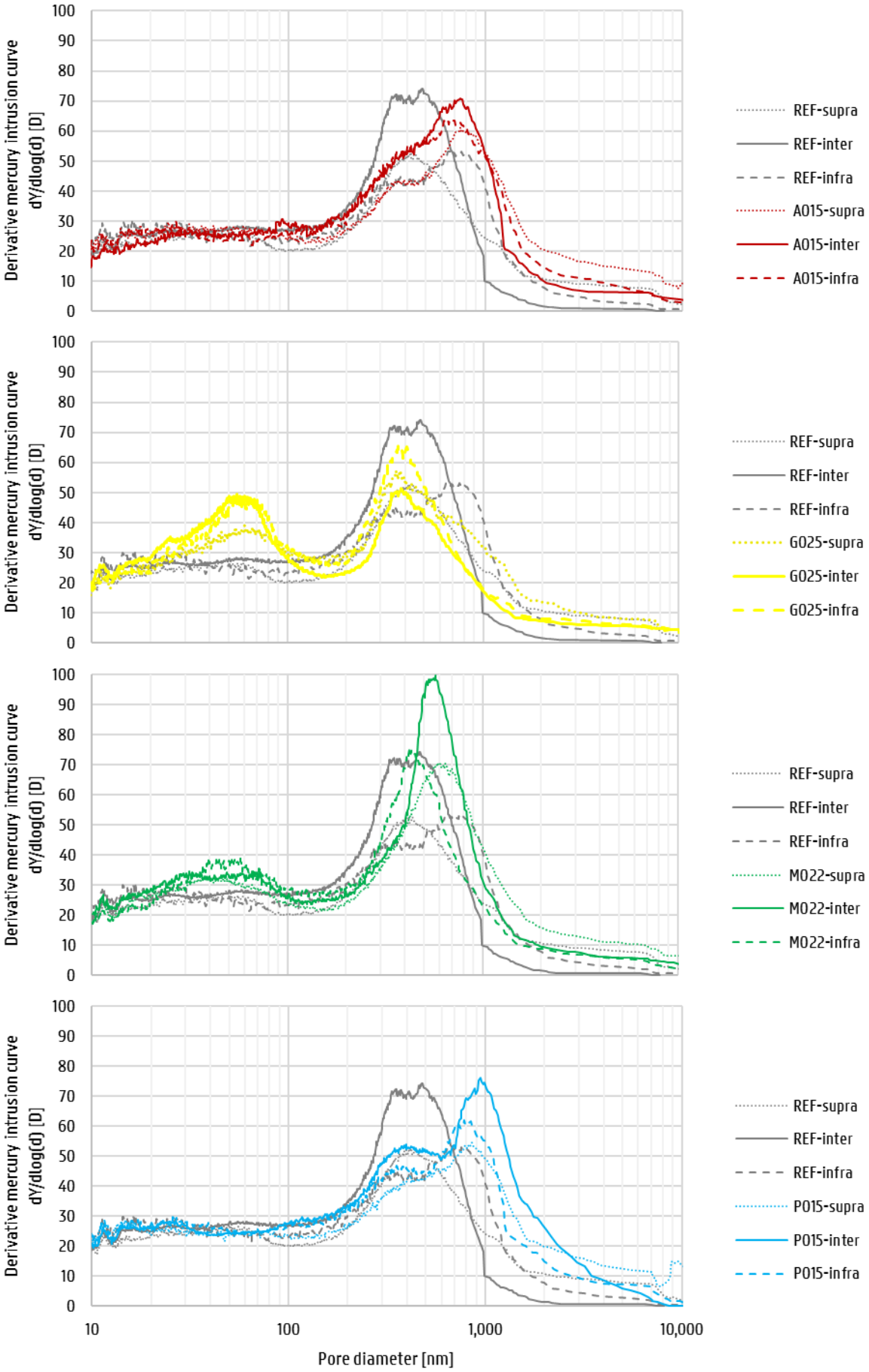

Figure 41: Derivative intrusion curves (MIP) (n = 1)

In general, SAPs tend to reduce the amount of nanopores in the range of 100 nm to 500 nm and increase the amount of voids with a diameter above 700 nm. This is ascribed to a better hydration rate around the SAPs, closing up the smaller pores, as well as to their autogenous shrinkage mitigation that reduces the amount of micro-cracking [42]. Their influence on sizes below 100 nm is inconclusive. G025 shows a distinct peak in its derivative intrusion curve (of each layer) for pore diameters ranging from 10 nm to 100 nm, while it shows a reduction in the amount of pores with a diameter above 400 nm, unlike all other studied mixtures. G025 is even denser than REF in every layer (Table 16), which would suggest a lower effective w/c. This is validated by previous printability tests, such as the flow table test and viscosity evaluation. The water that is released by the swollen particles over time, will migrate away from the polymer and take part in hydration, reducing the diameter of the porous path it followed. As such, it is believed the water will close off the porous network by chemically connecting the sides. The water might not be able to penetrate the smallest pore connections as an air pocket is entrapped for example, under cohesion to the matrix, adhesion and/or capillary tension from a larger water mass in its proximity. This would explain the relatively large fraction of small pores ($<$ 100 nm) that get closed off, and small fraction of intermediate nanopores (400 nm to 1,100 nm) in G025, that keep reducing in pore diameter as type G SAPs provides them with water to maintain hydration. Accordingly, the other mixtures would seem less efficient in supplying water to their surroundings as they show a greater presence of larger nanopores (500 nm to 1,000 nm) associated with accumulated water that was not able to migrate away and take place in hydration. M022 shows a tendency similar to G025 as its second peak (ca. 550 nm) lies closer to the peak of G025 (400 nm) compared to A015 and P015 (800 nm, respectively 1,000 nm) and as M022 does show a relative fractional increase in pore diameters below 100 nm, while the mixtures with SAPs A and P do not. The behaviour is believed to be explained in more detail by the swelling kinetics of each respective SAP type.

Snoeck [42] determined the overall nanoporosity in R0.35 as defined above, to be 16.9 % which is similar to the value for REF (Table 16). The order of magnitude of the results in Table 16 is therefore validated. However, the mixtures A0.5a and A1a have a lower nanoporosity of respectively 16.6 % and 13.2 %. The mixtures with SAPs in this research do not reduce the total nanoporosity with respect to REF, though they are known to stimulate hydration. Future research with respect to the influence of sample preparation on the total nanoporosity is advised (cf. § 5.2.4.1).

5.3. Early age shrinkage

In this chapter the early age shrinkage behaviour is investigated in protected and unprotected environmental conditions. The protected condition refers to the autogenous shrinkage testing procedure by means of Auto-Shrink dilatometry as the mortar is shielded from the environment and cannot lose water to it (§ 4.4.2). The unprotected condition refers to the camera and automated laser measurements as the printed specimens are subject to evaporation (§ 4.4.3, respectively § 4.4.1).

5.3.1. Autogenous shrinkage

Figure 42 shows a longitudinal autogenous strain plotted in time (zeroed out at t_{fs}, the final setting time according to Vicat testing) measured for the reference mixture ($n = 3$). The two distinct bending points are indicated. The first bending point marks the first real change in chemical structure: i.e. the initial setting time or the moment the specimen goes from a pure suspension state to a percolated structure. This denotes the end of vast plastic shrinkage, be it chemically induced by a loss of water to hydration rather than by evaporation, bleeding, and by the elasticity of the corrugated tubes that may slightly deform in the first minutes after filling. The second bending point indicates the final setting time and as such a completely percolated structure of irreversible chemical bonds. From this point on the overall shrinkage is mostly due to the apparent volume change rather than the absolute, as the latter stagnates when the hydration rate diminishes. Consequently, from that moment on, the autogenous shrinkage is self-desiccative. By definition the knee-point coincides with the second bending point. Similar bending points are observed in measurements of different mix designs.

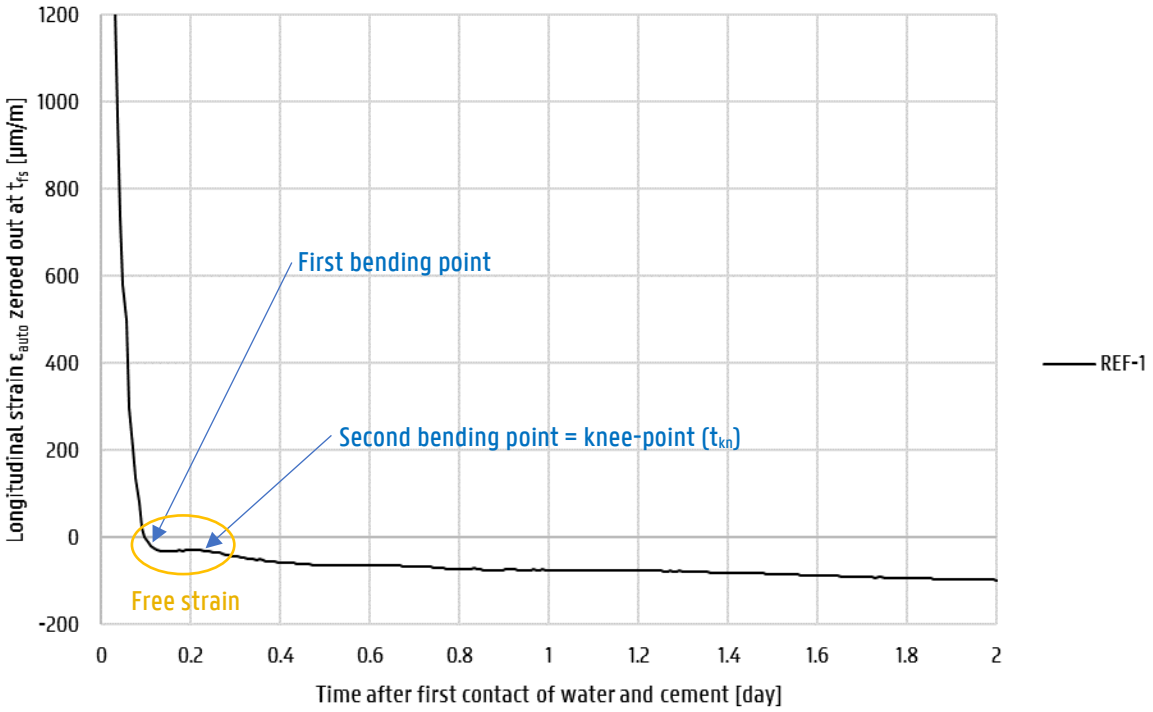

Figure 42: Observation of knee-point in ε_{auto} (1 of 3 measurements for REF), originally zeroed out at t_{fs} (Vicat)

In between the two bending points, the so-called free strain occurs: its name referring to the autogenous shrinkage that happens fairly unrestricted, making the absolute and apparent volume identical [35].

Figure 43 plots the curves of autogenous strain zeroed out at t_{kn}. Discussion on the free strain is postponed to § 5.3.3 in comparison to other test results.

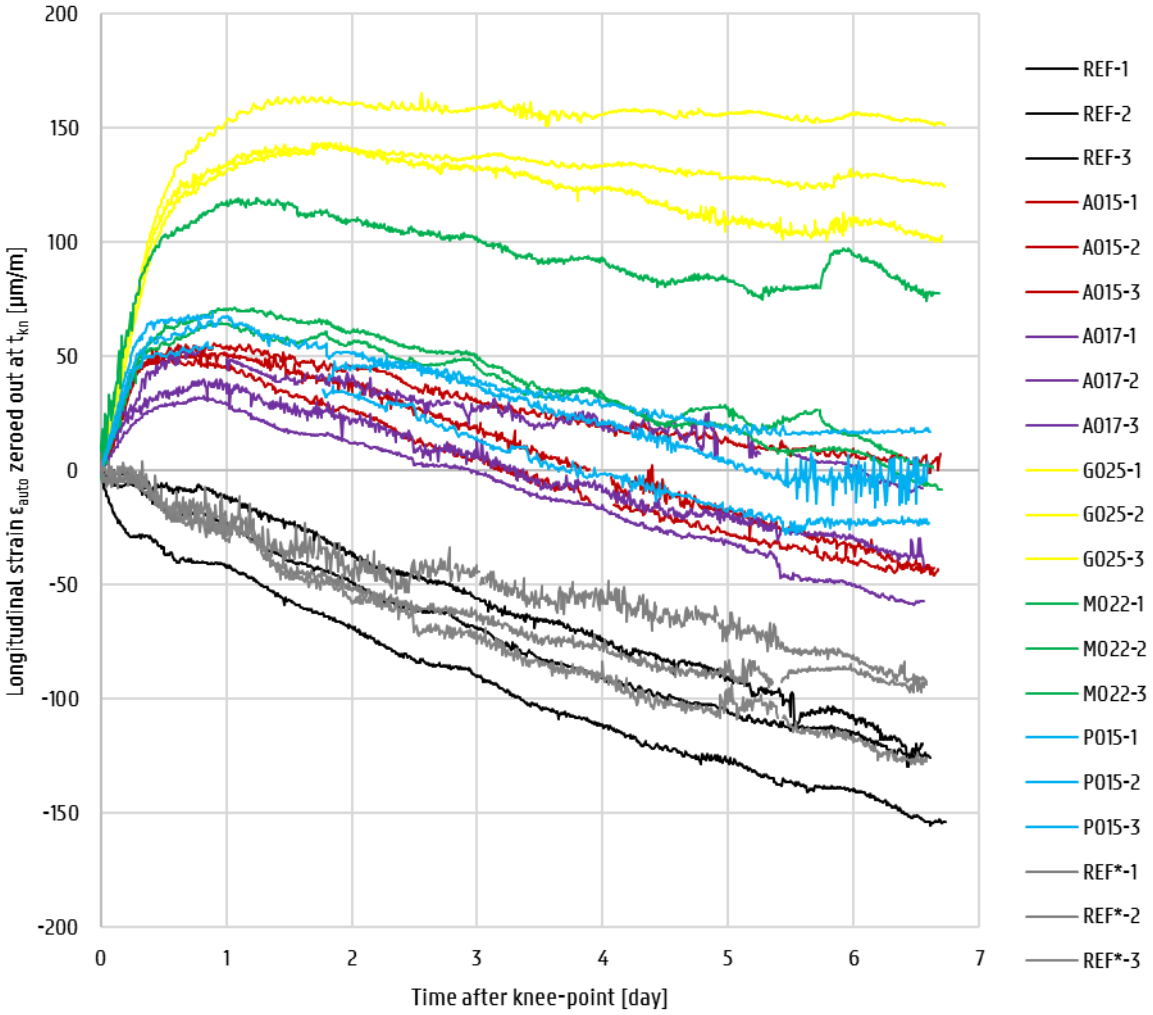

Figure 43: Autogenous shrinkage after knee-point (self-desiccation)

The following trends become apparent.
Both reference mixtures, with and without additional water (REF*, respectively REF) continue to shrink at the same rate after the knee-point. They show no swelling behaviour as do the mixtures with SAPs.
The swelling behaviour immediately after final setting (t_{kn}) up to about a day after is present in all mixtures with SAPs. This is ascribed to their capacity to recapture possible bleeding water that has risen to the interface between tube and mortar specimen as well as to them mitigating the additional water. These are two abilities REF* does not have, despite the same w_{add}, and since it cannot recapture or mitigate water, it shows a similar shrinkage behaviour as REF, though marginally better. Mixtures with higher w/c have a less dense matrix and are hence

subject to smaller capillary pore tension. As will be discussed in the case of unprotected shrinkage, an overall chemical-structural swelling is present in all specimens. However, it can only manifest in combination with a water mitigation capacity, as otherwise capillary tension will annihilate it. And since in protected samples the evaporation to the environment is prevented, the capillary tension will be lower than in unprotected samples (see § 5.3.2).
All SAP-mixtures show statistically identical shrinkage rates after swelling and equal to the rates of the reference mixtures (− 13.9 µm/m/day on average). They are also statistically indistinguishable from each other (except for M022, due to its outlier in Figure 43), but differ significantly from both similar references. These conclusions do however not hold for G025 which differs from all other mixtures with an effective significance of less than 0.176. G025 has a shrinkage rate after swelling of – 4.9 µm/m/day on average. It is not clear why one of three measurements of M022 shows such an uncharacteristic behaviour, though it is only described as an outlier as the general trend is believed to follow the majority of two.
G025's best autogenous shrinkage mitigation is explained by former conclusions for the mixture. With respect to its printability it was remarked that: (1) during mixing (procedure 2) it is slower to reach full swelling capacity; (2) during printing it is most viscous; (3) after printing it seems driest, though most dimensionally stable as well. From swelling capacity tests and microscopy, it was concluded that SAP G: (1) has one of the best swelling capacities in cement filtrate; and (2) has the largest ratios of saturated and set diameter (or volume) to dry particle size (or volume). It also has the shortest setting duration (i.e. period of free strain; see § 5.3.3), starting the latest in comparison. As such, its shrinkage mitigating behaviour is explained as follows. SAP G, which is abundantly present in G025 (0.25 m% was considered a little too much in § 5.1.1) is able to take up more of the mixing water than it was designed for (w_{add}) due to its good SC. It seems to retain the water the longest as well, as the onset of free strain is delayed the longest and since it has the largest ratio of set to dry size. Therefore, less bleeding water will be lost to the interface of tube and specimen compared to other mixtures and the effective w/c will be relatively lower too. It is known from literature that hydration is stalled longer for lower w/c [42] [73]. When the period of free strain commences, SAP G is more efficient in providing the surrounding cement particles with water for the following reasons: (1) internal curing water is only provided within a 2 mm range around the reservoir [79]; (2) the particles are relatively small, abundant (largest mass percentage) and therefore well spread out over the specimen; (3) the type G particles still hold most of their initially absorbed water while other SAPs might have lost part to bleeding that localises water at the top and therefore on average further away from unhydrated cement particles. All of these lead to an efficient supply of water to cement by the SAP G particles and as such a reduction in setting duration (i.e. the period of free strain). And since the autogenous shrinkage is self-desiccative from final setting on, induced by capillary tension, it is countered more in G025 for the same three reasons as latterly mentioned – or in short: for its efficiency of providing water to compensate the capillary tension.
This notion of efficiency can be used to describe the behaviour of SAPs as well. Though statistically equal, the reasons for a lower swelling tendency right after t_{kn} are believed to be: for SAPs A and P, the loss of water due to bleeding and a relatively small void period of around 3.5 mm (cf. Table 14); and for SAP M, the loss of water due to bleeding and a lack of swelling capacity and reabsorption in mortar.

It is remarked that G025 has the largest macro- and micropore content (7.6 %, Table 12) but the smallest nanopore content as well (17.1 %, Table 16), in comparison to other mixtures with SAPs. It is known from literature (§ 2.3.3.1) that internal curing contributes to a reduction of autogenous shrinkage microcracking. The relatively low nanoporosity of G025 specimens may as such be explained as it is clear from Figure 43 and the previous discussion that G025 mitigates autogenous shrinkage the best. More detailed studies are required to fully comprehend its mechanism.

Snoeck [42] found the autogenous shrinkage of the mixture R0.35 to be about – 700 µm/m at 6 days after first contact of water and cement (t_0). This amounts to a difference of roughly 600 µm/m between REF and R0.35. It is unclear as to why this difference is so substantial (i.e. a reduction of shrinkage of ca. 80 %) as the knee-points were determined around the same time instant: 540 min after t_0 for REF and 650 min after t_0 for R0.35. Other reference mixtures (i.e. without SAPs) of research by Justs et al. [82] and Dudziak et al. [83] on ultra-high performance concrete (UHPC) showed autogenous shrinkage values at the same age in the range of – 250 µm/m to – 100 µm/m respectively. It is therefore accepted that the mixture of REF differs from R0.35 and the difference is simply attributed to the different chemical composition (or cement even, cf type Strong in Table 2). The order of magnitude of the reduction in autogenous shrinkage by addition of SAPs (and w_{add}) was similar to those of comparable mix designs in the researches by Justs et al. [82] and Dudziak et al. [83].

5.3.2. Unprotected early age shrinkage

The test results from ALM, which would have been used to evaluate the shrinkage evolution in height, were not useful. Over time, the plots of mean technical strain fluctuated substantially, once in expansion then in contraction again. This was, among other flaws, caused by an incremental deviation on each subsequent measurement – which was of course corrected for by using the reference surface measurements, but in vain –, a seemingly random number of laser dots per path and the vulnerability of the test setup to the slightest movement. The only conclusion for these tests is that ALM fails to adequately monitor the shrinkage in height.

Figure 44 shows an unprotected shrinkage strain [%] measurement of the reference mixture, by means of photographic image analysis, zeroed out at 10 min after the first contact of water and cement. In it the two distinct bending points are marked, as was done for the autogenous shrinkage curves as well. It is important to note that the bending points are not the same as the ones obtained in the previous paragraph, as will be discussed in § 5.3.3.

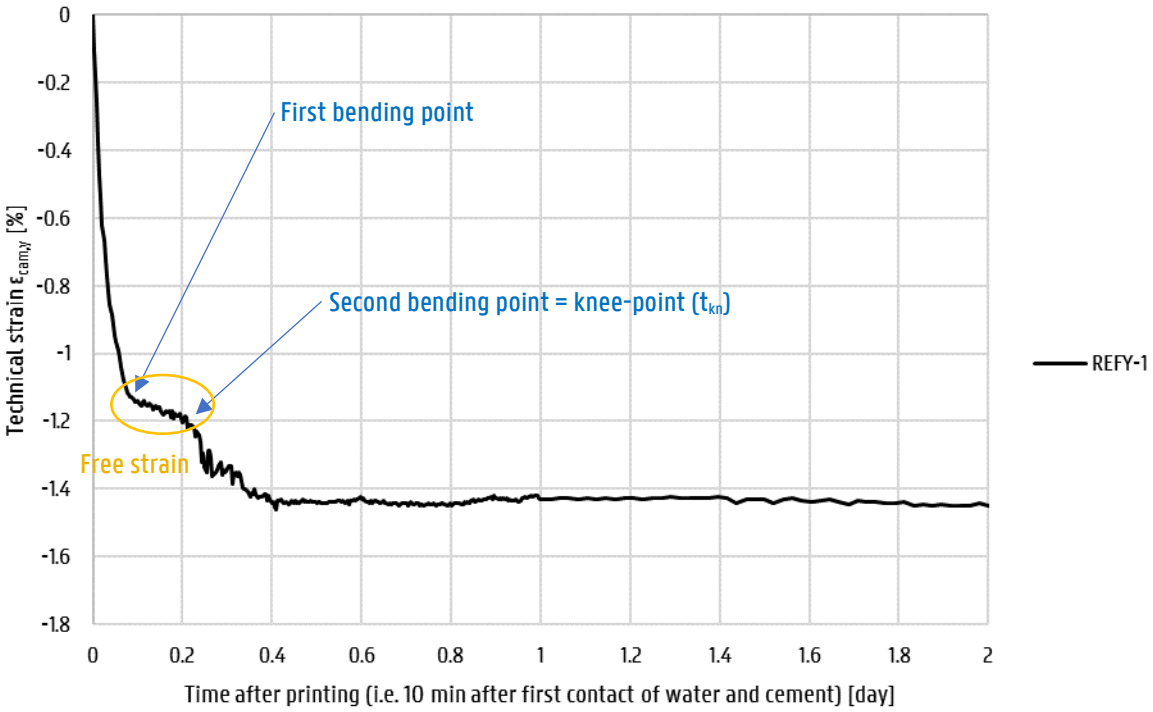

Figure 44: Observation of knee-point in $\varepsilon_{cam,y}$ (REF), originally zeroed out at t_0 + 10 min

Figure 45 and Figure 47 plot the unprotected shrinkage along the printing direction, starting from t_{kn} and respectively ending at 5 days and 1 day after. The unprotected free strain is discussed in the next paragraph.

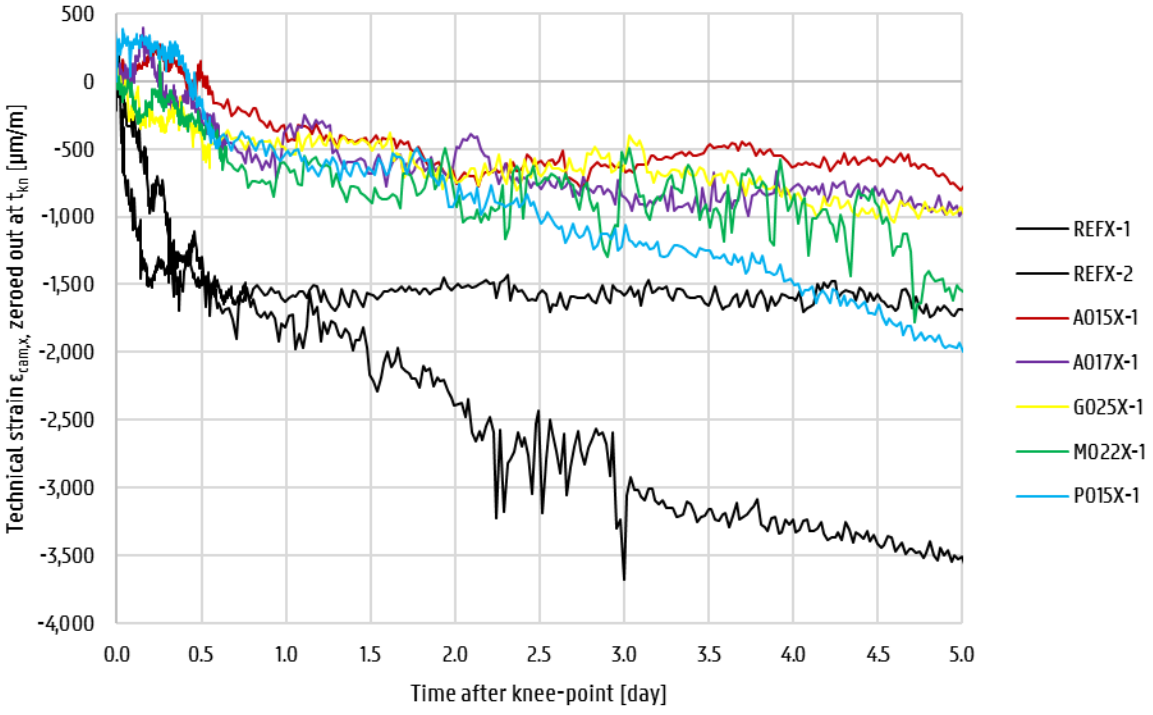

Figure 45: Unprotected shrinkage along the printing direction, $\varepsilon_{cam,x}$ zeroed out at t_{kn} (5 days)

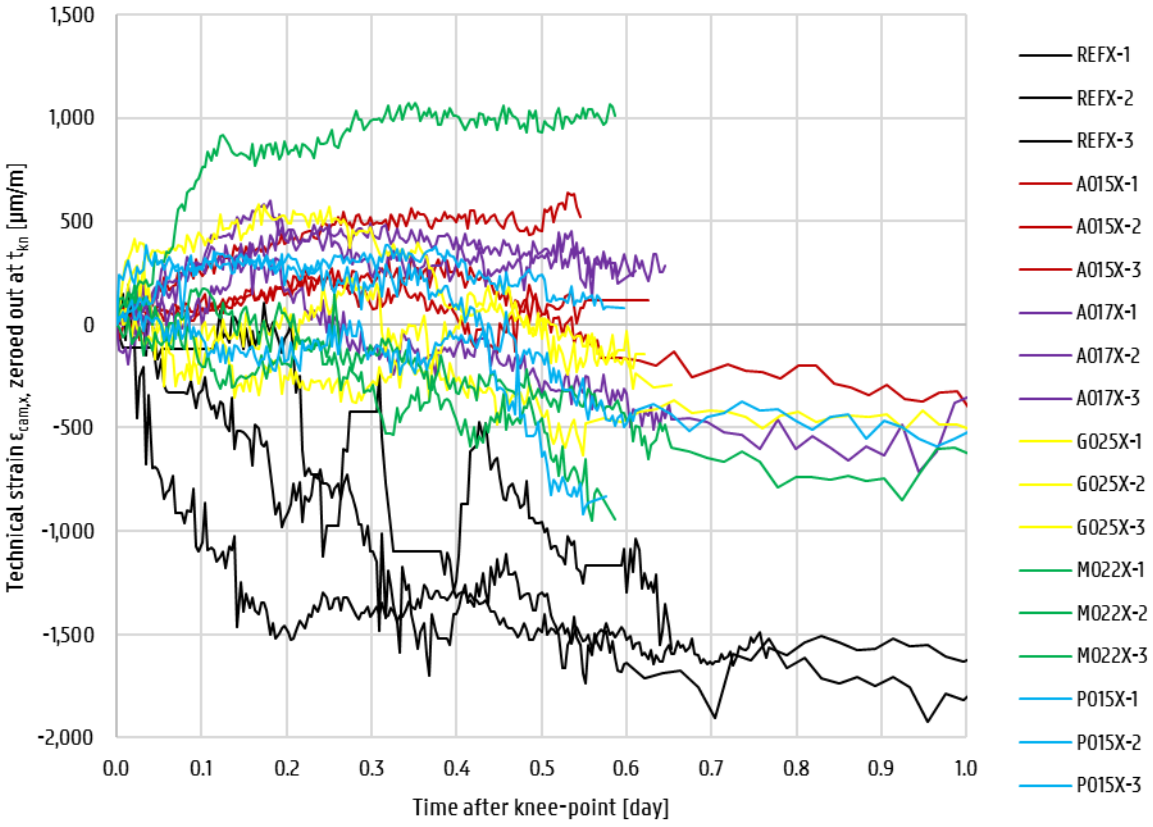

Figure 46: Unprotected shrinkage along the printing direction, $\varepsilon_{cam,x}$ zeroed out at t_{kn} (1 day)

With respect to the unprotected shrinkage along the printing direction, the following observations are made. All mix designs will shrink, however mixtures with SAPs know a minor expansion of about + 300 µm/m during the first 12 to 24 hours after knee-point. During this period the reference specimens show a relatively big shrinkage of about − 1,500 µm/m.
The expansive effect of SAP addition is ascribed to a combination of their water mitigation capacity and a chemical swelling present in all mixtures, but in the case of REF not strong enough to overcome the omnipresent capillary tension. After final setting chemical-structural swelling can occur due to the relatively late formation and growth of calcium hydroxide and to a lesser extent alumina ferric oxide sulphates (which will be present since their reactants are present in the cement mix: see Table 2) [68]. This will create a crystallisation pressure that counteracts the capillary pore water tension that induces self-desiccation. In the case of samples with SAPs, the solid matrix is believed to be more elastic as there is still water being supplied to unhydrated cement particles and as such the structuration continues more actively than in the case of REF, which is quite dry in comparison. Also, the fresh CSH rims that are formed around these unhydrated particles surrounded by water, are larger in volume than their unhydrated counterparts [68]. But as the specimens are unprotected from continued evaporation, only the ones with a water mitigation capacity can benefit from this swelling tendency. It would seem the reference mixture is not able to counteract the self-desiccation as it cannot produce enough continued chemical-structural swelling.
Once hydration slows down as it reaches its optimum, i.e. about a day after the knee-point, all mixtures can only shrink under endured evaporation. The shrinkage rates then align for all

mixtures to about − 200 µm/m/day. On average, this rate is about − 40 µm/m/day lower for the reference mixture. More measurements are required to make a significant conclusion around the difference in rate at later age.
As to why G025 does not show a noticeably better shrinkage mitigation, is attributed to the difference in testing conditions: protected from loss of water to the surroundings, in which case the polymer particles can hold on to their absorbed water; or not, in which case they will lose some to the environment under capillary tension.

Figure 47 and Figure 48 plot the unprotected shrinkage transverse to the printing direction, starting from t_{kn} and respectively ending at 5 days and 1 day after. The unprotected free strain is discussed in the next paragraph.

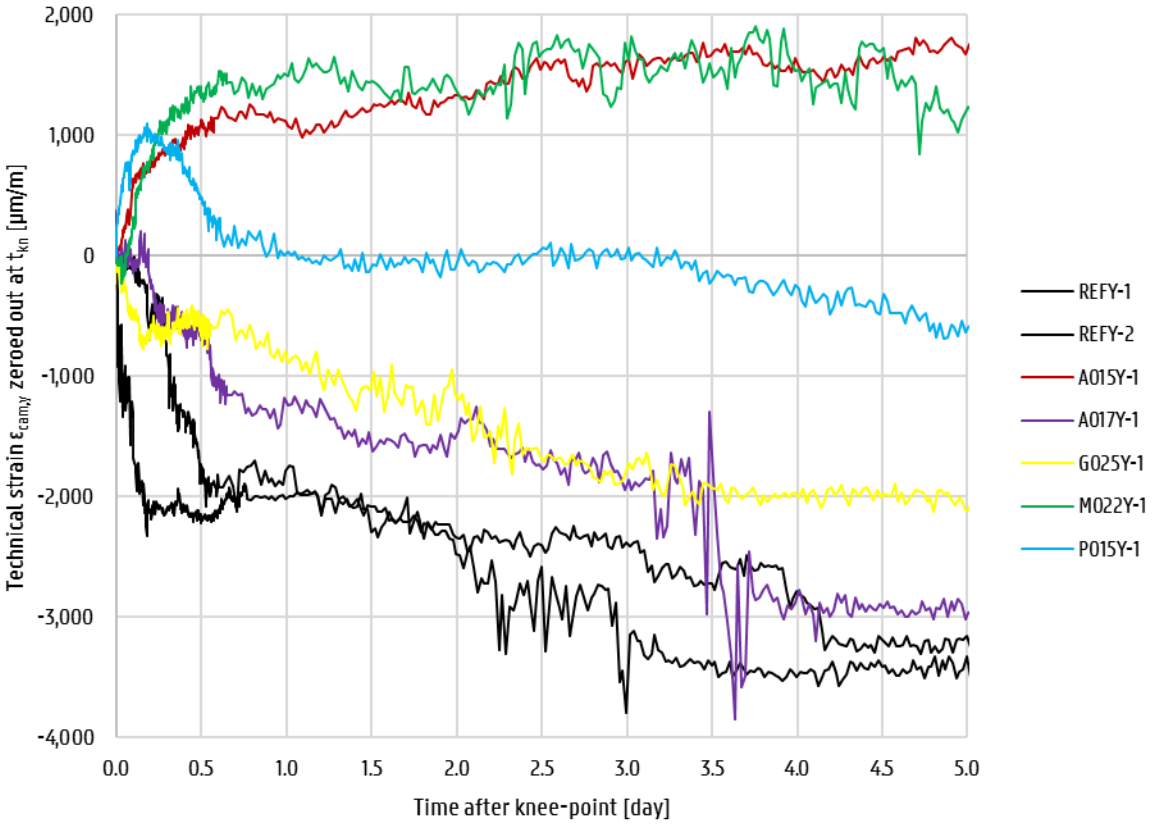

Figure 47: Unprotected shrinkage, transverse to the printing direction, $\varepsilon_{cam,y}$ zeroed out at t_{kn} (5 days)

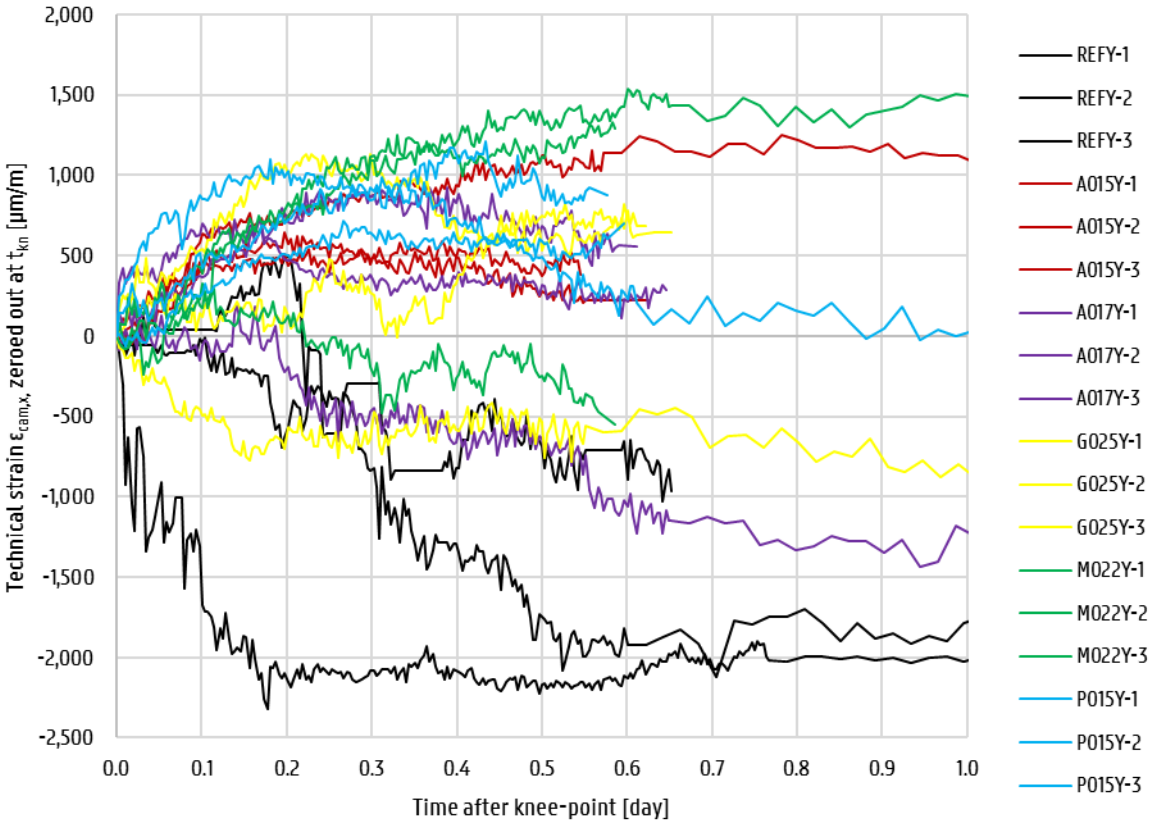

Figure 48: Unprotected shrinkage, transverse to the printing direction, $\varepsilon_{cam,y}$ zeroed out at t_{kn} (1 day)

With respect to the unprotected shrinkage transverse to the printing direction, the same general trend as observed in longitudinal direction holds: SAPs tend to mitigate the shrinkage. The reference mixtures have both in longitudinal and transversal directions the same outcome. The results in transverse direction of mixtures with SAPs are greatly dependent on their behaviour in longitudinal direction, in combination with the length of the sample (along the printing direction).

Figure 49 compares the strains in both directions, and the following observations are made:

- For samples of sufficient length, i.e. around 15 cm, the shrinkage in transversal direction seems a magnification of the one in longitudinal direction: when $\varepsilon_{cam,x}$ shows swelling in the first 12 hours after final setting, $\varepsilon_{cam,y}$ will do too; when $\varepsilon_{cam,x}$ continues to shrink after t_{kn}, $\varepsilon_{cam,y}$ will do as well.
- The only exception to this rule is M022. This mixture expands the most in transverse direction, while it shrinks considerably in longitudinal direction. In this case, it was later remarked that the sample length was only about 11 cm, explaining the opposing phenomenon: less length means less material to restrict $\varepsilon_{cam,x}$, creating a greater expansion transversally (i.e. Poisson deformation).

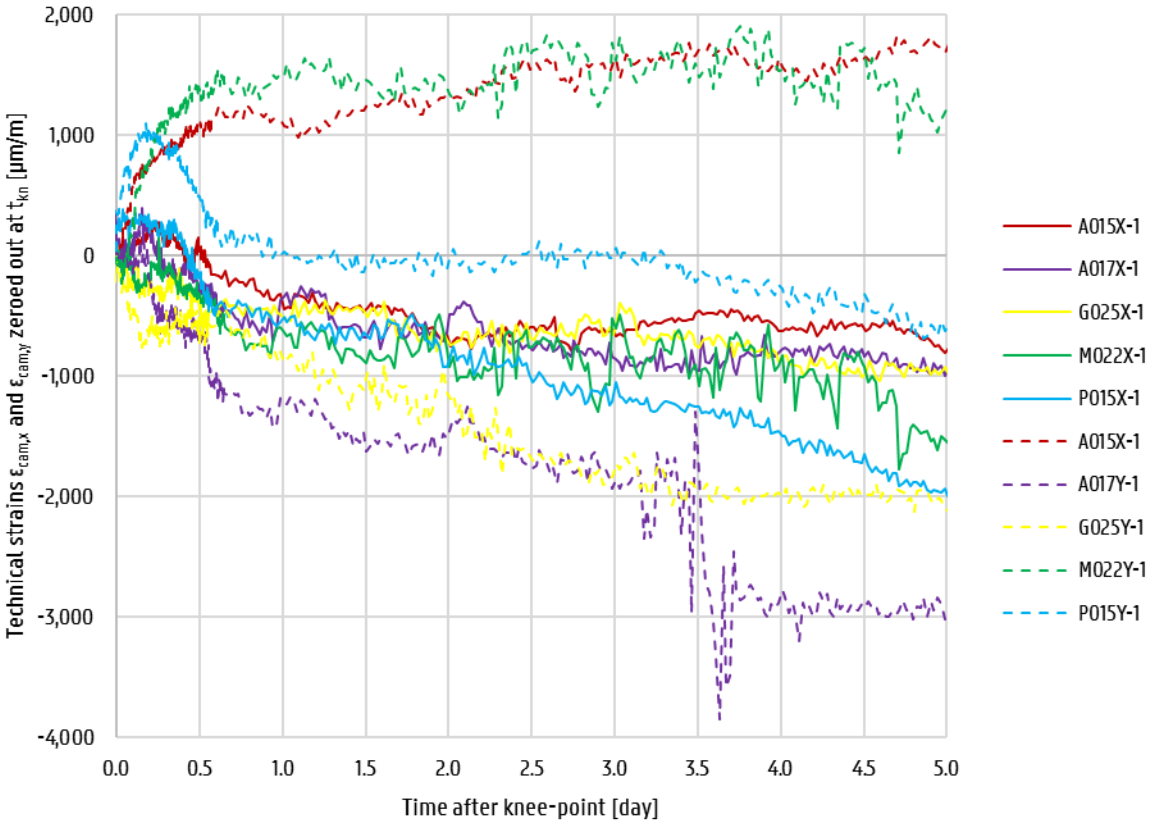

Figure 49: Comparison of unprotected shrinkage strains, along and transverse to the printing direction

Of course, in the field of 3DPC, the longitudinal shrinkage will be of greater importance than the transversal shrinkage, as their linear dimensions are considerably different. From the last observations (Figure 49) it follows that the unprotected shrinkage will depend on the continues length (or dimensions, in general) of the printed specimen. As the perimeter increases, the volume will do too and as such the specimen will restrain itself more from shrinking. Besides, the photographic tests executed in this research were carried out on printed filaments of small size (ca. 15 cm) and able to shrink relatively free (on the manipulated substrate; § 4.1.3).

Dudziak et al. [83] measured free plastic shrinkage in UHPC mixtures according to the setup designed by Slowik et al. [84] shown in Figure 50.

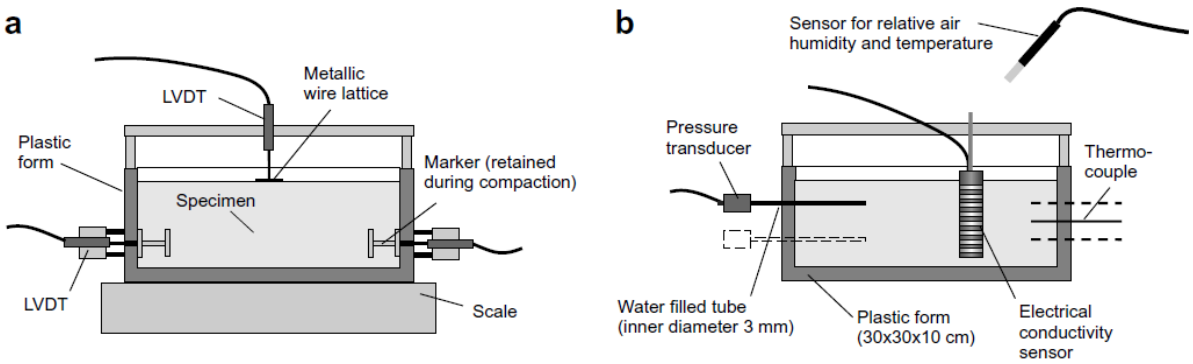

Figure 50: Experimental setup by Slowik [84]

The setup consists of two plastic forms in parallel to enable multiple measurements to be carried out: linear variable differential transformer (LVDT) dilatometry, air humidity sensors, temperature sensors, electric conductivity, capillary pressure, etc. This experimental setup is much more elaborated than the photographic analysis technique used in this research. However, the order of magnitude of free plastic shrinkage (i.e. unprotected shrinkage) from $t_0 + 50$ min on to t_{kn} lies in the same range for both techniques: between $-2.8{\cdot}10^3$ µm/m to $-5.9{\cdot}10^3$ µm/m in [83] versus $-2.3{\cdot}10^3$ µm/m to $-8.0{\cdot}10^3$ µm/m in this research. It would be good to include more comparative experiments in future research (with the same reference mixtures) to evaluate the adequacy of the technique defined in § 4.4.3. However, based on the latter resemblance, the technique is deemed valuable and suitable for conclusive discussion.

5.3.3. Comparison of free strain periods

Table 17 and Figure 51 hold the time instants of all distinct bending points, as well as the durations and rates of free strain.

Table 17: Mean free strain rates in protected and unprotected shrinkage (n = 3)

Mix	Mean free strain rate [µm/m/day]		
	Protected	Unprotected, X	Unprotected, Y
REF	-167.6	$-6.7 \cdot 10^3$	$-8.9 \cdot 10^3$
A015	-5.4	$-7.6 \cdot 10^3$	$-6.0 \cdot 10^3$
A017	-3.3	$-8.0 \cdot 10^3$	$-12.0 \cdot 10^3$
G025	+36.5	$-4.1 \cdot 10^3$	$-2.8 \cdot 10^3$
M022	-20.1	$-7.9 \cdot 10^3$	$-10.1 \cdot 10^3$
P015	-46.7	$-7.6 \cdot 10^3$	$-9.0 \cdot 10^3$
REF*	+33.9	N.A.	N.A.

The free strain rates in protected condition are insignificantly different except for the reference mixture REF. All other mix designs have a more moderate shrinkage rate and sometimes even expansion. This is solely ascribed to the difference in w/c: a lower one leading to more capillary tension. The difference in free strain rates in unprotected condition is statistically insignificant. Though it is remarked that in both conditions, G025 shows the best shrinkage mitigation, undoubtedly due to a combination of one of the previously discussed reasons.
The vast difference in order of magnitude (10^3) of shrinkages (and rates) monitored in both conditions is ascribed to: (1) evaporation of water to the surroundings; (2) the photographic measurement technique which leaves room for improvement (e.g. a higher precision camera); and (3) the calculation of unprotected shrinkage as technical strain that is translated into an equivalent linear shrinkage in µm/m. However, a similar factor was noted in research by Dudziak et al. [83].

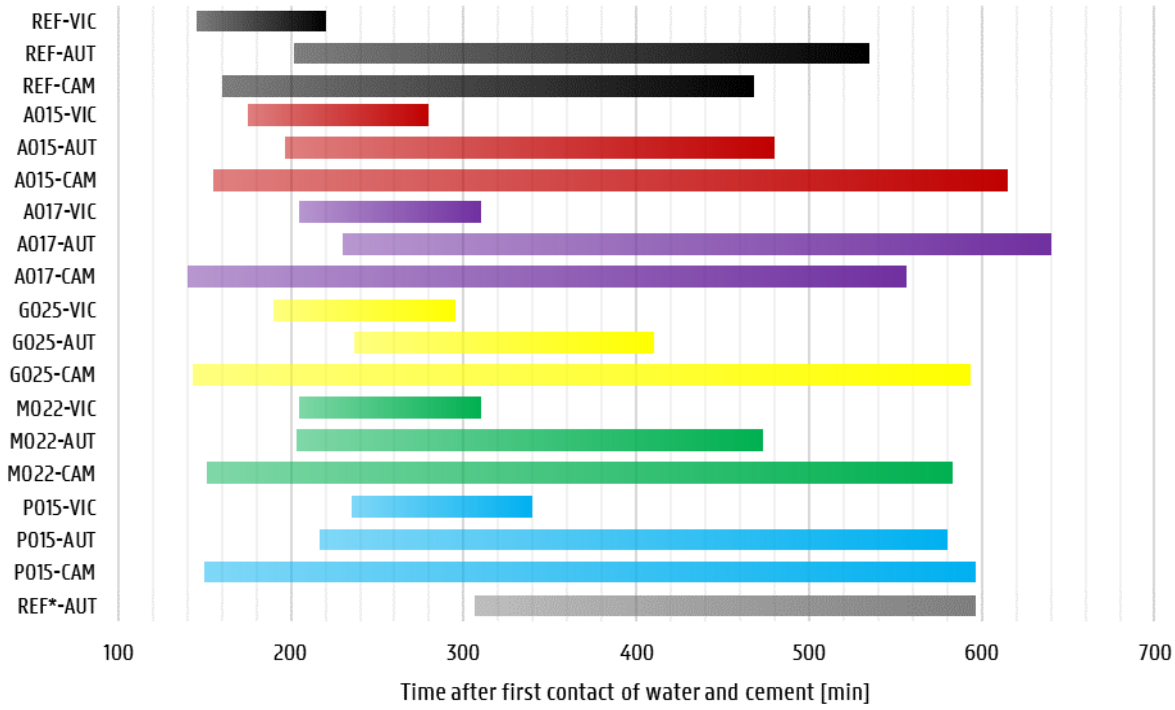

Figure 51: Time instants and durations of free strain periods
(VIC = Vicat, n = 1; AUT = autogenous shrinkage, n = 3; CAM = camera testing, n =3)

The onset of setting according to Vicat ($n = 1$) is postponed with the addition of SAPs (and w_{add}). It takes about 30 min longer to reach final setting, compared to REF. This is due to the SAPs mitigating the additional water to compensate the loss due to evaporation at the top surface, which is bare to the environment. Since the Vicat test will conclude final setting as the moment the needle can no longer penetrate the top surface, its state of freshness (i.e. moist) is crucial for the results. The REF mixture surface will be drier sooner and as such the needle will not be able to penetrate it sooner than for mix designs with SAPs.

The same analogy explains the difference in initial setting time for different techniques. All unprotected shrinkage tests (less distinct for REF) conclude an initial setting time before the one from the Vicat testing. This is explained by the fact that relatively more outer surface is subject to evaporation in the camera tests, creating a drier outer surface with a lower elasticity than the underlying part. On photographs especially, they will appear set, though it might not be completely so. It seems that specimens shielded from the environment in the corrugated tubes harden later, as no mixing water is lost and keeps the mortar fresh. Depending on the retention capacity of the polymers the effective w/c is different, leading to the small differences observed in Figure 51. The larger the effective w/c, or equivalently the less retaining the SAPs are, the later the initial setting time is marked, cf. REF* with the highest $(w/c)_{eff}$ equal to $(w/c)_{tot}$.

The duration of free strain in unprotected specimens is longer than in protected specimens as the latter have a higher effective water-cement ratio, expediting the hydration reaction and as such the hardening process.

For all mix designs with superabsorbent polymers the onsets and durations in unprotected condition differ significantly from the series REF but not from each other. The onsets in

protected conditions are all statistically identical except for REF* and the durations differ too with α_{eff} ranging from 0.047 to 0.221.
The conclusion drawn by Justs et al. [82] and Dudziak et al. [83] that internal curing retards the setting behaviour of cement mixtures, is also valid for the results of this research (Figure 51).

As final remark to this section, the sensibility of the camera setup for unprotected shrinkage measurements is reported. Several data sets of longer periods of monitoring were discarded as the photographing software (operating ceaselessly for months on end) malfunctioned and freezed the image due to movement nearby.

5.4. Mechanical properties

5.4.1. Compressive strength

Figure 52 shows the compressive strength of double-layered specimens printed with a zero time gap.

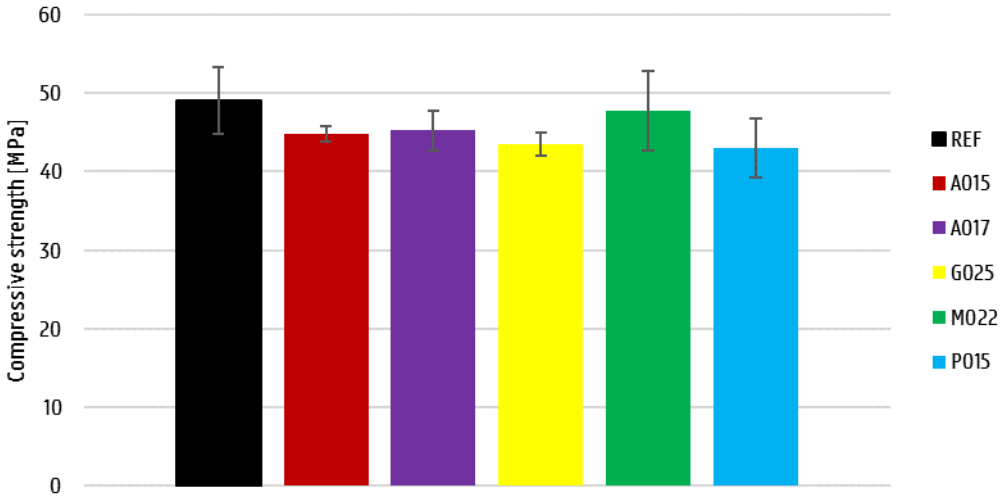

Figure 52: Compressive strength of double-layered specimens at zero time gap

Statistically the difference in compression strengths of all mixtures is insignificant, however two observations stand out: the values of REF and M022. The observation that REF has the largest compressive strength is explained by its low total air content and low void frequency (Table 14) that result in a denser matrix. Contradictory to this result is the high compressive strength in case of M022 which has the largest air content. In this case the result is explained by the fact that SAP M particles are the largest in dry and swollen state. This means that the larger total air content compared to other mixtures is actually divided over a smaller amount of voids in the specimen (cf. $E(\#)$ in Table 15). Consequently, the matrix connections between the voids are thicker and stronger to compression and enable some kind of dome action around the SAP particles (in the proximity of SAPs the matrix reaches a higher hydration rate). Also, by having a larger volume the irregularly shaped voids create less stress concentrations than they would do if they were smaller. M022 has the least total horizontally projected area of SAPs of all mixtures with SAPs: 8,090 mm^2 of SAPs M compared to 14,390 mm^2 of SAPs G in G025 (based on $E(\#)$ in Table 15 and the mean set void diameter in Table 12; see next paragraph: Table 18). This could explain the relatively low compression strength of G025 as well.
In general, the compressive strength is reduced with 2.4 % to 14.0 %. This trend conforms to the reduction of 10 % at the age of 28 days mentioned in the literature review [45], and the reduction of 9 % to 19 % in the research of Justs et al. [82].

Figure 53 shows the compressive strength of double-layered specimens of REF, A015 and A017 printed at different time gaps (of 0, 15 and 30 min; with notations: T0, T15 and T30).
Though not significantly different, neither with respect to mixture nor time gap – except for A015-T15 which differs from A015-T0 and A015-T30 –, there are distinct trends visible. The compressive strength is the largest at T15. This is ascribed to the denser first layer, which can

shrink more freely compared to double-layered specimens (T0) since the second layer will increase the outward hydrostatic pressure that counteracts the longitudinal contraction. From Figure 44 it is clear that even after 15 minutes the unprotected shrinkage strain can amount to −4 ‰, proving the importance of duration of time gap. The second layer that follows after 15 minutes is then also restricted more in its early shrinkage and results in a denser matrix as well. Values for a time gap of 30 minutes are lower than for 15 minutes but seem larger than zero time gap values for SAP mixtures and lower again for the reference mixture. But it is not the case that at T30 specimens obtain greater compressive strength, despite densification of their matrix due to shrinkage. The difference between T15 and T30 is then ascribed to air that gets entrapped more for older sublayers as it is drier at the surface (Figure 37), more rigid and therefore disables air to be squeezed out of the interface when another filament is superposed. The difference in strength between different mixtures is explained by the difference in retention capacity of the polymers or the lack of water retention at all. A017 can retain more water due to its larger SAP mass percentage added compared to A015, loses less permanently to the environment and is therefore more able to connect the fresh and older layers by gradual release over time. This is reflected in the surface moisture of Figure 37 as well: A017 seems drier at the surface as it retains the water longer internally. This figure holds the answer to why REF-T30 does not perform better under compression than REF-T0 as well: it has lost the most water to evaporation since it has no retention capacity.

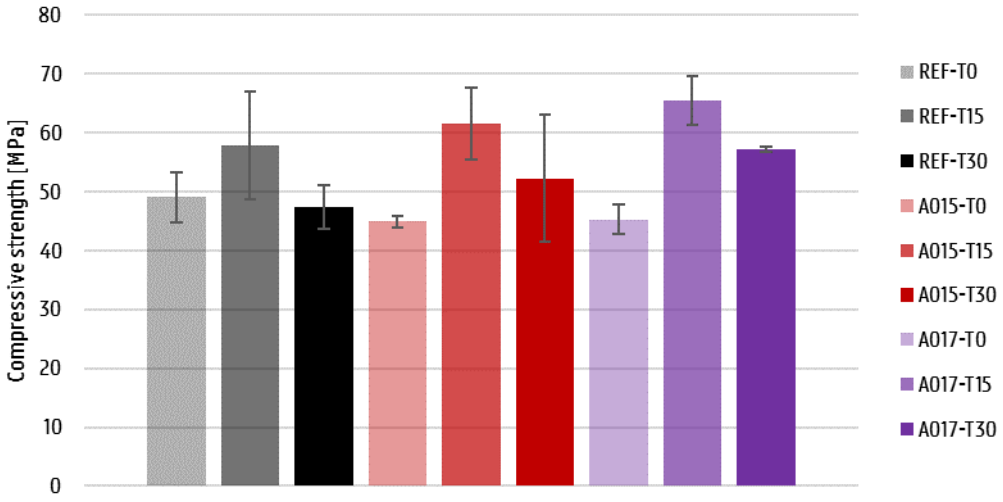

Figure 53: Compressive strength of double-layered specimens at different time gaps

5.4.2. Interlayer bonding strength

Figure 54 shows the interlayer tensile strength at zero time gap. Statistically the results do not differ significantly, however a clear trend becomes apparent.

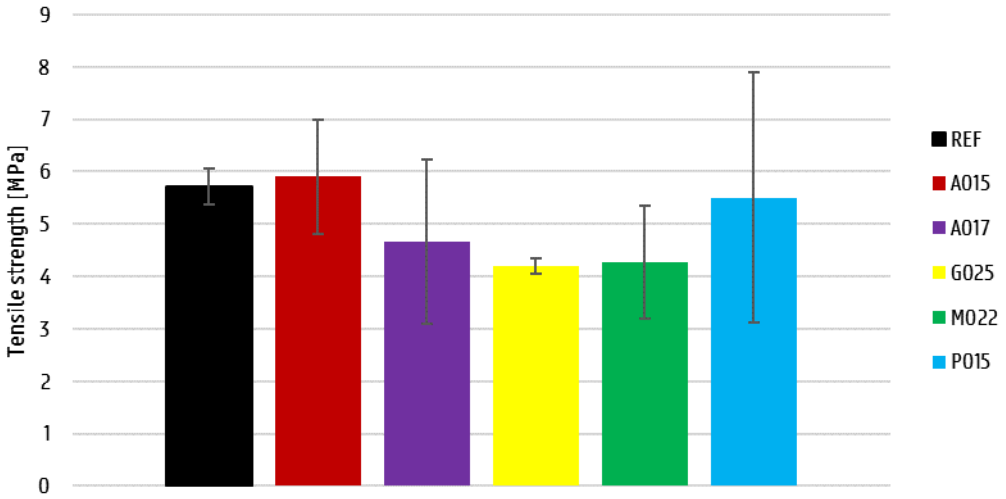

Figure 54: Interlayer tensile strength of double-layered specimens at zero time gap

It would seem there is an inversely proportional relationship between the amount of superabsorbent polymers added and the tensile strength of the interlayer. Crack initiation will generally happen at the interface as air gets entrapped between two superposed filaments, but the propagation will cross a normally dense matrix which as such defines the overall tensile strength. The density of the matrix depends on the air content and since that is proportional to the amount of polymers added (cf. Table 14 and Table 15), the latter will govern the tensile strength.

Table 18 holds the calculation of total horizontally projected area $A_{\perp}$ [mm^2] of SAP particles over the whole volume of one mortar batch, based on the expected number of SAPs in each mixture ($E(\#)$, Table 15) and the mean set void diameter (μ_{set} in Table 12). It would appear there is a linear relationship between this value and the tensile bonding strength of the interlayer (coefficient of determination equals 0.72). The tensile strength reduces with increasing projected area.

Table 18: Calculation of total horizontally projected area of SAP particles

Mix	E(#)	μ_{set} [mm]	$A_{\perp}$ [mm²]	f_t [MPa]
A015	8,708	0.308	8,418	5.91
A017	9,869	0.308	9,540	4.66
G025	8,769	0.522	14,390	4.20
M022	2,549	1.010	8,090	4.27
P015	4,160	0.492	8,444	5.50

The expected result for the tensile strength of the mixture M022 is according to the linear relation 5.81 MPa. This estimation does not agree with the value obtained from testing, as the latter is the lowest strength of all. This is ascribed to the greater amount of entrapped air at the interlayer (see Figure 40, § 5.2.4.1).
It is remarked that both M022 and G025 show the largest amount of nanopores below 100 nm. However, the previous reasoning is believed to be more influential for the tensile strength. Future research might include more detailed study to the exact effect of nanoporosity on the mechanical properties.

Figure 55 compares the interlayer tensile strength for different time gaps.

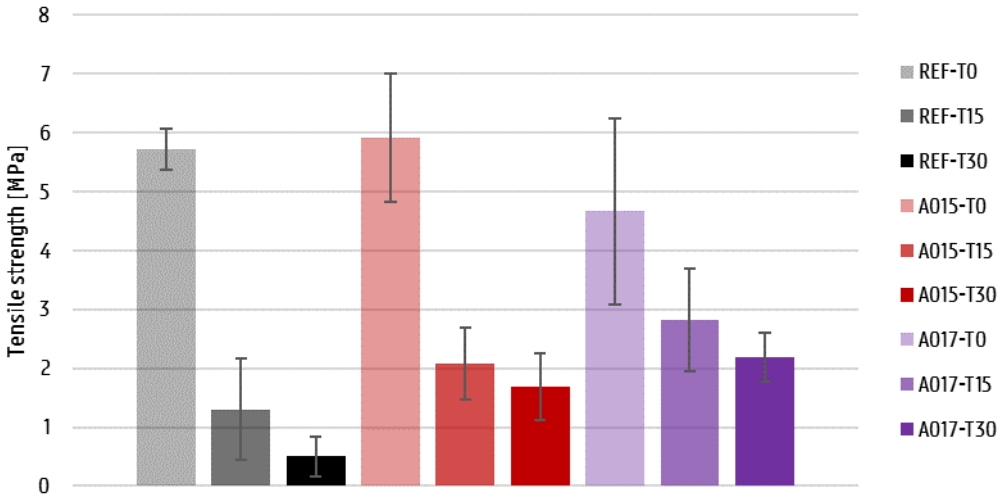

Figure 55: Interlayer tensile strength of double-layered specimens at different time gaps

The longer the time gap, the drier (Figure 37) and more rigid the outer surface of the first filament will be, obstructing entrapped air to be squeezed out of the interlayer (cf. § 5.4.1). Longer time gaps lead to more big air voids at the interface and these are destructive to the tensile strength as the crack propagates, connecting them one by one.
A more important influence is accounted to the difference in shrinkage rates between the two superposed filaments. In the case of compressive strength this might be beneficial as the two layers end up with a denser matrix. The restriction of the sublayer to the free shrinkage of the upper layer might however lead to (micro-)cracking in the connections between the layers. These reduce the resistance to tensile (and shear) loading.

The fact that A017-T15 and A017-T30 lose less of their initial strength as the time gap increases, compared to REF and A015, is due to their better water management as elaborately discussed before. The lack of such a capacity in the reference mixture leads to the lowest values in comparison. This was also stated by Buswell et al. [17] as the temporary lifetime of cold joints in SAP mixtures: cold joints may disappear when hydration between the layers commences.

Figure 56 and Figure 57 respectively show the interlayer shear strength for zero time gap and for comparison of different time gaps.

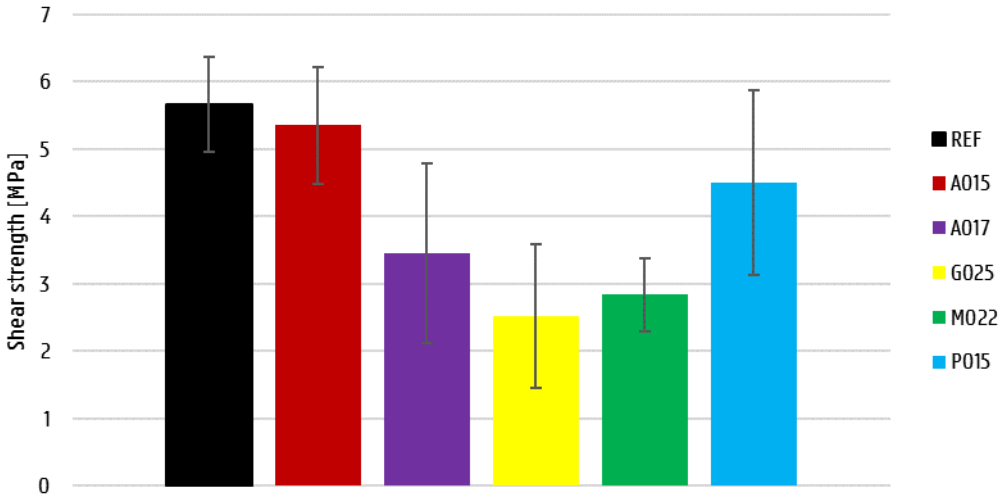

Figure 56: Interlayer shear strength of double-layered specimens at zero time gap

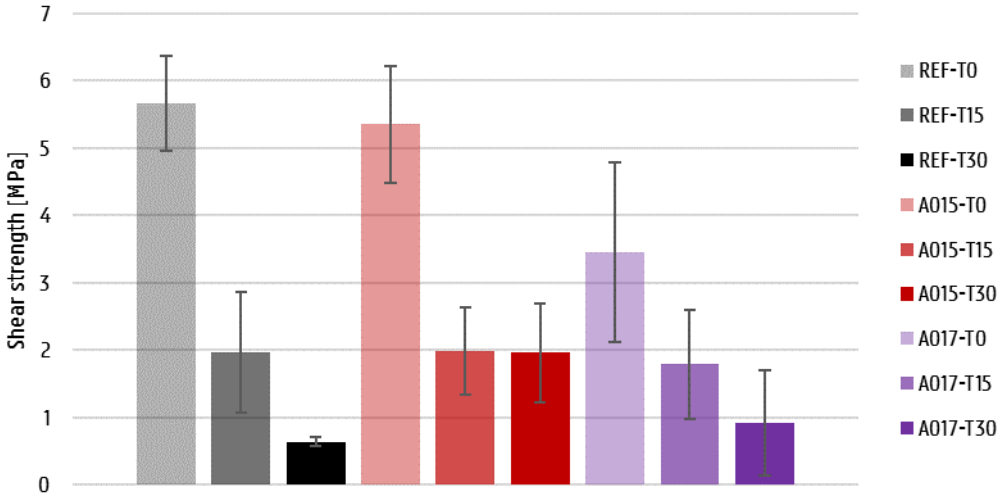

Figure 57: Interlayer shear strength of double-layered specimens at different time gaps

The same trends hold as observed for the tensile strengths, which makes sense as both quantities evaluate the resistance to a tensile stress (or a combination of tension and compression in the case of shear). In general, the shear strengths are lower (ca. 1 MPa) than the tensile strengths, which is to be expected according to Equation (21):

$$f_s \leq \sqrt{2} f_t \tag{21}$$

stated as the shear strength of unreinforced concrete in [80]. The measured value of f_s also depends on the testing procedure itself, which induces bending tension, and on local weaknesses around the interface of two superposed layers. These may lead to a lower shear force registered than might actually be the resistance.

It is believed the surface moisture (Figure 37) is more like a necessity rather than a sufficiency with regards to good interlayer bonding strength, as there exists no one-on-one relation between the two, according to the results of previous tests. The surface of printed layers of mixtures with SAPs will be more moist over time, compared to the reference mixture, but this is a consequence of the water management of SAPs. The temporary character of a cold joint confirms this as well.

CONCLUSIONS

Distributio autem est copiarum locique commoda dispensatio parcaque in operibus sumptus ratione temperatio.

MARCUS VITRUVIUS POLLIO

DE ARCHITECTURA | LIBER PRIMUS | CAPUT SECUNDUM

Economy consists in a due and proper application of the means afforded according to the ability of the employer and the situation chosen; care being taken that the expenditure is prudently conducted.

6. Conclusions and future research

This chapter holds the essential conclusions and recommended topics for future research, organised per main subject.

6.1. Conclusions

6.1.1. On printability

A good estimation of the SAP amount needed to compensate an additional mass of water w_{add} and keep the effective w/c unaltered, is found by taking the swelling capacity in mortar as half of the one in cement filtrate. The optimal amount of added superabsorbent polymer, resulting from trial-and-error workability testing, should not deviate much from the initial estimate, i.e. only a couple of mass percentage points. If that is however the case, this either indicates a flaw in the mixing procedure or an incapability of the polymer to absorb any of the mixing water.

Regular-shaped superabsorbent polymers, generally produced by suspension polymerisation and/or finalised by extrusion (i.e. SAPs D, F and H), are less efficient than irregularly shaped polymers produced in bulk, when it comes to retaining mixing water in mortars. In the case of the grapes-like particle D, the inadequacy lies in the swelling kinetics in combination with the fact that during mixing the polymer in swollen state gets broken. Though the initial addition of D leads to a huge reduction in effective water-cement ratio, it does not last long. And as in its broken state the overall polymer volume has more specific surface, it should show a larger swelling tendency which it does not. The exact reason should be found in its swelling kinetics. As such, a large and uneconomic amount of the polymer (> 0.5 m%) needs to be added for redundancy, making it unfit for practical applications. The F fibres meet the same fate as they are broken in the mixing procedure and lose their absorbed water. In this case the effect is not especially ascribed to the chemical structure but rather to its geometrical shape. The spherical SAP particles H are not broken down in the mixing procedure but cannot compete in water attraction with the cement particles due to their shape and small size of only around 70 µm. They have a relatively small surface per mass added compared to the other irregular-shaped SAPs studied and it is confirmed again that the activity of the outer surface is less than that of the bulk material. Another explanation of SAP H's reduced effect on workability lies in its spherical particles, which do not restrict the mortar mass as much as irregularly shaped particles. However, the marginal workability influence of a substantial addition of 0.6 m% cannot solely be ascribed to its geometrical properties, but to its swelling kinetics and possible balling effect as well. Further research is required to provide a definitive explanation.

The flow table test results depend on the preceding mixing procedure, i.e. its effect on the behaviour of the superabsorbent polymers. Small (dry ∅ ca. 100 µm), irregular and fast-swelling (< 10 s) polymers, such as SAP A, are less affected by the hindrance of sand granulates that tend to slow down the swelling rate and sometimes destroy the (swollen) polymers altogether. Indeed, the SAP particles initially blend in with the largest cement particles and fit in the voids between the inert sand granulates, as well as are almost unaffected by a change in

duration of mixing procedures by swelling fast. Big (dry ∅ ca. 500 µm), irregular and slow-swelling (> 60 s) polymers, alike SAP M, seem not influenced by the mixing procedure. Their size, elasticity and shape help them against possible sand attack and their swelling behaviour is quite inert to a variation in mixing duration. SAPs with intermediate properties (cf. G and P) show a greater susceptibility to flow dissimilarities as they are more vulnerable to sand, especially in (quasi)-swollen state and more influenced by a change in mixing order or duration. The discrepancy between flow curves following different mixing procedures generally becomes smaller as the mix design reaches its optimal SAP amount to compensate w_{add}.

Larger polymer particles (200 µm ≲ dry particle size < 500 µm) tend to make the mortar less viscous as they have a lubricating capacity that reduces the internal shear and friction to the sides of the pumping system, when put in motion. The lower viscosity will in turn lead to a smoother surface of the printed filament but a lower dimensional stability when a second layer is put on top as well.

The chemical structure of the SAPs and their associated properties are of paramount importance. This in combination with the physical, especially geometrical characteristics, defines their behaviour in fresh mortar. More specialised research is required to perfect and validate the previous theories.

6.1.2. On the printing process

Both the printing process and the mixture to be printed influence each other's characteristics:

Mixtures with SAPs tend to retard the onset and duration of setting compared to the reference mixture without SAPs. This influences the duration of open time of printing and the choice of time gap.

The workability reduces quite quickly over time: flow table diameter from 21 cm to 18 cm in 30 min. This will influence the printing procedure in the mortar production (e.g. volume of a batch, continuity of production, …) and in time gap as well.

Mixtures with larger SAP particles (200 µm ≲ dry particle size < 500 µm) tend to show a lubricating behaviour that reduces the energy loss due to friction on the sides of the pumping hose. The possibility of swollen SAP particles segregating and migrating to the outside of the printed filament was noted, but nothing conclusive follows from this research.

Air can get trapped at the interface of two superposed layers. The likeliness to find a higher air content in the interlayer is dependent on the printing procedure as well as on characteristics of the printed mixture. The nozzle standoff distance and shape, printing speed and flow rate influence the surface quality of the printed filament, making it rougher or smoother and consequently more susceptible to entrapped air, respectively less so. In this research these parameters were held constant throughout. The dimensional stability of a printed layer under its own weight or that of a superposed one, in combination with their respective states of viscosity

influence the interlayer quality. Layers with a low buildability and high viscosity (M022) show more entrapped air at the interlayer than layers with a high stability and low viscosity (G025). Air entrapment may also result from slight variations in the process or mixture, which are variable in nature and cannot be eliminated.

The bottom layer has, in comparison to the inter- and top layer, a lower nanoporosity, ascribed to its denser matrix under increased hydrostatic pressure of superposed layers. The density of the matrix at the interlayer is influenced by entrapped air and water pockets that might have influence on both micro- and nanoporosity.

Comparison with other research showed that it is likely the air content in printed specimens is higher than in mould casts of the same mixture, especially if the latter are compacted.

From simultaneous research on 3D printing of cementitious materials, it showed that mixtures optimised for 2D printing could not be used in 3D printing as the delivery system of the machines greatly differed.

The duration of time gap is an important influencer of the degree of free (i.e. less restrained) shrinkage. The latter also depends on the perimeter of the printed specimens. A newly printed layer is restricted in its shrinkage by its own size (the larger, the more restriction) and by the layer underneath that, depending on the time gap, has reached a higher shrinkage strain. This differential shrinkage may lead to (micro-)cracking of the connections between the two layers and as such to a reduction in interlayer bonding strength.

6.1.3. On early age shrinkage

The automated laser measurement of height in time proved inadequate to substantiate the respective shrinkage evolution. This was due to a multitude of inaccuracies inherent to the technique: incremental deviations from the reference level, varying number of coordinates per laser path and vulnerability to movement by neighbouring activities.

For both environmental conditions (protected from evaporation or not) the shrinkage plots in time show two distinct bending points, between 2 and 10 hours after first contact of water and cement, marking changes in the chemical structure of the specimen. The first bending point is observed at the transition of suspension state to percolation and will as such slow down the vast plastic shrinkage. The second bending point, i.e. by definition the knee-point, indicates the final setting time after which the autogenous shrinkage is mostly self-desiccative. In between lies a period of free (autogenous) strain, so-called as the apparent volume is not different from the absolute.

The shrinkage mitigation capacity of any mixture can be explained by the notion of efficiency in water supply, based on the spatial distribution, retention and recapture tendencies of its internal water reservoirs. Right after final setting (i.e. the knee-point) a chemical-structural swelling can occur due to the formation and growth of more voluminous hydration products,

such as calcium hydroxide and ettringite. Possible reabsorption of bleeding water will also lead to swelling of the apparent volume. In the case of mix designs without SAPs, this swelling ability goes almost unnoticed as the shrinkage due to capillary pore tension is more dominant, especially for low w/c. In order to enable the swelling to manifest, an active internal water management is needed, for example by adding superabsorbent polymers. They can recapture bleeding water, locally maintain chemical-structural swelling, and most importantly reduce the capillary tension forces. G025 shows the best shrinkage mitigation, especially shielded from evaporation, as it has a good void frequency, is more abundant (small size and large m%) and shows the best water retention capacity. Other SAP mixtures in this research showed more or less the same shrinkage reduction (for both environmental conditions). The reference mixtures without SAPs knew the largest shrinkage strains.

The water management characteristics of superabsorbent polymers will influence the onset of setting and its duration. SAPs who absorb more than the additional mass of water, reduce the effective water-cement ratio and stall as such the hydration. Their spatial distribution and chemical ability to supply water to the unhydrated cement particles determine the duration of free strain: a better efficiency leads to faster setting. Setting times and durations also depend on the condition of testing: a greater surface subject to evaporation will commonly lead to faster initial setting and later final setting.

It is remarked that the optimal mix design in mitigating autogenous shrinkage, i.e. G025, shows relatively good reduction of (longitudinal) unprotected shrinkage. Future research could establish whether this correlation is generally valid.

The unprotected shrinkage development, transverse to the printing direction is dependent on the longitudinal shrinkage evolution. It will show some kind of magnification of the longitudinal effect, except for when the length over width ratio of the printed specimen drops below 3.5: in that case it will expand as the specimen contracts in length, and vice versa, due to increased effect of Poisson deformation.

There is a difference in order of magnitude of shrinkages (and rates) monitored in both environmental conditions, of about 10^3 (unprotected conditions amount to substantially more shrinkage). This is ascribed to the influence of evaporation and the photographic measurement and calculation technique of the unprotected shrinkage. It is believed that camera equipment with a higher resolution will lead to more precise results. However, the clearly observable trends suggest the method is already useful for qualification. Moreover, the same order of magnitude of strains and ratios was stated in other research with different experimental setups.

6.1.4. On mechanical properties

The compressive strength is not substantially reduced by the addition of SAPs: a reduction of 2.5 % to 14.0 % depending on the mixture, which is comparable to the range resulting from other researches in literature. But it is remarked that a lower number of larger polymers is less compromising than an equal total swollen volume divided over smaller and therefore more

particles. This is due to the effect on a continuous matrix and the shape of the particles creating stress concentrations. Relatively big but less abundant irregular particles thicken the matrix connections in between and are able to transfer the compressive stress by dome action.

For layers printed with an intermediate time gap of 15 minutes, the compressive strength is larger than for a zero time gap. This is ascribed to the difference in restriction of shrinkage between one- and two-layered specimens. In the latter the initial unprotected shrinkage is counteracted more by a larger hydrostatic pressure, as it has double the height of a single filament. The more freely deforming single sublayer has a denser matrix after 15 minutes and will in turn restrict the shrinkage of the second layer more. A denser matrix leads to a higher compressive strength. From a time gap of 30 minutes on, the gain in strength has become marginal as the outer surface of the sublayer is believed too dry and rigid, enabling air being stuck at the interface.

The interlayer tensile and shear strengths are inversely proportional to the air content of the specimens, being in turn proportional to the mass of SAPs added. A linear relationship exists between the total horizontally projected area of SAP particles over the volume of specimen and its bonding strength. The larger the total projected area of SAPs, the greater the reduction in continuous mortar matrix and as such the greater its reduction in resistance to tensile loads. Most of the time, a crack will initiate near the interface as this is the preferred location for larger entrapped air voids, but it propagates through a regularly dense matrix, which determines the final strength. The influence of nanoporosity was noted but no conclusive relation could be remarked. In the same respect, the influence of a good hydration stimulation by SAPs is noted (e.g. G025) but deemed of minor importance compared to the micro- and macroporosity of the matrix.

The interlayer bonding strength reduction at longer time gaps is ascribed to the entrapment of air between a drier and more rigid first layer and a new layer, as well as to their differential shrinkage strain. In the case of compressive strength this might be beneficial as the two layers end up with a denser matrix. The restriction of the sublayer to the free shrinkage of the upper layer might however lead to (micro-)cracking in the connections between the layers. These reduce the resistance to tensile (and shear) loading.

The surface moisture is believed to be a necessity rather than a sufficiency in the bonding strength of the interlayer. It is a sign of active water management by SAPs but, as a possible cold joint is temporary in nature (in SAP mixtures), not an exclusive one.

6.2. Future research

Future research could include:

- microscopy of fresh mortar and paste (without sand), focusing on the state of the SAPs: unsaturated, swollen, broken, clustered, …
- testing the influence of more diverse mixing procedures in order to evaluate the influence of the printing parameters;
- test repetitions on normally cast (compacted and uncompacted) samples;
- rheological research with more precise tools on the influence of SAP addition on the viscosity and the latter in turn on the aspects of printability;
- detailed study of the exact kinetics of each of the SAPs and their influence on the swelling behaviour in mortar over time;
- test repetitions with slightly altered mix designs to validate the robustness of the theories described in this research;
- repetitions of photographic shrinkage tests for seven days and comparative tests of the unprotected shrinkage measurement setup used in this research and other techniques mentioned in literature;
- unprotected shrinkage measurements for longer periods of time, to include drying shrinkage amongst others;
- measuring the internal relative humidity evolution and heat production, to be able to link it to the bending points and chemical or physical alterations of the specimens;
- scanning electron microscopy (SEM) to study the chemical structure in more detail, focussing on the outer surface and interface of printed specimens;
- microscopy (and MIP, RapidAir and/or SEM) of sections of hardened single-layered printed filaments and specimens in corrugated tubes;
- microscopy (and MIP, RapidAir and/or SEM) of sections of hardened single-layered and double-layered printed specimens in different directions to the printing direction;
- mechanical test repetitions in the other orthogonal directions to the printing direction;
- test repetitions for different intermediate time gaps, for example: every five minutes between 0 and 30 min.

APPENDICES

Harmonia autem est musica litteratura obscura et difficilis, maxime quidem quibus graecae litterae non sunt notae. Quam si volumus explicare, necesse est etiam graecis verbis uti, quod nonnullae eorum latinas non habent appellationes.

MARCUS VITRUVIUS POLLIO

DE ARCHITECTURA | LIBER QUINTUS | CAPUT QUARTUM

Harmony is an obscure and difficult
musical science,
but most difficult to those
who are not acquainted with
the Greek language;
because it is necessary to use many
Greek words to which there are none
corresponding in Latin.

References

[1] ASTM F42, Standard Terminology for Additive Manufacturing Technologies, American Society for Testing and Materials, Pennsylvania, United States, 2015.

[2] Lloret E., Shahab A. R., Linus M., Flatt R. J., Gramazio F., Kohler M., Langenberg S. (2015). Complex concrete structures: merging existing casting techniques with digital fabrication. Comput-Aided Des 60, 40–49.

[3] Rouhana C. M., Aoun M. S., Faek F. S., Eljazzar M. S., Hamzeh F. R. (2014). The reduction of construction duration by implementing contour crafting (3D printing), in: Proceedings of the 22nd Annual Conference of the International Group for Lean Construction: Understanding and Improving Project Based Production (IGLC). The International Group for Lean Construction Oslo, Norway, pp. 1031–1042.

[4] Nematollahi B., Xia M., Sanjayan J. (2017). Current progress of 3D concrete printing technologies. Proceedings of 34th International Symposium on Automation and Robotics in Construction, Taiwan, pp. 260–267.

[5] Sanjayan, J. G., Nematollahi, B., Xia, M., & Marchment, T. (2018). Effect of surface moisture on inter-layer strength of 3D printed concrete. Construction and Building Materials.

[6] Marchment, T., Xia, M., Dodd, E., Sanjayan, J., & Nematollahi, B. (2017). Effect of delay time on the mechanical properties of extrusion-based 3D printed concrete. In International Symposium on Automation and Robotics in Construction.

[7] Le, T. T., Austin, S. A., Lim, S., Buswell, R. A., Gibb, A. G. F., & Thorpe, T. (2012). Mix design and fresh properties for high-performance printing concrete. Materials and Structures/Materiaux et Constructions.

[8] Jolin, M., Burns, D., Bissonnette, B., Gagnon, F., Bolduc, L. S. (2009. Understanding the pumpability of concrete. Proceedings: Shotcrete for Underground Support XI, Engineering Conferences International.

[9] Beaupré, D. (1994). Rheology of High Performance Shotcrete. Civil Engineering Department, University of British Columbia, Canada. Ph.D. Thesis.

[10] Roussel, N. (2018). Rheological requirements for printable concretes. Cement and Concrete Research.

[11] Chapdelaine, F. (2007). Étude fondamentale et pratique sur le pompage du béton. Ph.D. Thesis, Laval University, Quebec, Canada.

[12] Kuder, K. G., & Shah, S. P. (2007). Rheology of extruded cement-based materials. ACI Materials Journal.

[13] Bos, F., Wolfs, R., Ahmed, Z., & Salet, T. (2016). Additive manufacturing of concrete in construction: potentials and challenges of 3D concrete printing. Virtual and Physical Prototyping.

[14] Miller, E., & Rothstein, J. P. (2004). Control of the sharkskin instability in the extrusion of polymer melts using induced temperature gradients. Rheologica Acta.

[15] Mettler, L. K., Wittel, F. K., Flatt, R. J., & Herrmann, H. J. (2016). Evolution of strength and failure of SCC during early hydration. Cement and Concrete Research.

[16] Mewis, J., & Wagner, N. J. (2009). Thixotropy. Advances in Colloid and Interface Science, 147–148, 214–227.

[17] Buswell, R. A., Leal de Silva, W. R., Jones, S. Z., & Dirrenberger, J. (2018). 3D printing using concrete extrusion: A roadmap for research. Cement and Concrete Research.

[18] Ma, G., Li, Z., & Wang, L. (2018). Printable properties of cementitious material containing copper tailings for extrusion based 3D printing. Construction and Building Materials.

[19] Papachristoforou, M., Mitsopoulos, V., & Stefanidou, M. (2018). Evaluation of workability parameters in 3D printing concrete. Procedia Structural Integrity.

[20] Li, Z., Wang, L., & Ma, G. (2018). Method for the Enhancement of Buildability and Bending Resistance of 3D Printable Tailing Mortar. International Journal of Concrete Structures and Materials.

[21] Roussel, N., Ovarlez, G., Garrault, S., & Brumaud, C. (2012). The origins of thixotropy of fresh cement pastes. Cement and Concrete Research.

[22] Perrot, A., Rangeard, D., & Pierre, A. (2016). Structural built-up of cement-based materials used for 3D-printing extrusion techniques. Materials and Structures/Materiaux et Constructions.

[23] Le, T. T., Austin, S. A., Lim, S., Buswell, R. A., Law, R., Gibb, A. G. F., & Thorpe, T. (2012). Hardened properties of high-performance printing concrete. Cement and Concrete Research.

[24] Paul, S. C., Tay, Y. W. D., Panda, B., & Tan, M. J. (2018). Fresh and hardened properties of 3D printable cementitious materials for building and construction. Archives of Civil and Mechanical Engineering.

[25] Panda, B., Chandra Paul, S., & Jen Tan, M. (2017). Anisotropic mechanical performance of 3D printed fiber reinforced sustainable construction material. Materials Letters.

[26] Roussel, N., & Cussigh, F. (2008). Distinct-layer casting of SCC: The mechanical consequences of thixotropy. Cement and Concrete Research.

[27] Roussel, N. (2006). A thixotropy model for fresh fluid concretes: Theory, validation and applications. Cement and Concrete Research.

[28] Panda, B., Paul, S. C., Mohamed, N. A. N., Tay, Y. W. D., & Tan, M. J. (2018). Measurement of tensile bond strength of 3D printed geopolymer mortar. Measurement: Journal of the International Measurement Confederation.

[29] Zareiyan, B., & Khoshnevis, B. (2017). Interlayer adhesion and strength of structures in Contour Crafting - Effects of aggregate size, extrusion rate, and layer thickness. Automation in Construction.

[30] ACI Committee 308. (2001). Guide to Curing Concrete. American Concrete Institute, ACI Special Publication.

[31] Mechtcherine, V., & Dudziak, L. (2012). Effects of superabsorbent polymers on shrinkage of concrete: Plastic, autogenous, drying. In Application of Super Absorbent Polymers (SAP) in Concrete Construction: State-of-the-Art Report Prepared by Technical Committee 225-SAP.

[32] Slowik, V., Schmidt, M., & Fritzsch, R. (2008). Capillary pressure in fresh cement-based materials and identification of the air entry value. Cement and Concrete Composites.

[33] Jensen, O. M., & Hansen, P. F. (2001). Autogenous deformation and RH-change in perspective. Cement and Concrete Research.

[34] Li, J., & Yao, Y. (2001). A study on creep and drying shrinkage of high performance concrete. Cement and Concrete Research.

[35] Barcelo, L., Moranville, M., & Clavaud, B. (2005). Autogenous shrinkage of concrete: A balance between autogenous swelling and self-desiccation. Cement and Concrete Research.

[36] Houst, B. F. (1997). Carbonation shrinkage of hydrated cement paste. In Fourth CANMET/ACI International Conference on Durability of Concrete, Sydney.

[37] Šavija, B., & Luković, M. (2016). Carbonation of cement paste: Understanding, challenges, and opportunities. Construction and Building Materials.

[38] Snoeck, D., Jensen, O. M., & De Belie, N. (2015). The influence of superabsorbent polymers on the autogenous shrinkage properties of cement pastes with supplementary cementitious materials. Cement and Concrete Research.

[39] Mechtcherine, V. (2012). Introduction. In Application of Super Absorbent Polymers (SAP) in Concrete Construction: State-of-the-Art Report Prepared by Technical Committee 225-SAP.

[40] Reinhardt, H. W., Cusson, D., Mechtcherine, V. (2012). Terminology. In Application of Super Absorbent Polymers (SAP) in Concrete Construction: State-of-the-Art Report Prepared by Technical Committee 225-SAP.

[41] Friedrich, S. (2012). Superabsorbent polymers (SAP). In Application of Super Absorbent Polymers (SAP) in Concrete Construction: State-of-the-Art Report Prepared by Technical Committee 225-SAP.

[42] Snoeck, D. (2016). Self-Healing and Microstructure of Cementitious Materials with Microfibres and Superabsorbent Polymers. Civil Engineering Department, Ghent University, Belgium. Ph.D. Thesis.

[43] Lura, P., Friedemann, K., Stallmach, F., Mönnig, S., Wyrzykowski, M., Esteves, L. P. (2012). Kinetics of Water Migration in Cement-Based Systems Containing Superabsorbent Polymers. In Application of Super Absorbent Polymers (SAP) in Concrete Construction: State-of-the-Art Report Prepared by Technical Committee 225-SAP.

[44] Toledo Filho, R. D., Silva, E. F., Lopes, A. N. M., Mechtcherine, V., & Dudziak, L. (2012). Effect of Superabsorbent Polymers on the Workability of Concrete and Mortar. In Application of Super Absorbent Polymers (SAP) in Concrete Construction: State-of-the-Art Report Prepared by Technical Committee 225-SAP.

[45] Kovler, K. (2012). Effect of Superabsorbent Polymers on the Mechanical Properties of Concrete. In Application of Super Absorbent Polymers (SAP) in Concrete Construction: State-of-the-Art Report Prepared by Technical Committee 225-SAP.

[46] Reinhardt, H. W., Assmann, A. (2012). Effect of Superabsorbent Polymers on Durability of Concrete. In Application of Super Absorbent Polymers (SAP) in Concrete Construction: State-of-the-Art Report Prepared by Technical Committee 225-SAP.

[47] Cusson, D., Mechtcherine, V. & Lura, P. (2012). Practical Applications of Superabsorbent Polymers in Concrete and Other Building Materials. In Application of Super Absorbent Polymers (SAP) in Concrete Construction: State-of-the-Art Report Prepared by Technical Committee 225-SAP.

[48] Imran, A. B. & Takeoka, Y. (2014). The development of novel “stimuli-sensitive” hydrogels for various applications. In Nature Communications (electronic version).

[49] Mönnig, S. (2009). Superabsorbing additions in concrete – applications, modelling and comparison of different internal water sources. Fakultät Bau- und Umweltingenieurwissenschaften, Universität Stuttgart, Germany. Ph.D. Thesis.

[50] Ye, G., van Breugel, K., Lura, P. & Mechtcherine, V. (2012). Effect of Superabsorbent Polymers on Hardening Process of Binder Paste and Microstructure Development. In Application of Super Absorbent Polymers (SAP) in Concrete Construction: State-of-the-Art Report Prepared by Technical Committee 225-SAP.

[51] Jensen, O. M. (2008). Use of superabsorbent polymers in construction materials. In 1st International Conference on Microstructure Related Durability of Cementitious Composites 13-15 October.

[52] Li, J., Zhang, K., Zhang, M., Fang, Y., Chu, X., & Xu, L. (2018). Fabrication of a fast-swelling superabsorbent resin by inverse suspension polymerization. Journal of Applied Polymer Science.

[53] Jensen, O. M., & Hansen, P. F. (2001). Water-entrained cement-based materials - I. Principles and theoretical background. Cement and Concrete Research.

[54] Nerella, V. N., Krause, M., Näther, M., & Mechtcherine, V. (2016). Studying printability of fresh concrete for formwork free Concrete on-site 3D Printing technology technology (CONPrint3D). Rheologische Messungen an Baustoffen, (March), 236–246.

[55] Feng, P., Meng, X., Chen, J. F., & Ye, L. (2015). Mechanical properties of structures 3D printed with cementitious powders. Construction and Building Materials, 93, 486–497.

[56] Snoeck, D., Pel, L., & De Belie, N. (2018). Superabsorbent polymers to mitigate plastic drying shrinkage in a cement paste as studied by NMR. Cement and Concrete Composites, 93, 54–62.

[57] Snoeck, D., Pel, L., & De Belie, N. (2017). The water kinetics of superabsorbent polymers during cement hydration and internal curing visualized and studied by NMR. Scientific Reports, 7(1), 9514.

[58] Audenaert, K. (2006). Transportmechanismen in zelfverdichtend beton en relatie met carbonatatie en chloridepenetratie. Civil Engineering Department, Ghent University, Belgium. Ph.D. Thesis.

[59] Snoeck, D., Van Tittelboom, K., De Belie, N., Steuperaert, S., & Dubruel, P. (2012). The use of superabsorbent polymers as a crack sealing and crack healing mechanism in cementitious materials. 3rd International Conference on Concrete Repair, Rehabilitation and Retrofitting, ICCRRR 2012, September 3, 2012 - September 5, (December 2013), 152–157.

[60] Mignon, A., Snoeck, D., Dubruel, P., Vlierberghe, S. Van, & De Belie, N. (2017). Crack mitigation in concrete: Superabsorbent polymers as key to success? Materials. MDPI AG.

[61] Buchholz, F., & L.; Peppas, N. A., E. (1994). Superabsorbent Polymer. Science and Technology. American Chemical Society: Washington, DC, 16, 193–202.

[62] Jin, Z. F., Asako, Y., Yamaguchi, Y., & Yoshida, H. (2000). Thermal and water storage characteristics of super-absorbent polymer gel which absorbed aqueous solution of calcium chloride. International Journal of Heat and Mass Transfer, 43(18), 3407–3415.

[63] Vandenhaute, M., Snoeck, D., Vanderleyden, E., De Belie, N., Van Vlierberghe, S., & Dubruel, P. (2017). Stability of Pluronic® F127 bismethacrylate hydrogels: Reality or utopia? Polymer Degradation and Stability, 146, 201–211.

[64] Snoeck, D., Schröfl, C., Mechtcherine, V. (2018). Recommendation of RILEM TC 260-RC: testing sorption by superabsorbent polymers (SAP) prior to implementation in cement-based materials. Materials and Structures, 51(116), 1-7.

[65] Esteves, L. P. (2011). Superabsorbent polymers: On their interaction with water and pore fluid. Cement and Concrete Composites, 33(7), 717–724.

[66] Snoeck, D., Velasco, L. F., Mignon, A., Van Vlierberghe, S., Dubruel, P., Lodewyckx, P., & De Belie, N. (2015). The effects of superabsorbent polymers on the microstructure of cementitious materials studied by means of sorption experiments. Cement and Concrete Research.

[67] Snoeck, D., Schaubroeck, D., Dubruel, P. & De Belie, N. (2014). Effect of high amounts of superabsorbent polymers and additional water on the workability, microstructure and strength of mortars with a water-to-cement ratio of 0.50. Cement and Concrete Research.

[68] Baroghel-Bouny, V., Mounanga, P., Khelidj, A., Loukili, A., & Rafaï, N. (2006). Autogenous deformations of cement pastes: Part II. W/C effects, micro-macro correlations, and threshold values. Cement and Concrete Research, 36(1), 123–136.

[69] Charron, J.P., Marchand, J. Bissonette, B. (2003). EARLY-AGE DEFORMATIONS OF HYDRATING CEMENT SYSTEMS: COMPARISON OF LINEAR AND VOLUMETRIC SHRINKAGE MEASUREMENTS. In A. Kovler, K; Bentur (Ed.), International RILEM Conference on Early Age Cracking in Cementitious Systems (pp. 245–256). RILEM Publications SARL.

[70] Boivin, S. (1999). Retrait au jeune âge du béton – Développement d'une méthode expérimentale et contribution à l'analyse physique du retrait endogène. Doctoral thesis of École Nationale des Ponts et Chaussées, Paris, 1999.

[71] Mounanga, P., Baroghel-Bouny, V., Loukili, A., & Khelidj, A. (2006). Autogenous deformations of cement pastes: Part I. Temperature effects at early age and micro-macro correlations. Cement and Concrete Research, 36(1), 110–122.

[72] Omidian, H., Hashemi, S.A., Sammes, P.G., Meldrum, I. (1998). A model for the swelling of superabsorbent polymers. In Polymer, Volume 39, Issue 26, 1998, Pages 6697-6704.

[73] Khalil, N., et al. (2017). Use of calcium sulfoaluminate cements for setting control of 3D-printing mortars. Construction and Building Materials, 157: p. 382-391.

[74] Boel, V. (2007). Microstructuur van zelfverdichtend beton in relatie met gaspermeabiliteit en duurzaamheidsaspecten. Civil Engineering Department, Ghent University, Belgium. Ph.D. Thesis.

[75] Huang, H. Ye, G. (2017). Examining the "time-zero" of autogenous shrinkage in high/ultra-high performance cement pastes. Cement and Concrete Research, 97 (2017), 107-114.

[76] Hamad, A.J. (2017). Size and shape effect of specimen on the compressive strength of HPLWFC reinforced with glass fibres. Journal of King Saud University - Engineering Sciences, Volume 29, Issue 4, 2017, Pages 373-380.

[77] Bentz, D.P., Garboczi, E.J., Haecker, C.J., Jensen, O.M. (1999). Effects of cement particle size distribution on performance properties of Portland cement-based materials. Cement and Concrete Research, October 1999.

[78] Taerwe, L., De Schutter, G. (2006). Betontechnologie. Vakgroep Bouwkundige Constructies. Laboratorium Magnel voor Betononderzoek. Cursustekst.

[79] Trtik, P., Münch, B., Weiss, W.J., Kaestner, A., Jerjen, I., Josic, L., Lehmann, E., & Lura, P. (2011). Release of internal curing water from lightweight aggregates in cement paste investigated by neutron and X-ray tomography. Nuclear Instruments and Methods in Physics Research Section A, 651(1), 244-249.

[80] Taerwe, L., (2016). Concrete structures: prestressed concrete and slabs. Department of Structural Engineering. Magnel Laboratory for Cocrete Research. Course notes.

[81] Quikpoint (2019). Quikpoint™ Mortar Gun (w/ Black & Decker, 5.2 Amps). [online] www.quikpoint.com. Available at: https://www.quikpoint.com/Quikpoint-Mortar-Gun-p/3600.htm [Accessed 13 May. 2019].

[82] Justs, J., Wyrzykowski, M., Bajare, D., Lura, P. (2015). Internal curing by superabsorbent polymers in ultra-high performance concrete. Cement and Concrete Research. Volume 76, 2015, Pages 82-90.

[83] Dudziak, L., Mechtcherine, V. (2010). Enhancing early-age resistance to cracking in high strength cement-based materials by means of internal curing using Super Absorbent Polymers. International Rilem Conference On Material Science. 3. 129-139.

[84] Slowik, V., Schmidt, M., Fritzsch, R. (2008). Capillary pressure in fresh cement-based materials and identification of the air entry value. Cement and Concrete Composites. Volume 30, Issue 7, 2008, Pages 557-565.

List of figures

List of tables

This page is intentionally left blank.